Insulin-based nanowire structures:
Production, characterization and catalysis potential

by

Kiersten Marie Batzli

A dissertation submitted in partial fulfillment
of the requirements for the degree of
Doctor of Philosophy
(Materials Science and Engineering)
in The University of Michigan
2015

Doctoral Committee:

Professor Brian J. Love, Chair
Professor John W. Halloran
Professor Joerg Lahann
Professor Ayyalusamy Ramamoorthy

About 10,000 years ago, [humans] began to domesticate plants and animals.
Now it's time to domesticate molecules.

-Susan Lindquist
Professor of Biology, MIT

Dedication

To my family:

To my dad for his advice and for not letting me give up on science.

To my mom for her unconditional support.

To my sister and brother for inspiring me and reminding me to laugh.

And to Ben for providing emotional support, creative input and an alternative perspective that made this journey not only possible but fun as well.

Acknowledgements

I'd like to thank my committee for their helpful comments which have helped to shape the direction of this thesis. The diverse perspectives that they bring to this topic has lead me to stretch to consider a complicated and interdisciplinary topic from different views and I am grateful for this experience. I'd also like to thank my advisor, Brian Love, for taking a chance on a philosophy major with an interest in biomaterials and developing this project. Thanks also to my colleagues in the Materials Science and Engineering Department who have also been supportive and helpful in getting through the degree process.

Many thanks are due to those who supported me throughout my many years of education, instilling a love of learning as well as patience and perseverance. Special thanks go to Mr. Wilkes, Mrs. Norton and Mrs. Golembeski for their unbelievable devotion to making high school science and math fun. Thank you to my high school English teacher Mrs. Van Pilsum, who planted the idea of pursuing a PhD so early, even though Materials Science is definitely not what she suggested. I owe a deep debt of gratitude to my undergraduate advisors, Ellen Feder and Nate Harshman for helping me to structure my undergraduate education and supporting my dreams of going to graduate school. Thanks to Paul Ruchhoeft at the University of Houston for taking me on as an REU student and introducing me to research in a lab for the first time. Thanks are also due to my fellow physics students at American University for keeping it fun through many late nights and long problem sets.

A huge thank you to my friends for their support during the completion of my Ph.D. The unwavering friendship and support of my friends in Ann Arbor and their unfailing willingness to hop on a bike or grab a cup of coffee for some stress relief has made these five years possible.

Thank you to my family for being supportive and believing in me throughout the years. And the largest thank you to Ben who has been there for me throughout all of the craziness of grad school.

I'm so thankful for the opportunity that I've had to stretch myself (and some proteins) and dig deeply into the problems presented in this thesis. I'm beyond excited to see what the next chapter of life brings. And I bet you're excited for the next chapter of this thesis!

Table of Contents

List of Figures

List of Tables

Abstract

Use of proteins as bio-templates for production of nanowires and materials is a burgeoning field of research making use of intrinsic protein characteristics and tendencies to self-assemble nanostructures for use in a variety of applications. Proteins are known to self-associate into a variety of aggregate structures with interesting qualities including high aspect ratios and large effective surface areas that can be coated with metals. These protein-based nanowires are of potential interest as high surface area catalytic surfaces.

Here we have developed a protocol for producing insulin-based protein-fibrils by heating and applying oscillatory strain to the proteins. Using this method we reliably produce numerous high aspect ratio fibrils that are characterized using TEM. The fibril structures and 2-D networks formed by deposition of the structures onto a substrate have been analyzed and a regime of appropriate applied strain has been identified for production of a large number of fibrils and highly connected networks upon deposition.

Aggregate development is explored using sigmoidal analysis of rheological data tracking initial stages of growth during the heating and deforming protocol. Use of the sigmoidal model allows for extraction of kinetic constants associated with aggregate production in the solution resulting in increased viscosity. The sigmoidal model may be applied to a variety of experimental techniques tracking fibril development, although they measure different aspects of the denaturing, nucleation and fibril growth process. The sigmoidal model is applied to ThT assay data compiled from the

literature and used to point to possible techniques for increased uniformity and better comparison amongst ThT assay tests.

A protocol for metallizing insulin fibrils is developed for coating the produced insulin fibrils with platinum using an electroless plating technique. The platinum completely covers the fibrils and is well-adhered, forming a metallic nanowire based on the insulin template. Dispersions of nanowires are used as efficient catalysts in reducing 4-nitrophenol to 4-aminophenol. This reduction is tracked by UV-Visible Spectroscopy, and associated reaction constants compares favorably with reaction constants of similar platinum-coated substrates used in the literature. Subsequently, the immobilization of the protein-based nanowires onto textile substrates has been demonstrated for potential use as retrievable catalysts.

Chapter 1.

Insulin aggregation and directed-assembly

1.1 Chapter Summary

The molecular mechanisms associated with unfolding and aggregation of amyloid proteins have been documented in the literature and are reasonably well-understood. Such studies employ methods including CD and NMR to understand and describe these mechanisms which are reviewed here. The macromolecular structures which can be formed from protein aggregates and fibrils are less understood but their potential for use in a technical applications such as electrodes, sensors and catalysts prompts the need for further study.

1.2 Introduction

Interest in biomolecules and their potential use as bottom-up building blocks to engineer self-assembled devices has exploded in recent years. Biomolecules are nanoscaled, self-associating building blocks that can be influenced to construct various structures with relative ease [1, 2]. The simplicity of biomolecule self-association into precise and diverse structures has fed the recent research into both understanding biomolecular self-association and directing the self-association into useful structures.

Controlling the organization and self-assembly of biomolecules begins with choosing the molecule which to build. Many proteins found *in vivo* may naturally self-associate into small oligomeric structures which are related to their function [3, 4]. Proteins are also influenced by environmental conditions that may drive them from their native conformation and cause them to misfold or unfold. The structures which are formed when unfolded proteins self-assemble depends on a variety of factors including the protein and environmental conditions such as pH, temperature and the presence of other molecules [5, 6].

Of particular interest for the self-assembly of useful structures are amyloid proteins as they form long fibrous aggregates known as fibrils under specific environmental conditions. These fibrils may be coated in various metals for use as self-assembled nanowires, electrodes, biosensing devices and solar cells as well as high surface-area catalysts [1, 7]. In this thesis, a protocol for preparation of insulin fibril structures and their subsequent platinum coating for use as catalytic surface is documented, as well as the characterization of the aggregates and aggregate networks.

1.3 Insulin misfolding and aggregation

1.3.1 Insulin as an amyloid protein

Insulin was chosen as a model protein on which to base our investigation of the macromolecular aggregate structures that can be formed because the mechanisms of insulin denaturing and misfolding are well understood. This provides us with a strong basis on which to begin investigation of the structures that we can form for use in other applications while having and understanding from other research of the mechanisms that we are manipulating to form these structures.

Insulin is expressed from the prohormone precursor proinsulin in pancreatic β-cells where it is stored as a zinc-stabilized hexamer [8, 9]. The pH change accompanying the release of insulin from the pancreas into the blood stream causes the insulin to dissociate from its hexameric conformation into three dimers and further into a monomeric form, which is its physiologically active form [8, 10]. Insulin naturally forms a three-dimensional structure sequestering its hydrophobic regions. It is also known that under specific conditions insulin misfolds into an unstable conformation with exposed hydrophobic regions encouraging self-aggregation [6, 8, 11, 12].

As an amyloid protein, insulin self-aggregates into fibrils rich in β-sheet formations [13, 14]. The potential interacting sites of the insulin protein have been identified on residue A8 on the A chain and residues 10, 16, 17, and 25 on the B chain [12, 15]. Residue substitutions in proinsulin have been shown to negatively affect proinsulin chain combination and folding [9]. Bovine insulin differs from human insulin in that it has different residues at the A8, A10 and B30 sites [15], and these substitutions make it more prone to fibrillation than human or porcine derivatives [12, 15].

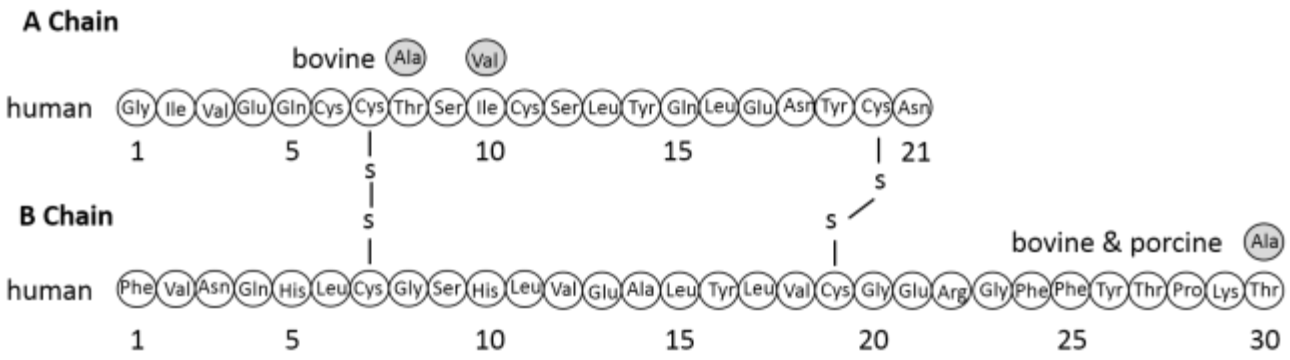

Figure 1. A and B chains of human insulin with bovine and porcine differences marked.

Insulin, like other amyloid proteins, form fibrillar aggregate structures under certain environmental conditions. In the case of insulin, exposure to temperatures of greater than 60°C is sufficient to produce unfolding of the protein, and in low pH solutions the resulting aggregate is fibrillar in structure [16, 17, 18, 19]. The addition of salts or urea is also known to cause unfolding and aggregation of insulin, although these conditions have been shown to produce amorphous and circular aggregates, respectively [13, 20]. The nature of the aggregates is influenced by the pH of the solution in relation to the isoelectric point (pI) of the protein. Near the pI proteins typically form globular aggregates, while farther from the pI aggregates are fibrillar [21, 22, 23].

1.3.2 Mechanisms of misfolding

The formation of fibrils is a common trait of proteins and is driven by interactions between polypeptide main chains [24]. Thus, the amino acid sequence of the protein leads to increased or decreased rate of aggregation and influences the resulting aggregate morphologies [12, 15]. The structure of insulin amyloid protein and insulin self-assembly to form fibrils has been studied by analysis of the crystal structure of the protein and its aggregates [14, 25], cryo-electron microscopy

imaging of formed fibrils [26] and x-ray scattering data [27] as well as circular dichroism (CD) [28, 29, 30, 31].

For insulin fibrillation to occur, the protein must first progress through a non-native, partially folded monomeric intermediate species [27, 32]. The unfolding of insulin has been traditionally achieved by heating which was shown early on in CD studies to result in a partially unfolded structure with reduced α-helix content and the appearance of β-pleated sheet structures [33]. Recently, the unfolding mechanism was further elucidated through use of NMR studies which showed a partial fold during which the N-terminal segments of both A- and B-chains detach from the core and the N-terminal α-helix of the A-chain unfolds [34].

Huus *et al* investigated the thermal stability of insulin using near-UV CD and differential scanning microcalorimetry to better understand the thermally mediated unfolding process. It was found that zinc-free insulin which is primarily dimeric at room temperature easily unfolds at 70°C but the association of insulin with zinc lead to biphasic thermal denaturation due to the presence of both a monomer/dimer species and a hexameric zinc-stabilized insulin species [35]. Their work supports the theory that the thermal stability of insulin is very closely linked to the association state. Exposure to denaturants such as urea and NaCl also result in unfolding of insulin that can be tracked by CD [36, 37].

Conformational changes accompanying misfolding and self-association continue with the tertiary and quaternary structures leading to organization into aggregate superstructures [5, 38, 39]. The creation of chiral superstructures from insulin protein formed in the presence of agitation has been investigated by Babenko *et al* by ThT fluorescence assay [40]. Babenko *et al* find that chiral superstructures are accessible by the insulin protein if certain specific structural features are

formed and precisely aligned to facilitate the formation of microarchitectures [40]. Chiral structures are also observed in vortexed insulin protein in ThT and Congo Red studies by Loksztejn *et al* as well as bifurcated fibril structures [36].

Work by Vestergaard *et al* made use of x-ray scattering to resolve the nuclei and elongating unit for insulin fibril formation. In investigating the kinetic fibrillation of insulin, they found insulin monomers, mature fibrils and an oligomeric species made up of five to six insulin monomers. These structures are determined to be the fibril repeating unit, with the helical oligomer identified as the structural nucleus. The oligomer content in the solution was found to be proportional to the fibril growth rate [27].

1.3.3 Bulk and surface-mediated aggregation

The self-association of the proteins occurs via interactions of amino acid residues, but the specifics of aggregation may follow a variety of pathways which have been suggested in the literature [41, 42, 43, 44]. Assembly can occur by a variety of pathways dependent on the environmental stimuli and conditions which result in aggregate formation specific to the peptide [6]. The present work promotes aggregation of insulin proteins in a bulk solution via heating and deforming. It is likely that aggregation is mediated both by association of proteins in the bulk and by interactions at the air/water interfaces.

Bulk mediated aggregation may occur via two different pathways. The aggregation may occur via chain polymerization, by which monomers are added to the ends of elongating protein fibrils. Assembly may also occur via aggregate association in which larger aggregate structures assemble [45]. Chain polymerization and aggregate association may happen concurrently and can also occur along with other types of aggregation behaviors and mechanisms [41].

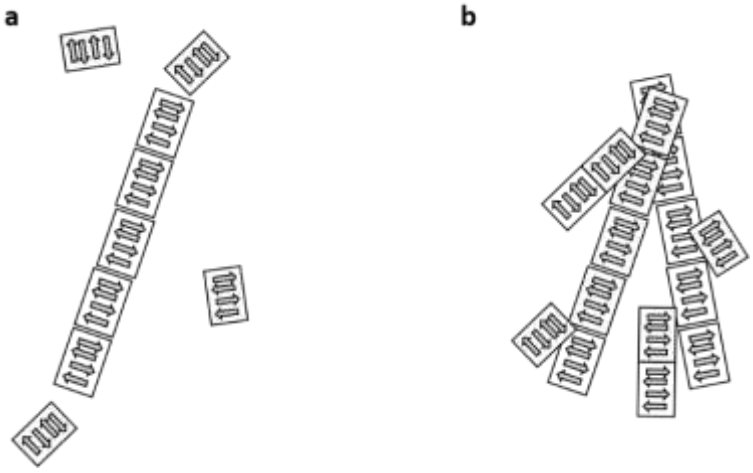

Figure 2. Bulk aggregation mechanisms a) chain polymerization and b) aggregate association.

An additional aggregation mechanism is self-association mediated by exposure to an air/water or other interface [41, 46, 47, 48]. Surface mediated aggregation is not entirely understood, though the interaction of the hydrophobic interface (such as a vapor/liquid or liquid/solid interface) and hydrophobic residues which are exposed on unfolded proteins is expected to play a role in the arrangement of proteins along these interfaces. One suggested mechanism for aggregation at interfaces is that these hydrophobic interactions attract a large number of proteins which adsorb to the interface and become entangled and associated with other proteins. The proteins adsorbed to the surface form a film of variously sized aggregates which become desorbed from the film, flaking off into the bulk of the solution where they may attract additional monomers and aggregates [41]. Whether these protein aggregates take the form of fibrils or larger amorphous or globular aggregates depends on the other conditions [41].

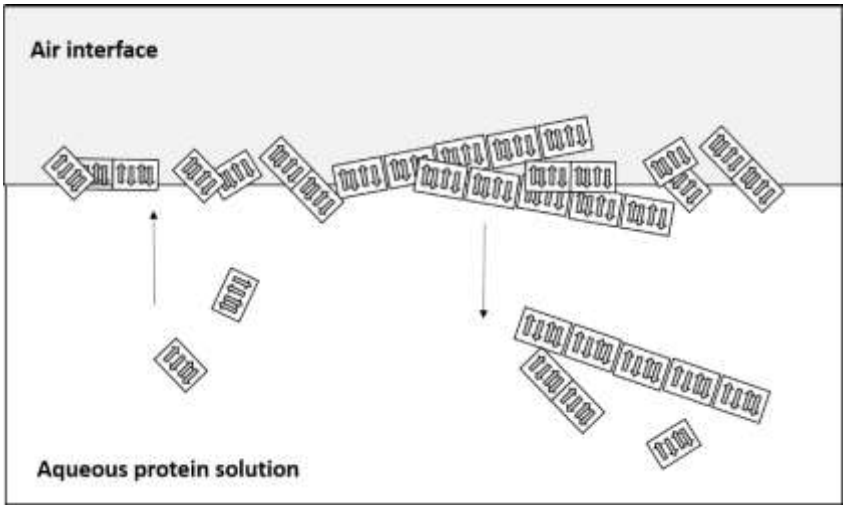

Figure 3. Surface mediated aggregation - unfolded proteins are attracted to the air/water interface due to hydrophobic interactions. At the interface the proteins interact and form aggregate structures which leave the surface and continue to aggregate in the solution bulk. Adapted from Amin et al, 2014.

Morphologies of aggregates can be influenced by the environmental stimulus that caused unfolding or other existing environmental conditions. Aggregates range from amorphous associations of proteins to spherical deposits of varying size to singular or bundled fibril structures [49, 50]. The association of the protein progresses according to a generally accepted aggregation pathway including the nucleation of an unfolded protein, association with other unfolded proteins and the continued aggregation to form a larger structure [6, 51, 52].

In the case of formation of fibrillar aggregates, the pathway that is generally agreed upon progresses through these phases as well as others specific to the fibrillar structure [6]. The aggregation begins with a protein subunit which is unfolded into a formation conducive to aggregation (with 'sticky' hydrophobic residues exposed) and is followed by the association of this protein with one or more other unfolded subunits to form an aggregating nucleus. Further association with other unfolded proteins results in the elongation of the nucleus into a protofibril. The protofibrillar protein is joined by other unfolded proteins which bind to the exposed residues

on the ends of the protofibril, elongating the aggregate into a fibrillar form. Fibrils can exist in a singular form, as a set of bound fibrils in a specific structure (such as helical fibrils formed of 3 single fibrils observed by Jansen *et al*) or as a more loosely arranged bundle of fibrils [53]. Fibrils and fibrillar bundles can further associate into networks of fibrils [54].

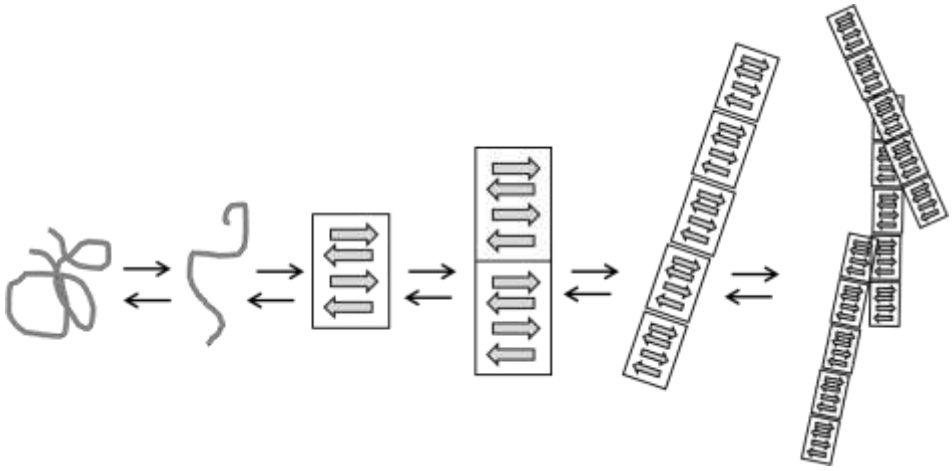

Figure 4. Generally accepted amyloid fibrillation pathway in which a folded protein becomes unfolded, forms a nuclei and elongates from the ends to form a fibril. Fibrils may also interact to form larger structures or networks. Under some conditions these steps may be reversible..

Both Krebs and Jansen observe the beginning stages of aggregation a short time after exposing insulin protein fragments to temperatures of 60°C or higher. This is followed by a further ordering observed by both Jansen *et al* and Krebs *et al* [20, 39, 53]. Krebs *et al* also observed that adding salt accelerated the initial fibril formation as well as spherulite formation [20].

1.3.4 Methods of studying amyloid proteins

Amyloid proteins are studied by a variety of methods. Chemical structure of amyloid proteins and ensembles thereof in various conformations, aggregate structures or complexes formed with other

compounds is often studied by NMR, SAXS, SANS or by computational methods [14, 55, 56]. The inhibition of aggregation is studied by ThT assay, Western Blot electrophoresis, microscopy, and less often, DSC [57, 58]. Aggregation behavior including kinetics can also be studied by ThT, circular dichroism, Congo red dye, microscopy techniques and light scattering techniques [17, 59, 60, 61]. Though this list is clearly not exhaustive, these are the biochemical and material tests which are most often encountered in the amyloid protein and aggregation literature, though the specific tests are dependent on the scientific question being pursued, as mentioned, as well as the scientific discipline of the group doing the research. Amyloid proteins are studied for a variety of reasons; most commonly to learn more about amyloid aggregation and its inhibition. More recently, a separate group of studies have emerged which leverage the natural tendency of amyloids to aggregate into specific conformations in a variety of technical applications including creation of metallized fibril-based nanowires.

1.4 Amyloid formation studies

1.4.1 Aggregation studies

The aggregation behavior of amyloid proteins and their influence on disease progression is a topic of much research. Of particular interest are the mechanisms of aggregation *in vivo* and the events that prompt aggregation to begin. Additional concerns include determinations of which aggregate conformations are cytotoxic and to which cell types, and how the aggregation might be stopped, slowed or reversed in general or at a particular aggregate formation stage. These studies occupy much space in the literature and in the biochemical and disease communities, as many of the mechanisms of amyloid-related diseases remain poorly understood and there are few, if any,

successful methods of disease reversal [57, 62]. As a result, most currently approved medical treatments of these diseases focus on palliative care and treatment of symptoms rather than addressing root causes of disease.

Understanding the processes by which proteins misfold and self-associate is interesting to other communities as well as protein aggregation is an issue of importance in food science, pharmaceutical production, anti-biofouling and others. Basic research into the mechanisms of protein aggregation and the kinetics associated with these processes furthers these research areas and others. Lastly, research is ongoing into how the mechanisms of aggregation can be controlled to manipulate the formed structures for use in engineering various devices [63, 64, 65, 66].

1.4.2 Materials applications of amyloid aggregates

Construction of nanodevices requires high precision deposition of material into two- and three-dimensional formats. As the need for nanoscale devices continues to grow, efficient means for creation of such devices are necessary. Though photolithography and other deposition techniques currently fill this need, the self-assembly of biomolecules both designed and native are an alternative mean for creation of nanodevices. The use of proteins and peptides as nanoscale building blocks from which to self-assemble nanoscale systems is appealing and research into the mechanisms by which they can be aggregated into controlled conformations is ongoing.

The natural tendency of amyloid proteins to form super high aspect ratio fibrils has been exploited in several recent studies for the creation of protein-templated nanowires. The protein side-chains allow for metallization of the nanowires using simple chemistry and the high physical and chemical stability of the protein aggregates are properties that make them appealing in a variety of applications [67, 68, 69].

Further association of protein aggregate structures lead to the formation of nanostructures networks. The properties of these nanostructures are determined by the morphologies of the protein aggregates which make up the structure [70]. In past studies aggregate morphologies have been controlled by tailoring the peptide design [70, 71]. Here we report on use of external parameters in controlling fibril morphology for a simpler and economical means of nanostructure control.

Peptide-based hydrogels and other nanostructured networks are of general interest in tissue engineering as extracellular matrix substitutes, sealants for wounds and as templates for inorganic-organic nanocomposites [72]. Metallized protein aggregates have been created and used in proof-of-concept constructions of devices such as solar cells [73] and biosensors [74, 75]. The potential for their use as nanowires has also been investigated in various studies utilizing amyloid proteins [76, 77, 78].

1.5 Contents of this dissertation

This dissertation includes development of one scheme for the reliable and efficient production of insulin-based nanowires for use in catalysis. Following this introductory chapter, chapter two documents the production of insulin fibrils using a protocol which relies on heat and deformation to denature the protein which then forms elongated fibril structures during incubation at room temperature. Possible mechanisms related to the rapid production of the fibrils with the addition of deformation are presented and general differences in fibril characteristics achieved with high and low magnitudes of deformation are described.

Chapter three goes on to describe the metallization of the prepared insulin fibrils to create insulin-templated platinum nanowires. Experiments related to the use of the nanowires as catalytic surfaces in the reduction of 4-nitrophenol to 4-aminophenol tracked by UV-Vis spectroscopy are

discussed and the catalytic efficiency of the produced nanowires is compared to other similar nanowire-like catalysts described in the literature.

In chapter four aggregation kinetics are described as related to the tracking of viscosity during denaturing and nucleation by rheology. The use of a sigmoidal model for the extraction of kinetic constants allows for better understanding of relative kinetics of varied test parameters including concentration dependence. The sigmoidal fitting of aggregation data can be extended to better understand and compare between other measures of protein aggregation including ThT fluorescence assay.

Chapter five includes preliminary work to extend the use of the insulin-templated nanowires as catalytic surfaces by immobilizing the nanowires onto textile substrates so that they can be reused in repeated reactions. The immobilization of the nanowires onto fabric swatches that can be immersed into a reaction vessel and then removed and used in additional reactions would greatly increase the value of these catalytic surfaces.

Lastly, chapter six contains a summary of the work presented in this dissertation as well as conclusions which are drawn from the experimental work and consideration of the theories related to the amyloid aggregation process. Recommendations for future work in the characterization, creation and use of protein-based nanowires are also included in this chapter.

1.6 Chapter conclusion

The natural self-assembly tendencies of peptides and proteins make their use as templates for creation of nanowires appealing. In particular, the fibrillar aggregates produced by amyloid

proteins are well-suited to metallizing for production of nanowires and other nanostructures. Other characteristics of these aggregate structures including stability and high aspect ratio add to their appeal and suggest other uses such as high surface area catalytic surfaces.

In order to best make use of proteins as nanostructured building blocks reliable methods for controlled assembly must be developed and the resulting assembled structures characterized. Methods for controlling the assembly of peptides into a variety of pre-determined nanostructures have been suggested which rely on the molecular design of peptides so that they will assemble into specific structures. However, the natural responses of proteins to their environments also dictate structural responses in produced aggregates and these environmental cues may be studied in order to simply and effectively control the natural aggregation of proteins.

Chapter 2.

Heat and deformation-produced fibrils and structures

This chapter is drawn largely from a manuscript which is in preparation for submission to the journal MSE C.

2.1 Chapter summary

A protocol for denaturing and aggregating insulin protein into fibrils and fibrillar networks is developed using heating and protein deformation by application of oscillatory shear strain. The produced fibril structures are investigated by TEM and optimum deformation for robust production of fibrils is identified. Differences in fibril morphologies attributed to the application of high and low strain resulting in larger and smaller protein deformation are characterized. Further, regions within the parallel plate structure of higher and lower deformation are suggested which lead to morphological differences in fibrils and aggregate structures produced within a single sample. Application of small amounts of deformation yields the production of many long fibrils, while application of very large strains result in fragmented and short fibril formation.

TEM imaging is used to determine network properties associated with the 2-dimensional projection of fibrils dispersed in solution. The network properties are investigated using a variety

of methods including fibril dimensions, areal calculations and nodal counts to determine connectivity. It is found that 2-D networks produced from fibrils formed with small deformations are denser and more interconnected than networks of fibrils formed in the presence of large deformations. The use of deformation in forcing proteins from their natural conformations and into nucleating aggregates is discussed.

2.2 Introduction

Amyloid proteins are known to aggregate into a variety of morphologies, including fibrils with high aspect ratios, which have potential use as templates for inorganic structures. Recent studies have demonstrated using these natural fibril formations as high aspect ratio templates for creating metallic electrodes and catalysts [76, 77, 78, 79, 80, 81, 82]. These studies focus on the metallic plating of fibrils formed in conditions known to cause aggregation such as low pH and high temperatures. Thus far, the ability to metalize proteins into nanowires and nanostructured networks has been shown, as have attempts to insert these bio-inorganic hybrid structures into working devices. However, the range of macromolecular structures and structure characteristics available through the tuning of fibril-forming parameters has not yet been documented.

Thermally-induced aggregation produces high aspect ratio fibrils in many amyloidogenic proteins, including insulin. However, while the denaturing and fibrillation process has been shown to begin nearly immediately upon exposure to elevated temperature, the formation of superfibrillar structures may take hours or days, though the rate depends on the incubation temperature [53, 60, 83]. Development of protein structures for use as nanowire templates has so far been undertaken using simple thermal denaturing techniques which involve long incubation times, often amounting to days [75, 76]. The present work reports on the development of a method for rapid creation of various fibrillar structures and subsequent quantification of the networks thermally nucleated in the presence of varied amounts of deformation.

Aggregation of insulin has been documented in denaturing conditions of altered pH [8, 13, 16, 84], elevated temperature [53, 83, 85], elevated pressure [53, 86], and added salts [87, 88, 89]. In the past decade, agitation or shearing of proteins during denaturing and nucleation has been shown to have a

significant effect on both the aggregation rate and resulting structure. The presence of shear has been shown to induce and facilitate aggregate formation in a variety of proteins, including β-lactoglobulin [90, 91], glucagon protein [92], amyloid-β [93, 94] and insulin [13, 95, 96, 97].

Shear, when applied at low rates, has been found to increase aggregate formation, although higher levels of shear can lead to the breakup of large aggregate clusters [98] or fibril degradation [90]. Several groups have shown that shear alone is sufficient to initiate fibril formation without the presence of heat [50, 90, 95, 99, 100]. Shear is thought to extend protein chain length, destabilizing it along the way. This leads to a preferential orientation that is conducive to aggregation [93, 95, 101]. Hamilton-Brown *et al* have found that nucleation and protofibril development of β-amyloid are enhanced by shear, but that mature fibril formation is inhibited, perhaps due to fibril breakage [91, 93]. Fragmented fibrils may then act as additional nucleation seeds and serve to speed aggregation further. At very high shear rates fibril formation may be hindered by the overstretching and severe deformation of fibrils. Hill *et al* have also observed enhanced aggregation in the presence of shear and report an increase in the aggregation rate of β-lactoglobulin measured by ThT fluorescence with increasing shear rates between 25 and 200 s^{-1} [90]. They find that the reorganization of protofibrils into β-sheet structures common to amyloid fibrils is inhibited in high shear environments with shear rates greater than 500 s^{-1}. Humblet-Hua *et al* have described the increased conversion of Hen egg-white lysozyme (HEWL) monomer to fibrils with increasing shear rate up to a critical shear beyond which no change in conversion rate is noted [102]. Similar findings have been published by Akkermans *et al* regarding β-lactoglobulin [100]. Insulin is exposed to shear forces during cardiovascular transport [103] as well as during pharmaceutical processing, and delivery either by manual or automated syringe injection. Though many amyloid proteins have been observed to undergo increased aggregation in the presence of shear, the mechanisms of protein interaction

leading to aggregation are complex and outside the scope of this work which aims to characterize and use the formed structures.

Manno *et al* have previously reported on tracking insulin aggregation kinetics by rheology and light scattering [104]. In the reported study, the protein was denatured at low pH and the formation of an entangled network was monitored by oscillatory rheometry. The results show that changes to the viscoelastic properties of the bulk solution occur with aggregation and that a large initial shear modulus results from the nucleation and growth of protofibrils in the early stages of aggregation.

Networks of amyloid protein fibrils are used as templates to create high-aspect ratio nanowires for use in electrodes and other technological applications [1, 64, 75, 105, 106]. While Zhang and others have documented the formation of metal-coated fibril networks created by thermally induced aggregation, the varied potential uses for such materials may require a larger control over the tunability of network structure and better characterization of the nanoscale networks produced [77, 78, 80]. In this paper, we focus on the effects of deformation and heat during fibril nucleation and the initial growth period on the resultant fibrillar network. We characterize the networks formed with various applied strains during the initial nucleation period and quantify the differences between resulting network structures.

2.3 Materials and Methods

Preparation of insulin solution: Insulin solutions were prepared by dissolving the appropriate amount of lyophilized porcine insulin (Sigma Aldrich) in a 0.01 M HCl solution (pH 2) for a final

concentration of 5 mg/ml. The solution is briefly mixed and stored at 4°C. Samples are used within 24 hours of preparation to minimize degradation.

Strained and heated samples: It is known that heating proteins above a denaturing temperature prompts the unfolding of the protein from the natural conformation, exposing hydrophobic residues and ultimately leading to the formation of nuclei for aggregation [12, 13]. Additionally, studies have shown the use of shear increases the speed at which aggregation takes place in a variety of protein solutions. The use of both temperature and applied strain as a means of deformation was hypothesized as a mechanism to reliably produce protein aggregates in a short time span. The protein aggregates formed by use of the heating and deformation protocol were compared to samples which were created by heat only and strain only to determine the effect of strain and heating on the formation of nuclei and eventual fibril networks.

Samples were heated with simultaneous application of oscillatory shear in parallel plate geometry using a TA ARES rheometer equipped with an air oven. The parallel plate geometry creates a direct relationship between displacement and strain within the sample compared with a Couette geometry which has different strain conditions comparing the axial and radial zones of the specimen geometry. The parallel plate geometry also allows for easy sample extraction post-processing with minimal turbulence to the strained fluid after the heating and straining protocol. All experiments were conducted with a working gap size of 0.5 mm ± 0.1 mm. Samples are loaded onto the bottom plate at room temperature followed by heating to 65°C at a controlled ramp rate of 10°C/min while applying strains of 1, 10, 25, 50, or 100% strain. Here, strain is expressed as a dimensionless percentage and defined as the ratio between the applied rotational displacement and the gap:

$$Strain\ (\%) = \frac{deformation\ (mm)}{gap\ size\ (mm)} \qquad \text{(eq. 2.1)}$$

Large amounts of strain result in larger deformations along the edges of the plate (Figure 5). The amount of deformation felt by proteins is smaller towards the center of the plate, and the amount of deformation to the proteins exists on a gradient between the edge and the center point. Since the gap and the frequency are maintained between different samples, the amount of applied strain is the only parameter which is varied in the tests.

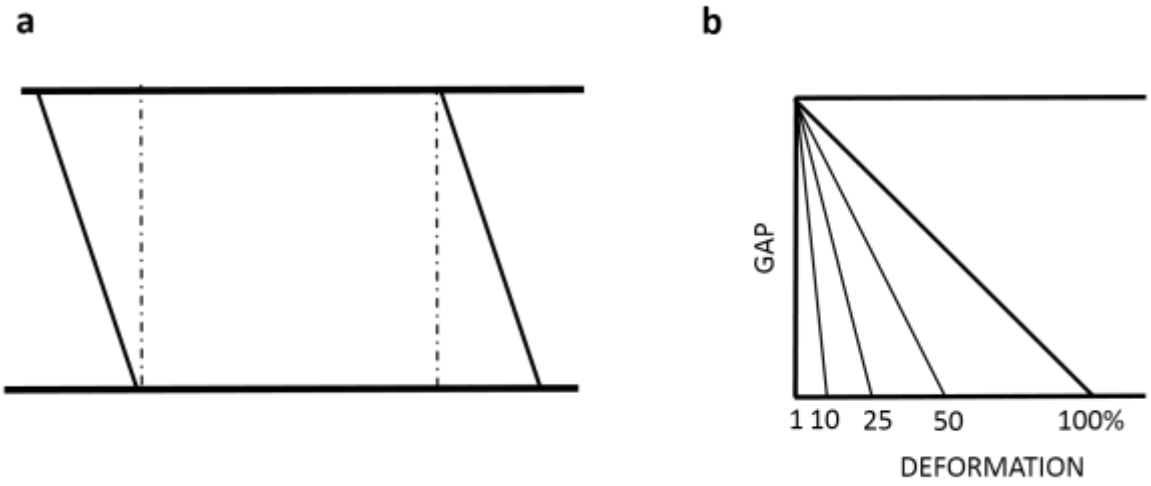

Figure 5. Illustrations of shear strain a) effect of shearing by lower plate b) large shear strain results in larger deformation and stretching near the edges of the plate.

Samples being prepared for TEM imaging are heated for 15 minutes on the rheometer with varied amount of strain (1%, 10%, 25%, 50%, and 100%) in order to initialize fibril formation and to minimize evaporation. Following the heating and deformation protocol, each sample is removed from the oven, cooled to ambient temperature (~23°C) and kept quiescently for 24 hours prior to further testing. Fibril growth triggered at elevated temperature continues at room temperature following the initial incubation [17].

Complex viscosity measurements were carried out using the same equipment but samples were heated and tracked for a longer time. Final complex viscosity was determined when a stable plateau was achieved. The samples are insulated by a layer of low viscosity silicone oil (Sigma Aldrich) dispensed around the circumference of the gap between the plates in order to minimize evaporation.

Preparation of heated or strained samples: For samples prepared in a static condition without shear, insulin is heated to 65°C in the air oven attached to the rheometer without the use of shear. To determine the complex viscosity of non-sheared samples the samples are prepared on the parallel plate but without shearing. Following 15 minutes of heating in static non-sheared conditions, the complex viscosity is measured.

A set of non-sheared samples which were denatured by heating only were prepared for TEM to visualize the differences in fibril morphologies with and without the presence of deformation. The non-deformed samples are prepared in the same manner but are only heated in the air oven and are not subjected to deformation by applied strain. Following incubation, each sample is removed from the plate and kept in quiescent conditions for 24 hours before preparation of the sample for TEM imaging.

Samples which are sheared at ambient temperature are prepared using the same frequency and strain settings as for preparation of samples with heating, but the air oven is not used. These samples are sheared for 15 minutes at room temperature and maintained in quiescent conditions overnight to allow for continued aggregation. These samples are then prepared for TEM imaging.

TEM Sample Preparation and Imaging: To quantify differences between fibrils and networks formed at different conditions, aggregated samples were analyzed by TEM. Samples for imaging

were prepared by drop casting 5 μl of solution onto carbon-coated copper TEM grids immediately following glow discharge treatment. Excess liquid is wicked away after 2 minutes to allow sufficient sample adsorption and the TEM grids are rinsed three times in distilled ultrapure water (Sigma Aldrich). This is followed by negative staining using 1% uranyl acetate stain (Sigma Aldrich). Excess stain is wicked away after 1 minute followed by imaging.

Imaging was conducted with a Philips CM-100 TEM and multiple areas of the sample were imaged in order to ensure observations were representative of the entire sample. Collected images were analyzed to quantify fibril dimensions, density of the fibrils within a network and the connectivity. A measurement of fibril density was obtained using area fraction calculations based on TEM images [107, 108]. It should be noted that TEM images produced from the fibril dispersion are 2-dimensional projections of the fibrils in solution. TEM images allow us to make measurements and observations about the individual morphologies, but the network calculations that we make based on these images are not necessarily representative of the fibrils suspended in the dispersion as TEM images are a 2-dimensional projection of the fibrils dispersed in solution.[109] Nonetheless, instances where an understanding of the 2-dimensional fibril network would be useful can be imagined, including use of the fibrils as templates for creation of nanowire electrodes.

TEM grids of strained protein networks were created from two separately prepared insulin solutions and each TEM session captured images from multiple networked areas on the grid. The connectivity of the fibril network was measured by assigning each fibril cross-over a number based on the number of spokes that come together at that node. Observed trends were validated by calculating connectivity and fibril density for one set of "test" images and then comparing the trends to calculations made for a second set of "validation" TEM images [110]. The results for the

two sets were similar and final numbers presented are averaged results of connectivity and fibril density for all captured TEM images.

2.4 Results

2.4.1 Rheological results

The effect of strain on the formation of nuclei and early aggregate structures was initially resolved using rheology to track the evolution of the complex viscosity with time during the heating and deformation protocol. By tracking the complex viscosity associated with the bulk solution during nucleation with shearing, we resolve the final complex viscosity achieved after heating to 65°C with 100% strain and incubating for 35 minutes. This is on the order of aggregation times observed by other methods. A rise in viscosity associated with initial denaturing of the protein, nucleation of aggregates and aggregate structure development is observed within 13 minutes with applied strain and heat, with a steady final state achieved after about 22 minutes. Additionally, non-sheared samples were produced by heating at 65°C for 15 minutes in the air oven without oscillatory shear. After heating for 15 minutes without strain, the complex viscosity was measured to resolve the behavior of the gel created with heat alone (Figure 6).

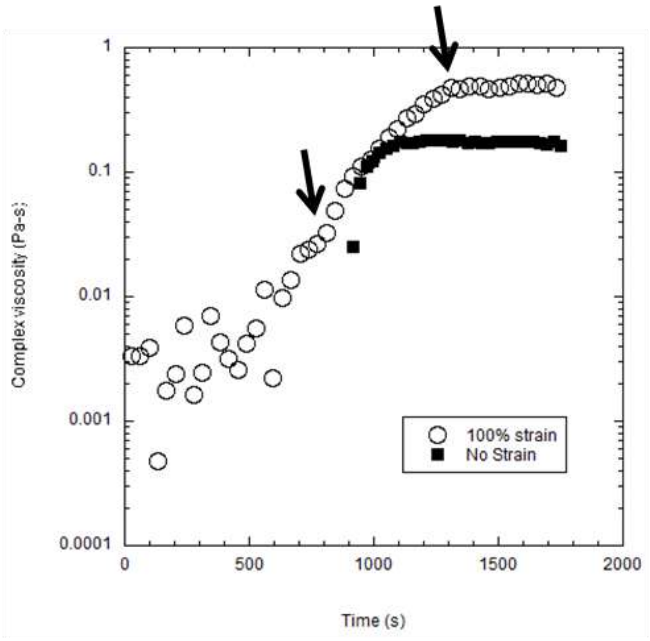

Figure 6. Rheological profile shows evolution of complex viscosity under 2 growth conditions: 100% applied strain (open circles) and no applied strain (filled squares).

The complex viscosity associated with these heated but un-sheared samples was higher than the initial complex viscosity of unheated solution. If no aggregation resulted from heating without strain, the complex viscosity at 15 minutes is expected to match the initial viscosity measured for 0 seconds of heating during deformation. Since this was not the case, some denaturing and aggregation resulting in an increase in the complex viscosity of the solution has occurred with heat alone. Some advancement of the complex viscosity relative to an unheated sample is observed after 15 minutes of heating without strain. The final complex viscosity of the non-sheared solution was observed to be 0.4 Pa-s less than the final complex viscosity of samples nucleated with both oscillatory strain and heat (Figure 6).

2.4.2 Influence of incubation time

Our results suggest the formation of unfolded proteins, nuclei and a subset of aggregate structures are present in the bulk sample volume after a short period of heating and shearing. The characteristics of the formed structures were further investigated by TEM in order to better understand the nature of the structures and the influence of strain during the initial heating and shearing treatment of the samples. Samples were prepared for TEM using the same frequency (10 rad/s) but varied strain (1, 10, 25, 50 or 100%) and were subjected to the heat and deformation regimen for a period of 15 minutes, as this was the approximate time required to onset of aggregation determined by our rheological data. Following the denaturing protocol, samples were incubated for 24 hours at room temperature for further fibrillation to occur before the sample was transferred to a copper grid for TEM imaging. Control samples were prepared without the effects of deformation by incubating samples at the temperature of 65^{o}C under no applied strain for 15 minutes, followed also by 24 hours at room temperature.

Figure 7 illustrates the change that occurs during the overnight incubation period. Figure 7a shows the protein solution taken directly from the rheometer plate following the shearing and heating protocol, while Figure 7b shows a TEM grid prepared from the same sample solution after incubation overnight. The 15 minute denaturing protocol results in denatured proteins which are prepared to form aggregates as well as a number of nuclei and small aggregate structures. Overnight, more of the denatured and aggregation-ready proteins come together to elongate nuclei into fibrillar nanostructures. Average fibril lengths immediately following the deformation protocol vary greatly, but are on average 300 nm with shorter fragments which are tens of nanometers in size. Following overnight incubation, the average fibril length increases to 800 –

3000 nm depending on the amount of fibril deformation during the denaturing protocol with large applied deformation yielding shorter fibrils.

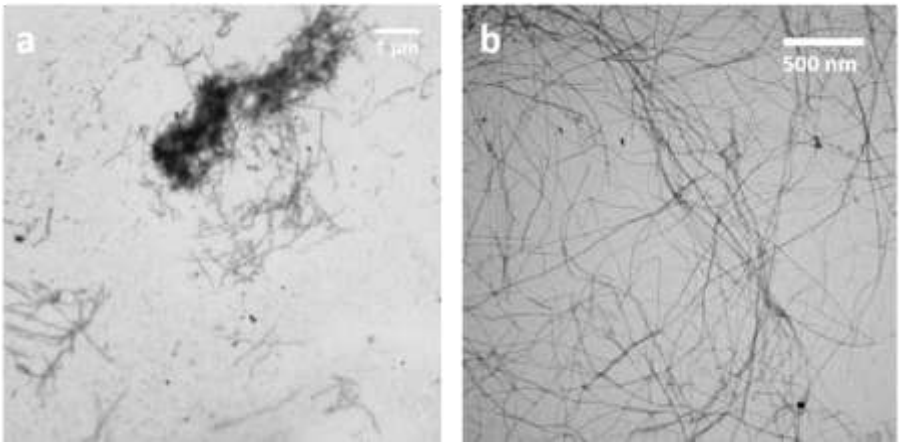

Figure 7. TEM images of protein solution (a) immediately following denaturing protocol and (b) after overnight incubation.

2.4.3 Influence of strain

Figure 8 illustrates commonly observed fibril morphologies, including bundled fibrils, curved fibrils and branched fibrils. These fibrils were prepared without applied strain (with heat only) those these morphologies are observed in strained and heated samples as well. The most identifying characteristic of non-strained samples which differentiates them from fibrils produced by the combined heating and straining protocol is that non-strained fibrils are found mostly in isolation. There are many times fewer fibrils observed in non-strained samples than in strained samples.

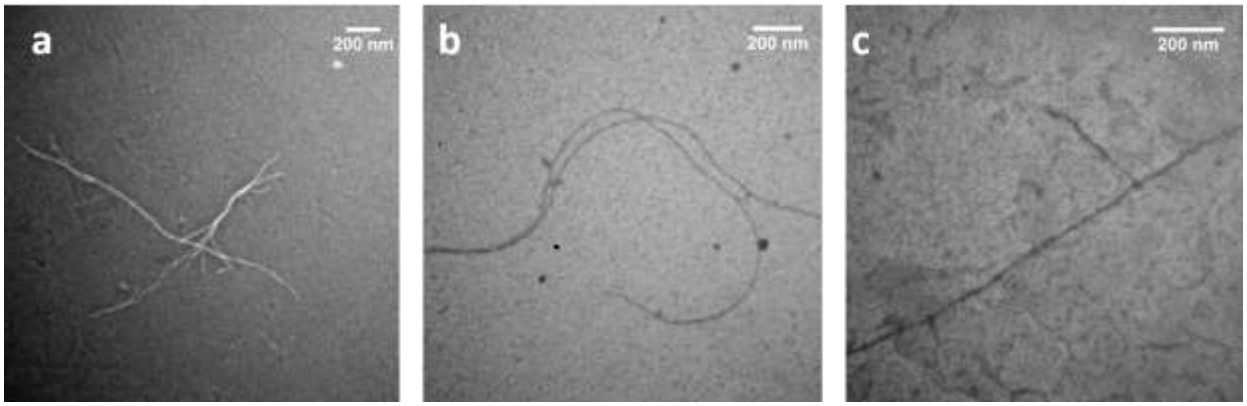

Figure 8. Common fibril morphologies include a) bundled fibril structures, b) curved fibrils and c) branched fibrils.

Fibrils which are produced using the heat and deformation protocol are more numerous and create dense fibrillar networks because of the large number of fibrils which exist in the solution. When the fibrils are deposited onto the TEM grid for imaging, the 3-dimensional structure of the fibrils suspended in the solution is reduced to 2-dimensions which can be studied both as an indication of the types of possibly more diffuse network structures which exist in solution as well as for potential 2-dimensional applications employing these fibril structures.

Samples nucleated during the combined heat and deformation protocol contain a higher density of fibrils producing an entangled network of fibers (Figure 9). Nucleation with as small as 1% strain significantly increases the density of fibers present and results in a fibrillar network. At 100% strain, identified as a large strain, there are a smaller number of fibrils present, and the fibrils are shorter and more heavily fragmented than fibrils created with lower strains. At intermediate strains (9c, 50% strain) we see an intermediate number of fibrils present which are neither as short as fibrils detected in 100% strained samples, nor as long as fibrils in 1% strained samples. There appears to be a gradient of fibrils number and length which is accessible based on the applied strain

which ranges from long fibrils grown from many nuclei to a smaller number of fibrils which are fragmented and stunted by application of large strain.

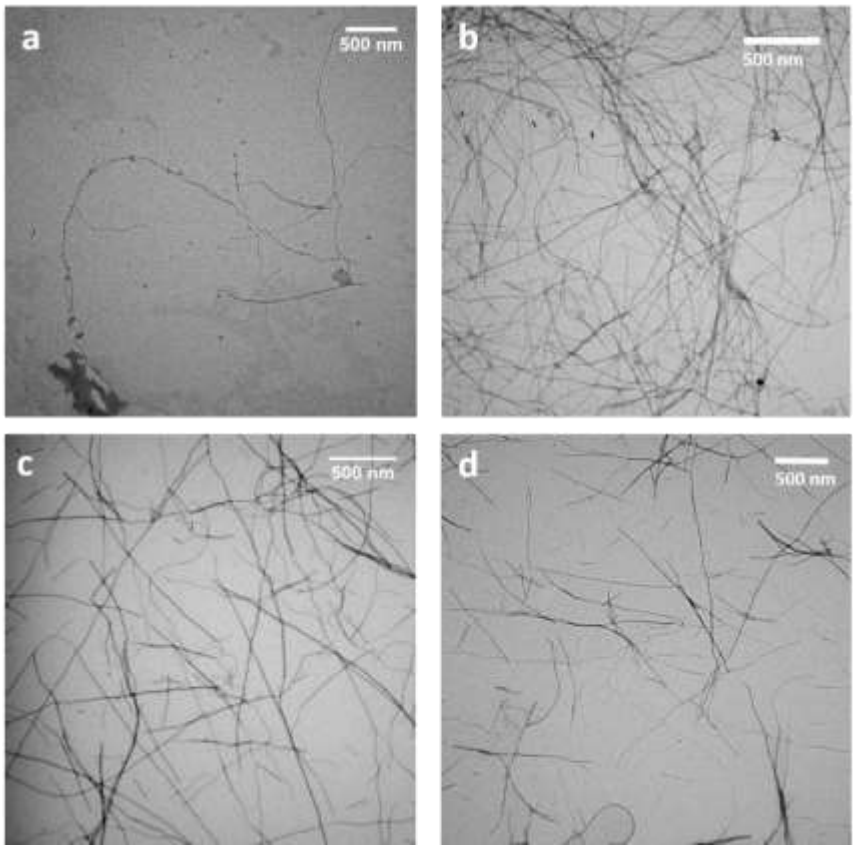

Figure 9. Fibril networks produced with varying strains from a) 0% b) 1%, c) 50% and d) 100% strain during heating.

The application of shear strain does not lead to a statistically different diameter of fibrils formed. For all nucleating conditions, single fibrils were found to have an average diameter of 12 ± 1.2 nm, as shown in Table 1. Similar minimal morphological variability in insulin fibril diameters has also been reported by Jansen *et al* [53]. Samples containing fibrils initiated with heat only and with heat and deformation both exhibit branching and bundling of fibrils. The bundles possessed

diameters which ranged from 20 nm - 50 nm. Fibril lengths observed in samples prepared with both large and small deformations vary greatly, but the average fibril length in TEM images of fibrils prepared with small amounts of deformation is larger than for those prepared with large deformations, 1750 nm compared to 1350 nm average length.

Table 1. Average fibril diameter with strain

	average fibril diameter	minimum measured (nm)	maximum measured (nm)
1	10.8 ± 3	6.2	17.6
10	12.2 ± 3	6.3	18.0
25	11.1 ± 3	4.2	17.8
50	12.0 ± 3	5.8	18.8
100	13.9 ± 3	9.7	18.9

2.4.4 Fibril Growth Mechanisms

Controlled deformation during denaturing influences the formation of fibril nuclei and the network characteristics of resulting fibrillar structures. Deformation of the protein in addition to heating creates larger numbers of fibrils and more complex fibril networks. The deformation of the proteins during denaturing likely increases stretching of the proteins at the outer edges of the plates where the deformation is highest and may also lead to increased adsorption, aggregation and renewal of proteins at the air/water interface. It has been shown that proteins readily adsorb to the bulk interfaces [111, 112, 113, 114, 115, 116] and that aggregate formation is accelerated by turnover at these

boundaries. This may be due to convective mass transfer,[117] compressing and dilating at the interface [118] or creating and destroying the interface through the formation and bursting of bubbles [119].

In samples which undergo surface-mediated aggregation in the presence of liquid and vapor phase interfaces, it is suggested that the amount of formed aggregates is proportional to the interfacial area between the protein solution and the air [41]. The processes by which interfacially-driven aggregation occurs is not entirely understood and may vary by protein species and the details of the experimental parameters. It is thought that surface-mediated aggregation is driven by interaction of the hydrophobic surface between air and water and the hydrophobic patches exposed during adsorption to the interface. Aggregates may form at the surface or as the misfolded proteins desorb from the surface and recombine into the bulk of the protein solution [72]. However the aggregation occurs, protein interactions at bulk interfaces are implicated in many aggregation studies [41].

While strained samples produce more fibrils, the application of large strains serves to fragment the developing fibrils and inhibit development of nuclei at the air/water interface due to overstretching of the protein at the extremities of the volume being sheared. Use of larger or smaller strains during the denaturing protocol results in creation of networks with different fibril densities and morphologies as well as fibril networks with different characteristics. In fact, the fibril characteristics vary with their positioning within the shear strain profile on the parallel plate.

Large applied strains result in the largest deformations on the outer part of the rheometer plate. The strain profile is varied as one moves in from this outer position – the proteins at the outer edge of the plate are being deformed by the full amount, but proteins which are positioned further in

toward the center of the plate experience a smaller deformation and are stretched less (Figure 10). A protein located at position d1 in Figure 10 would feel much less deformation and stretching than a protein located at position d2. Moreover, it is hypothesized that there is a critical distance from the central point of the plate past which proteins are exposed to extreme deformation and overstretching resulting in fragmentation of proteins and inhibition of aggregation which is observed in highly strained samples illustrated in figure 10 by the dotted line. Varying the applied strain may change where the critical diameter is, with high strains resulting in a larger annulus at the edge of the plate in which proteins are overstretched and low applied strains resulting in a smaller annulus and a smaller number of overstretched proteins. This would help to explain the variation in the number of protein fibrils which are apparent in aged samples exposed to varying applied strain during denaturing.

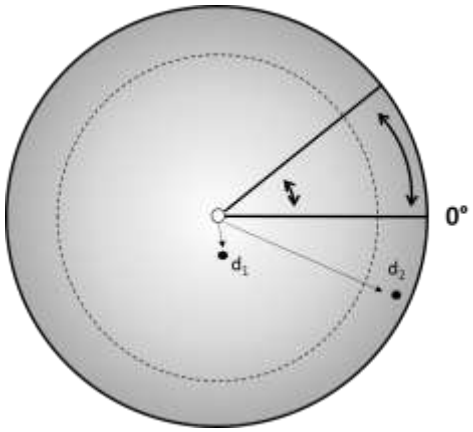

Figure 10. Illustration of magnitude of deformation of proteins on the parallel plate and regions of overstretching determined by applied strain.

As a result of placement on the rheometer plate and within the shear field, individual proteins, nuclei and fibrils fell varying amounts of deformation and stretching. In order to investigate the

effect of placement on the plate and within the shear field on the fibril and network morphology, samples were prepared according to the protocol but instead of removing the protein solution from the rheometer plate after denaturing, samples from the solution was removed directly from the plate onto TEM grids. In this way, grids were produced which are representative of specific locations within the shear field.

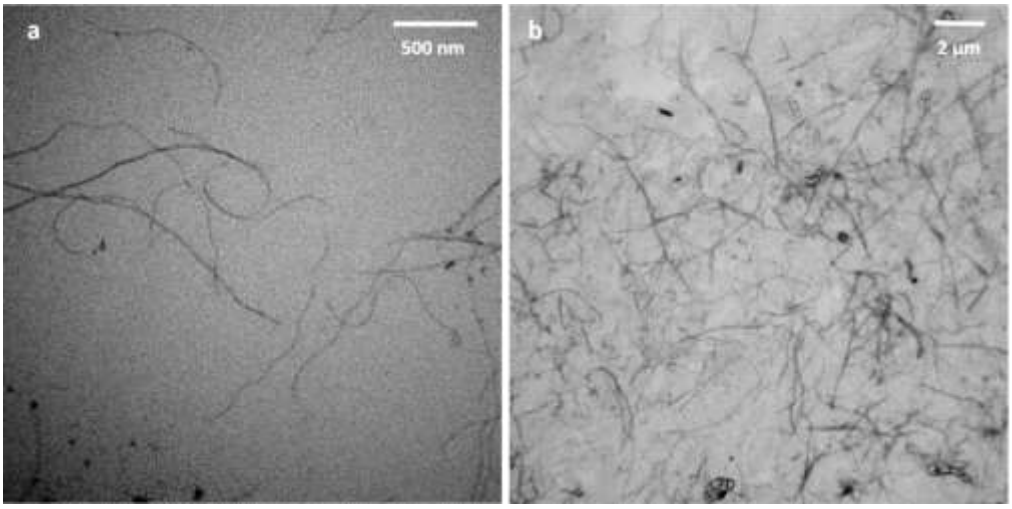

Figure 11. Fibril morphology changes with the shear field proteins are exposed to due to positioning a) center of plate, lower magnitude of deformation b) edge of plate, larger deformation

Figure 11 shows representative TEM images from the center and the edge of the plate. Proteins in the center of the plate experience a lower magnitude of stretching than proteins on the edge of the plate. In addition, there is less opportunity for nucleation events due to distance from the air/water interface. It is likely that nucleation continues to occur in the center of the plate due to thermal denaturing events, the presence of nucleating surfaces on the plate and as artifacts within the solution and by diffusion of nuclei from the edges to the center of the plate. However, nucleation in the center is limited when compared to formation of nuclei at the edges of the plate. The figure

illustrates the difference in number of fibrils produced after the straining and heating protocol and a limited period of incubation in the center of the plate (11a) and the edge of the plate (11b).

In addition to variation in the number of nuclei and fibrils produced, there are additional differences observed in the morphology of produced fibrils. Samples which are retrieved and imaged from the center of the plate where there is less deformation contain fibrils which are longer, more curved and form more complex aggregate structures with other fibrils. Images of fibrils which are sampled from the high-deformation edges of the plate show more fibrils which are shorter and more angular. The average length of fibrils retrieved from the center of the plate following denaturing and a 30 minute incubation period is 1250 ± 200 nm while protein aggregates retrieved from the edges are shorter with an average length of 825 ± 200 nm. Stretching makes percolation of denatured proteins through the growing nuclei and fibrils more difficult and may interfere with the attachment of these proteins to the ends of fibrils resulting in shorter fibrils and fibril fragments.

The variation of produced fibril morphologies across the deformation profile of the parallel plate is important to take into account. The method that we have developed for producing insulin fibrils with heating and deformation results in a non-uniform application of strain across the volume of the sample. However, in the subsequent removal of the sample and mixing of the regions within the sample the protein morphologies are homogenized into a single solution and allowed to continue growth overnight. The creation of fibrils with different morphologies due to the strain field may be of interest in specific applications of the fibrils. We focus here on the growth of a large number of fibrils rather than a specific morphology.

2.4.5 Network characteristics

Network morphology has a profound effect on other network characteristics including network rheology properties, solute diffusion and the nature of entanglements in the network [70]. The network structure created by the fibrils was quantified using areal fraction calculations as well as node-counting to determine connectivity of the fibrils in the network. The connectivity of the network was determined by a nodal count method by which the number of protein spokes which come together at each node in a TEM image of known magnification and size are counted [120]. The minimum number of spokes which can constitute a node are 3, so the higher the average number of spokes per node is above 3, the more connected the structure is. Additionally, the number of identified nodes in the TEM image give another indication of connectivity and the number and length of proteins available in the structure. This type of analysis gives information which is useful in comparing networks and could be used in determining the network reproducibility and performance for a specific usage like an electrode. Area fraction calculations were also conducted from TEM images to determine the fibril density in the network. In these calculations the percent of the TEM image which is covered by fibrils is determined using stereology methods [109, 121]. The area fraction and the average number of spokes at each node are compared in figure 12.

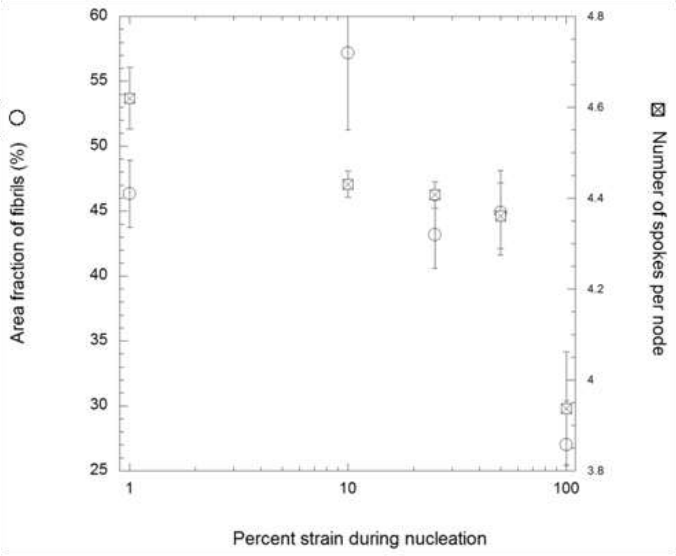

Figure 12. Quantitative analysis of network structures formed as a function of applied strain during nucleation protocol.

The density of the fibrillar networks and the connectivity are both influenced by applied strain during nucleation and early growth. We see a clear distinction between the areal fraction and node count results for applied strains of 50% and below and the samples which are produced with 100% strain. We see similar distinctions in the network morphologies observed by TEM. This suggests that there is an optimum amount of applied deformation which results in protein stretching, fragmentation, optimal orientation and disruption of the air/water interface to promote the formation of nuclei. At deformations which are too high, the overstretching and large disruptions of the air/water interface are fracturing fibrils and disrupting formation of nuclei and growth. Based on the results of network analysis and areal fraction calculations, it seems that this divide occurs at 100% applied strain, when too large an amount of the parallel plate surface is being overstretched.

The connectivity of the network is approximately 4.4 – 4.6 spokes per node for strains ranging from 1% to 50%. With 100% applied strain, the average number of spokes per node decreases to less than 4. The density of the network as measured by area fraction also decreases between low applied strains and 100% strain. At strains from 1% to 50% the area fraction ranges from 45 – 55% fibril coverage but at 100% applied strain it falls to less than 30%. The isolated fibrils and lack of network structure observed in unstrained samples render a fibril network density moot. Only samples exposed to the combined heating and shearing protocol reliably resulted in a dense network structure.

2.5 Discussion

Our results show that a protocol of combined heating and deformation of insulin solution leads to the robust production of protein fibril structures. The application of large or small amounts of deformation as controlled by the amount of strain applied to the system results in variations in the fibril morphologies produced as well as 2-D network characteristics. TEM results show a higher network density and connectivity are achieved with low applied strain as opposed to high strain procedures. It is commonly held that strain increases the nucleation of protofibrils, likely by distorting the stable protein structure and extending the protein backbone [98, 122]. The presence of shear serves to align the proteins preferentially such that aggregation is enhanced [90, 94, 98]. Shear has also been reported to contribute to fibril fracture [98], which may result in broken fibrils acting as nucleation sites for more fibrils. The preferential orientation and deformation of proteins has been observed by others in sheared conditions [90, 98]. Lowered fibril density as well as connectivity measurements at 100% strain are in agreement with reports that higher strain hinders fibril

formation, as the protein cannot perform the reorganization required to form stable fibrillar structures in the presence of large deformations. The results presented here using heat and deformation are consistent with prior reports of shear-dependent fibril formation in amyloid fibrillar networks [90, 93, 123]. Comparing between the strained and non-strained samples, deformation during heating increases the number of nucleated fibrils which leads to strain-dependent characteristics observed in the TEM samples of networks formed over 24 hours after the strain and heat protocol.

The presence of strain leads to the rapid creation of fibrillar networks. A short 15 minute exposure to combined heating and deformation followed by incubation at room temperature leads to the creation of dense networks of fibrils which might be used for a variety of technological purposes. Nielsen *et al* have shown using ThT fluorescence that fibrils form in the absence of agitation after approximately 1 hour at 60°C in moderately concentrated insulin solutions like our own. Fibrils were alternatively observed by ThT fluorescence to form within 2 hours by their agitation protocol of vigorous shaking at 960 rpm at 37°C [13]. It is difficult to make an absolutely direct comparison as our solution formulations are subtly different. But doing this kinetic comparison to our own evaluations, we find that a shorter period of 15 minutes at elevated temperature combined with strain is sufficient to trigger the fibril formation. That period is shorter than what is required for either the continuous elevated temperature exposure or shaking agitation strain exposure shown by Nielsen. It is also possible that the strain condition imposed by the rheometer could be more controlled than the more chaotic turbulent flow induced by shaking. Similarly, Webster *et al* have shown that the aggregation of insulin is speeded by applied strain in Couette flow in solution, observing the onset of fibrillation within 10 minutes by Raman spectroscopy [99].

The use of combined heat and deformation through shearing in our work here results in the formation of a network structure when allowed to continue growth overnight in ambient and quiescent conditions. The density of the network has been observed to increase with the application of heat and deformation during denaturing. The application of strain during denaturing results in a solution of higher complex viscosity than solutions which are heated by not strained during denaturing. With low applied strain, the final complex viscosity of bulk protein solutions is higher than for samples with larger deformations due to higher strain. The complex viscosity associated with the bulk solution is in large part due to the volume fraction of fibrils present, but also due to the entanglement of the existing fibrils. Large amounts of applied strain may orient the fibrils in such a way so as to diminish the entanglement of the fibrils hence reducing entanglements and leading to a rise in complex viscosity consistent with the work by Loveday *et al* using solutions of β-lactoglobulin [50].

At low applied strain, fibrils formed denser networks. The change from a static denaturing method using only heat to denaturing with applied strains as low as 1% causes dramatic differences in network formation. Strain between 1% and 50% appear to produce similar network characteristics based on TEM images, connectivity and area fraction calculations, while increasing the strain to 100% causes the density of the formed networks to drop off. These highly strained samples are approaching a regime where the formation of mature fibrils is inhibited by overstretching. The dense networks formed by application of 1 50% strain are likely the confluence of destabilization, preferential alignment and fibril breakage contributing to enhanced nucleation as well as formation of mature fibrils in solution [90, 93, 95, 101]. The influence of strain allows us a mechanism by which to tune the density of the formed network in a limited way.

The magnitude of rotation and size of the parallel plate rheometer disc may bias the test towards observation of apparent compression/dilation effects possibly exaggerating the impact of the air/water interface on the nucleation and formation of fibrils. Small applied strains result in minute oscillations of the disc which although small still create a turbulent flow due to the oscillatory nature of the applied strain and seem to lead to a clear effect in the fibril density after incubation which is likely due to increased nucleation.

2.6 Chapter conclusions

Controlled deformation during the nucleation and initial growth stages can regulate the density of formed fibrils and the resulting network structure. These results show that the presence of varying amounts of deformation during the nucleation phase causes significant differences in the morphology and density of fibrils produced, which are different from fibril morphologies present when nucleation and growth occur without shear. With any controlled oscillatory shear, a dense network of overlapping fibrils can be produced depending on the amount of strain.

We show that low strain results in denser networks, as quantified by both area fraction and node connectivity from TEM images. The density and connectivity of the network can also be related to the amount of strain applied during fibril nucleation with low amounts of deformation (1-50% strain) resulting in dense networks with high connectivity while large deformation (100% strain) causes fibril fracture and inhibits nucleation and growth. The influence of strain on the resulting fibril microstructures is likely due to increased nucleation at the air/water interface as well as increased fibril fragmentation during strain-induced stretching in the outer regions of the plate. The center of the plate has a different shear profile which results in longer and more curved fibril

structures. Removal of the sample from the plate results in mixing of the nuclei, fragments and fibrils such that the solution is somewhat homogenized. The ability to control the microstructure of formed protein networks using strain is likely crucial in producing robust peptide-based hybrid inorganic templates.

Chapter 3.

Platinum-fibril nanowires with large surface area for reduction of 4-Nitrophenol to 4-Aminophenol

This chapter is largely drawn from a manuscript published in MSE C as "Formation of platinum-coated templates of insulin nanowires used in reduction of 4-nitrophenol."

3.1 Chapter Summary

A protocol for metallizing insulin protein fibrils is presented which is used to coat the fibers in platinum creating insulin-templated metallic nanowires. The nanowires are characterized by TEM and other methods. These nanowires have a high surface area and are used as catalytic surfaces for the reduction of 4-nitrophenol to 4-aminophenol by $NaBH_4$ which can be tracked by UV-Vis spectroscopy. Catalytic efficiency in reducing nitrophenol is calculated and reaction constants are extracted for comparison with other works. The method produces robust nanowires which are successful in catalyzing the reaction and are highly efficient compared to other studies of catalytic efficiency of metallic nanowires with regard to this reaction.

3.2 Introduction

The controlled production and subsequent deployment of metallic nanostructures, such as nanowires and nano-networks, offers new pathways to produce more efficient and more active chemical catalysts, electrode materials and sensors. These structures have high aspect ratios, surface/volume ratios and few defects and lattice boundaries [77]. They are often constructed by the reduction or electroless deposition of colloidal suspensions of metal complexes onto polymeric nanofiber precursors [124]. More controlled nanostructure production hinges on the robust production of the polymeric nanofibers onto which these colloids are templated.

Studies have demonstrated using these natural fibril formations as high aspect ratio templates for creating metallic nanowires for use in devices [76, 77, 78, 79, 80, 81, 82]. Previous studies explore the metallic plating of fibrils and characterize the resulting protein-templated nanowires [125]. Preliminary studies integrating these bio-inorganic hybrid structures into working devices are forthcoming [75, 106]. Though protein-based nanowires have been created and individual wires have been characterized, the range of network structures and characteristics available by tuning of the fibril-forming parameters has not been fully investigated.

Ultrathin nanowires have been synthesized in a variety of ways, including on carbon black nanotubes [126], DNA [64], yeast derivatives [127] and more recently through amyloid protein templating [76, 77, 78, 79, 80, 81, 82, 105]. Amyloid proteins reliably form thin and long fibrils in specific environmental conditions [14, 19, 128] including high temperature [13, 53, 83, 85], altered pH [8, 13, 16, 84, 129], elevated pressure [53, 86] and the presence of salts or urea [13, 88, 95, 96, 97, 130]. Agitation [36, 97, 131], shear [90, 91, 94, 95, 96, 104] or the presence of other surface modulators can also affect the amyloid fibril structure and raise the aggregation rate, though the mechanisms of influence are not well understood. The effects of shear

and agitation on protein aggregation are highly debated. Some studies attribute aggregation of proteins not only to shear forces but rather to the effects of surface-liquid interactions of proteins resulting from various methods of agitation and shear [117, 132, 133, 134, 135]. Other studies have shown shear and agitation to effectively induce aggregation in proteins which are prone to fibrillation, including β-lactoglobulin [90, 91], glucagon protein [92], amyloid-β [93, 94] and insulin [13, 95, 96, 97]. It is thought that shear in polymer and protein solutions can orient the macromolecules in the direction of shear and that the driving force for orientation can be enough to favor misfolded chain conformations and aggregation.

Insulin amyloid fibrils have been used extensively in templating of nanowires and nanowire networks, though α-synuclein has also been used by Padalkar *et al* to create Cd and Pb nanowires [82]. Insulin fibrils are highly stable after formation and amino acids expressed on the insulin fibril can interact with inorganic substrates, making the amyloid precipitates ideal for the subsequent templating. The produced metallic nanowires can be integrated into sensors, high surface area electrodes or used as a catalytic surface to facilitate reactions, such as converting 4-nitrophenol (4-NP) to 4-aminophenol (4-AP). 4-NP is used in producing pharmaceuticals, fungicides, insecticides and rubbers and is found as a residue associated with explosives production and testing. 4-NP is relatively toxic with a low LD_{50} level, and its conversion to 4-AP yields a product that is less lethal to surrounding species and potentially more biodegradable in the environment. 4-AP is also used in the production of pharmaceuticals, corrosion inhibitors and anticorrosion lubricants [136]. The reduction of 4-NP by $NaBH_4$ in the presence of noble metal nanoparticles as catalysts is efficient in producing 4-AP [137, 138]. Thus, the catalytic reduction of 4-NP with an excess of $NaBH_4$ was used as a model system to evaluate the catalytic activity of the platinum coated (Pt-coated) insulin fibers.

The production of insulin fibers and their use as templates to form Pt-coated catalyst nanowires for conversion of 4-NP to 4-AP is documented here. We also present our determination of amyloid attributes arising from the controlled formation experiments. The influence of fibril morphology on the produced nanowires and their catalytic response is also reported on, as is the effect of temperature during 4-NP conversion. If the morphologies of nanostructured materials are more controlled these templated materials might be more effective catalysts.

3.3 Materials and Methods

Preparation of Insulin Solution: Insulin solutions were prepared by dissolving the appropriate amount of lyophilized porcine insulin (Sigma Aldrich) in a 0.01 M HCl solution (pH 2) for a final concentration of 5 mg/ml. The solution is briefly mixed and stored at 4°C. Samples are used within 24 hours of preparation to minimize degradation.

Fibril Production: Insulin fibrils were produced using a combined heating and straining protocol described in chapter 2. Briefly, a TA ARES Series oscillatory rheometer with 25 mm parallel plates was used to heat and strain aliquots of insulin. The parallel plate geometry creates a direct relationship between the deformation and strain in the sample and allows for easy sample extraction post-processing for metallizing.

All experiments were conducted with a working gap size of 0.5 ± 0.1 mm. Samples are loaded at room temperature followed by heating to 65°C at a controlled ramp rate of 10°C/min with applied strain of 1%, 10% or 100% and 10 rad/s frequency for 15 minutes to create different network structure morphologies. Strain is expressed as a dimensionless percentage defined as the ratio between the applied rotational displacement and the gap described by the equation:

$$strain = \frac{deformation}{gap\ size} \quad \text{(eq. 3.1)}$$

Following heating and straining, the insulin solution was stored at room temperature for 24 hours before metallizing.

A subset of unstrained fibrils were produced for comparison. These include fibrils that were heated without strain using the same heating protocols and for the same length of time and fibrils that were made by seeding an aliquot of non-aggregated insulin solution with a small amount of strained fibrils (1% strain). Both of these fibril solutions were stored at room temperature and otherwise treated according to the same metallizing protocols as the strained fibrils.

Metallizing Protocol: Fibrils were metallized using a method adapted from Zhang *et al* [77]. The protein solution was diluted to its final concentration of 0.2 mM and mixed with 2.5 mM aged Pt(IV)Cl salts in a 1:5 molar ratio and stirred using a magnetic stir bar for 24 hours. The platinum-fibril solution is then reduced by adding cold $NaBH_4$ dropwise to the chilled solution with 40 µL added every 5 minutes to achieve a final $NaBH_4$ concentration of 2.5 µM. The solution is chilled and mixed for 12 hours before testing.

UV-Vis Spectroscopy Probing of Catalytic Activity: The catalytic activity of the Pt-coated fibrils was measured by tracking the catalysis of 4-NP to 4-AP by the presence of Pt-coated fibrils and an excess of $NaBH_4$ based on work by Chang *et al* [125]. The transformation of 4-AP from 4-NP, illustrated in Figure 1, occurs by electron transfer on the catalytic surface of the Pt- coated fibril using $NaBH_4$. It should be noted that this is a heterogeneous mixture with additional ions present in the solution.

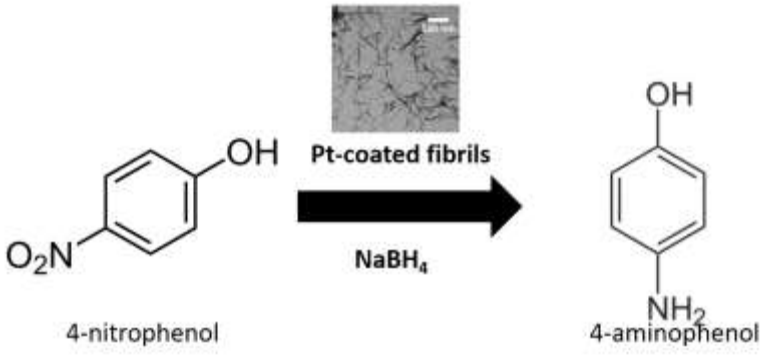

Figure 13. Schematic illustrating the reduction of 4-nitrophenol to 4-aminophenol by Pt-coated fibrils in an excess of $NaBH_4$.

The formation of 4-AP from 4-NP can be easily tracked using UV-Visible absorption spectroscopy. Cuvettes were prepared from 1.5 mL ultrapure H_2O and 250 µL of 4-NP mixed with $NaBH_4$ (1.5 4-NP:1 $NaBH_4$). UV-Vis spectra were obtained from a Cary Bio UV-Vis Spectrometer using fast collection time from 500 nm to 250 nm wavelengths with automatic background subtraction using a cuvette filled with water. After an initial spectrum was obtained of the cuvette containing 4-NP and $NaBH_4$, an aliquot of Pt-coated fibrils was added and another spectrum was immediately taken to capture the immediate response with subsequent spectra collected every 10 seconds to observe the transformation. In most cases, the spectra were taken until the reaction was complete, though in some cases where a minimum concentration of added Pt-coated fibrils was not met, the reaction failed to complete within the experimental time scale. A color change was observed from yellow to clear by adding Pt-coated fibrils and subsequent conversion of 4-NP to 4-AP. Unless otherwise noted in the text, the final concentration of Pt-coated fibrils added to the cuvette was less than 12 nM.

Additional dynamic UV-Vis spectroscopy was conducted in order to understand the kinetics of the catalysis using only platinum nanoparticles. The nanoparticles were diluted to the same concentration that they are present in the coated-fibril samples and incubated with $NaBH_4$ for 12 hours in the same way as for the fibrillar samples. The nanoparticle solution was added to the cuvettes containing 4-NP and $NaBH_4$ and spectra were taken using the same protocol as for catalysis using Pt-coated fibrils.

Experiments designed to determine any thermal retardation on the kinetics of conversion were conducted using cuvettes of 4-NP and $NaBH_4$ solution which were chilled in a controlled water or ice bath to temperatures of 7°C, 15°C and 20°C. Pt-coated fibril solutions were also equilibrated at the temperature before addition to the cuvette and UV-Vis tracking.

TEM Sample Preparation and Imaging: To quantify observational differences between fibrils and networks formed at different conditions, aggregated samples were also analyzed by TEM. Samples for imaging were prepared by drop casting 5 μl of solution onto carbon-coated copper TEM grids immediately following glow discharge treatment. Excess liquid is wicked away after 2 minutes to allow sufficient sample adsorption and the TEM grids are rinsed three times in distilled ultrapure water (Sigma Aldrich). This is followed by negative staining using 1% uranyl acetate stain (Sigma Aldrich). Excess stain is wicked away after 1 minute followed by imaging. Metallized fibrils were imaged without staining. Imaging was conducted with a Philips CM-100 TEM and multiple areas of the sample were viewed in order to ensure observations were representative of the entire sample. TEM grids of strained protein networks were created from two separately prepared insulin solutions and each TEM session captured images from multiple networked areas on the grid.

3.4 Results

3.4.1 Formation of insulin fibrils with deformation

Formation of insulin fibrils was reliably accomplished using the combined heat and deformation protocol. Varying the amount of oscillatory strain induced during the denaturing and nucleation phase resulted in different morphologies of insulin fibrils and network characteristics as observed by TEM as described in chapter 2. The presence of any deformation resulted in more fibrils than samples which were quiescently heated without stretching. The fibrils produced with heat and deformation were also shorter and straighter than fibrils which result from heating alone. Low amounts of deformation during initial denaturing produced many fibrils which are packed into dense networks. More deformation produced fewer fibrils with more space between them (Figure 14 a, b). Coating the fibrils with platinum did not significantly alter the observed fibril and network morphologies, although the fibrils were diluted in the coating process and there is some evidence of minimal fibril breakage as a result of the coating process (Figure 14 c, d).

Deforming the proteins during the initial aggregation has been studied by others and has been shown to often result in accelerated aggregation and fibril formation. Though the method of shearing in other studies is not always well-defined, studies such as that by Humblet-Hua *et al* and Akkermans *et al* have linked the dependence of fibril formation to the amount of strain present [100, 102]. Low amounts of added shear have accelerated fibril growth, with increasing shear producing shorter and more rod-like fibrils. Too much shear results in depleted fibril formation, likely due to fibril breakup. Akkermans *et al* further found that the duration of shear was less important to the fibril aggregation than the onset of strain which they describe as similar to a nucleation event [100].

The oscillatory strain on the heated proteins provided by the rheometer stretches the proteins and acts as a series of nucleation pulses such that aggregation is accelerated.

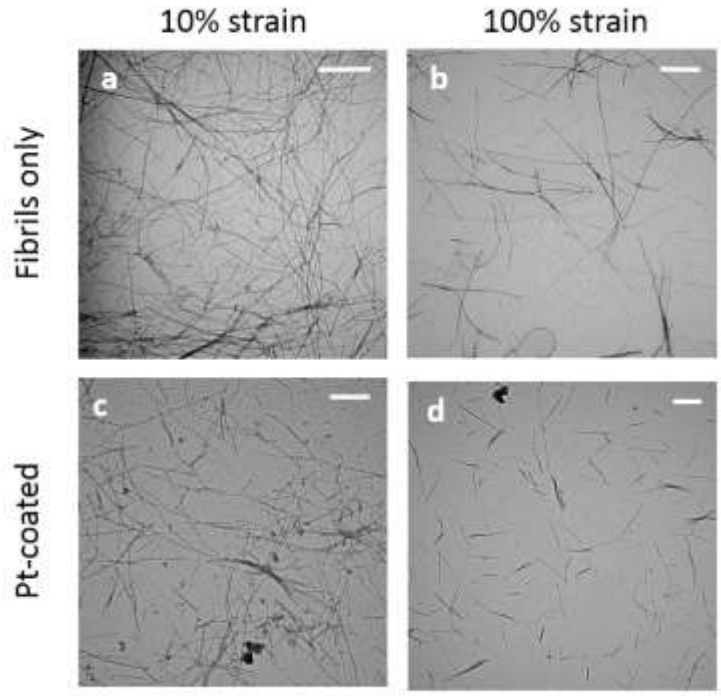

Figure 14. Insulin fibrils produced with heat and strain. a) Fibrils produced with 10% strain b) Pt-metallized 10% strain fibrils imaged without negative staining agent c) Fibrils produced with 100% strain d) Pt-metallized 100% strain fibrils. Scale bar = 500 nm.

3.4.2 Characterization of metallized fibrils

Fibrils metallized with platinum could be imaged in the TEM as produced. The platinum coats the entire length of the fibril and the network characteristics observed in TEM images of the uncoated fibrils largely remain (Figure 14 c, d). The width of the produced insulin fibrils are invariant with strain during the initial aggregation phases, but coating the fibrils with platinum results in an

increased width of 7-12 nm due to 3.5-6 nm coating by platinum on each side (Figure 15 a, b). The width of Pt-coated fibrils does not change with rinsing, indicating that the Pt-coating is well adhered to the insulin fibril. It is possible that longer exposures to the platinum solution or exposure to solutions of larger concentration may result in thicker platinum coating. The corresponding EDS of the Pt-coated fibrils is shown in Figure 3c with peaks corresponding to the fibrils (oxygen, carbon), sample substrate (aluminum) and Pt-coating (platinum).

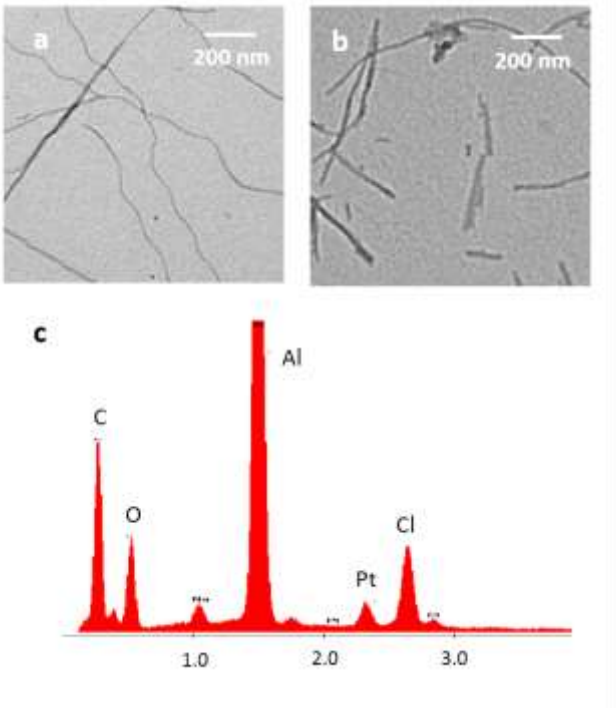

Figure 15. Magnified images of insulin fibrils a) before platinum coating and b) after coating, c) EDS of the prepared Pt-coated insulin fibrils.

It is expected that the platinum is initially associated with the insulin fibril due to strong attraction between the negatively charged platinum ions and the insulin fibril which is positively charged in the pH 2 aqueous HCl environment due to protonation of the amino acid residues.[78] Chlorine ions

may associate with the positively charged fibrils as counter ions which may then be exchanged with other ions such as platinum when the inorganic platinum complex is introduced to the solution.[78] The platinum is then further reduced onto the fibril with $NaBH_4$. It is unlikely that platinum would be dislodged or replaced via ion exchange by the introduction of other ions such as zinc, despite the strong affinity between insulin and zinc under physiological conditions. Zinc is far more electropositive than platinum and the potential for ion exchange is nonexistent. It is because of this that platinum has been used in this study and that other studies incorporate other stable noble metals as they have no native oxide.[139]

3.4.3 Catalytic efficiency of produced Pt-coated fibrils

The catalytic activity of the Pt-coated fibrils was determined by converting 4-NP solutions to 4-AP and tracking the reaction kinetics. The conversion of 4-NP was chosen as a model system as conversion occurs rapidly and can be easily characterized by methods such as UV-Vis spectroscopy [140, 141, 142, 143]. The UV-Vis absorption spectra for 4-nitrophenol in a solution of $NaBH_4$ includes one peak at 400 nm, while that of its derivative, 4-AP has a peak at 300 nm (Figure 16 a). Figure 3a illustrates the difference between the spectra before and after 4-NP conversion to 4-AP using both platinum-based nanoparticles and platinum-coated fibril nanowires. The 4-AP absorption peak is higher when the conversion occurs in the presence of platinum-coated nanowires rather than nanoparticles due to the increased cloudiness of the solution containing both reduced platinum and protein fibrils. In addition there is an additional bump in the lower wavelengths near the 4-AP peak for the absorption spectra following reduction with Pt-coated fibrils due to the absorption signature of the fibrils themselves which occurs at the low wavelengths around 260-270 nm.

The kinetics of the reaction were tracked by capturing absorption spectra every 10 seconds during conversion with the first spectra captured within 10 seconds of the addition of platinum coated fibrils as catalytic surfaces (Figure 16b). The peak associated with 4-AP (noted as 1 in Figure 16b) increases with time as the 4-NP peak (noted as 2) decreases. The activity was found to vary with the concentration of added fibrils, as to be expected as higher concentration leads to more catalyst surface.

The use of Pt-coated fibrils in the catalysis was similar in efficiency to the use of platinum nanoparticles. The rate of reaction was similar, though the absorption spectra associated with the fibrils make the final spectra slightly different from the nanoparticle only spectra (figure 16a). We observe an asymmetry to the absorption spectrum for the protein aggregates perhaps due to the larger distribution in size.

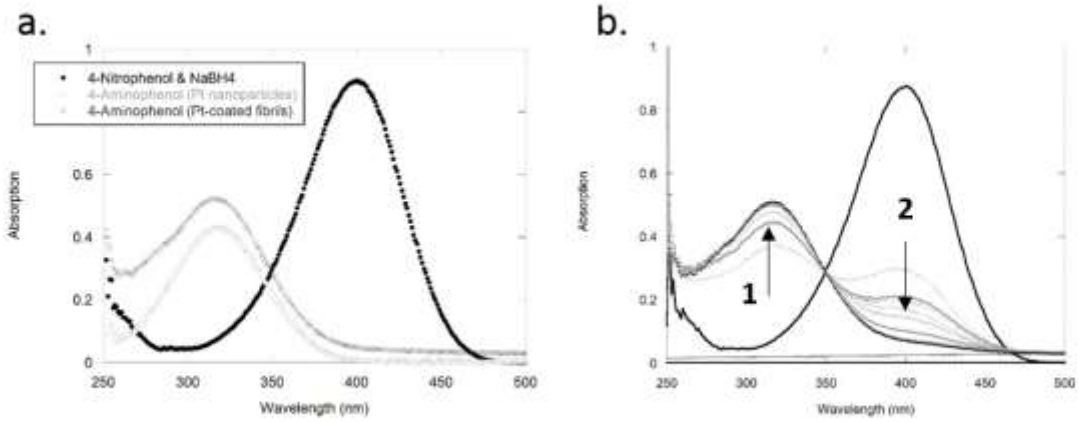

Figure 16. a) UV-Vis absorption spectra for reduction by platinum nanoparticles or Pt-fibrils, b) UV-Vis tracking of reaction.

3.4.4 Extraction of reaction constants

Focusing on the peak absorption wavelengths, the ratio of the height of the 4-NP peak at 400 nm at time *t* (A_t) compared to the initial peak height before adding catalyst to the solution (A_0) can be used to track the reduction of 4-NP. This ratio of the absorption peak height A_t/A_0 is taken to be equivalent to the relative concentration of 4-NP in the solution at a given time C_t/C_0. The use of this ratio allows for comparison between the relative rates of reduction and also allows for the extraction of reaction rate constants for comparison between various test parameters.

The catalysis of 4-NP by Pt-coated fibrils in the presence of $NaBH_4$ requires adsorption of 4-NP onto the catalytic surface. Such surface mediated reactions can be described by the Langmuir-Hinshelwood kinetic model:

$$r_0 = \frac{dC}{dt} = k\frac{K_F S_t C}{1+K_F C} \qquad \text{(eq. 3.2)}$$

Where r_0 is the reaction rate of the 4-nitrophenol reduction, C is the concentration of 4-NP in the solution, k is the limiting-step reaction constant under the given conditions, S_t is the total number of available reaction sites and K_F is the adsorption coefficient of 4-NP. In this case, with a low concentration of 4-NP and an excess of $NaBH_4$, the reaction equation can be simplified to pseudo-first-order kinetics [144]:

$$\ln\left(\frac{A_t}{A_0}\right) = \ln\left(\frac{C_t}{C_0}\right) = -k_{app}\, t \qquad \text{(eq. 3.3)}$$

In pseudo-first-order reactions, a reaction constant k_{app} can be extracted from the linear relationship between ln (Ct/C_0) and time *t* (figure 17).

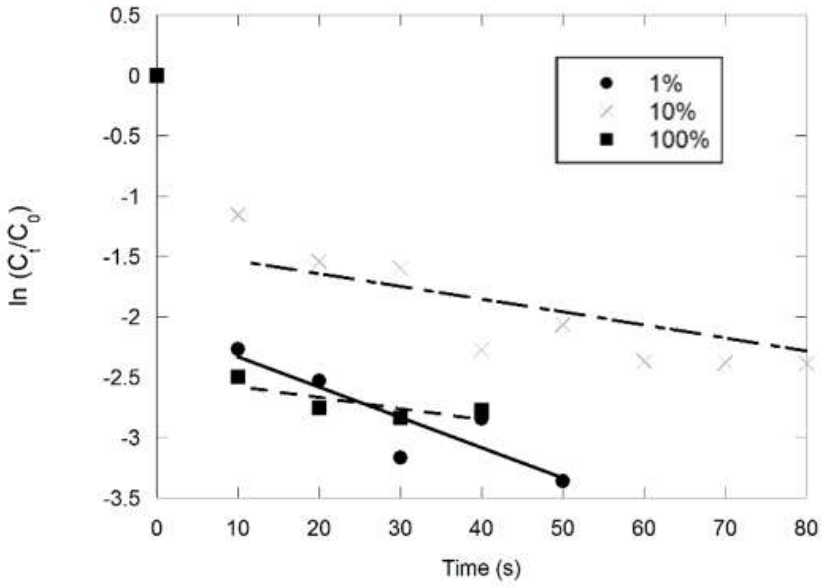

Figure 17. Extraction of reaction constant k_{app}.

In this case the reduction of 4-nitrophenol by Pt-coated fibrils in an excess of $NaBH_4$ results in a linear region which begins with the second spectra taken or at about 20 seconds after the beginning of the reaction. The immediate reduction in 4-NP absorption peak following the addition of the platinum-coated fibrils is due to the initial filling of the reaction sites on the fibrils and the first reactions that result. Following the filling of the reaction sites, the reaction becomes rate limited by the requirements that reacted 4-AP must desorb from the fibril surfaces before unreacted 4-NP can move into place, absorb on the surface sites and react. Thus, the initial reduction in 4-NP which occurs in the first 20 seconds is not included in the calculation of the reaction constant. This initial reaction rate is commonly observed in the literature but the steady-state reaction constant is reported. The extracted rate constant k_{app} is described in Table 2.

Table 2. Rate constants for varying fibril morphologies at 20 C.

Aggregation protocol	k_{app} (s^{-1})
Heat only	0.003 ± 0.002
Seeded with 1% strain nuclei	0.006 ± 0.003
1% strain	0.03 ± 0.01
10% strain	0.01 ± 0.002
100% strain	0.009 ± 0.006

The amount of added Pt-coated fibrils strongly impacted the rate of the reaction. The catalysis of 4-NP to 4-AP could be tracked visually, as well as by UV-Vis spectroscopy, as the initial 4-NP solution is yellow and clarifies with continued reaction. Additions of Pt-coated fibrils which totaled 5 nM concentration or less led to incomplete conversion over the time scale of the experiment. The addition of fibrils or nanoparticles to achieve slightly higher concentrations lead to the slow completion of the reaction with local catalysis occurring as a reaction front where the fibrils were dropped in and then further catalysis as the fibrils are dissipated throughout the solution by natural convection. This type of catalysis resulted in UV-Vis results showing fluctuations in the height of the 4-NP peak, with an initial decrease in the peak followed by an increase toward the initial height. The reaction eventually reached completion on a slow time scale, though this depends on the added concentration of coated fibrils. Additions of Pt-coated fibrils to achieve concentrations of 10 nM or more resulted in complete conversion of 4-NP to 4-AP over the course of 5 minutes or less.

The reaction was considerably slower using Pt-coated fibrils formed without induced strain. Metallized fibrils which had been created by use of heat only or through seeding with strained

nuclei succeeded in conversion of 4-NP but at a much slower rate than strained Pt-coated fibrils. This is not unexpected, as smaller numbers of fibrils are observed in TEM samples of fibrils created without strain or agitation. Fewer fibrils will result in a smaller number of available catalytic surface sites compared with solutions with a larger number of fibrils.

The effect of temperature on the reaction kinetics was tested by chilling the cuvettes of 4-NP solution as well as the metallized fibril solutions until they achieved a uniform temperature. The temperatures tested were 7°C, 15°C and 20°C. It was expected that lowering the temperature of the solution would retard the reaction. Though there were slight variations in the rates of conversion at temperatures below ambient, the kinetic differences are not statistically significant. The apparent rate constants associated with the different temperatures for a single fibril morphology are listed in Table 4. We found no other thermal kinetics studies of 4-NP reduction by metallic protein-based nanowire in the literature.

3.5 Discussion

The use of metal-coated protein fibrils as catalytic surfaces to speed reactions is based on the supposition that the amyloid fibrils are produced with large surface to volume ratios which, after metallization, allow for more reaction sites which is favorable for reaction kinetics. Additionally, the metal-coated fibrils might withstand aggregation, a problem in colloidal solutions of nanoparticles alone. Based on the greater surface area available, it was expected that given the ability to produce different morphologies of fibrils, protein-based nanowires could be created which would optimize the catalytic activity and increase reaction kinetics.

The Pt-coated fibrils that were produced successfully catalyzed the reduction of 4-NP to 4-AP with an efficiency equivalent to the catalysis of the reaction using platinum nanoparticles alone. The concentration of Pt-coated fibrils added to the 4-NP solution must overcome a threshold concentration in order to completely reduce the 4-NP to 4-AP within the experimental time of approximately 10 minutes. Though a minimum concentration of catalyst is required for completion within this time frame, catalytic agents are not used up in the reaction and it is expected that even reactions which occur below the minimum concentration would eventually reach completion. Convection of the catalyzing agent throughout the solution allows local catalysis followed by fluctuations in 4-NP concentration due to the mixing of the fibrils through the liquid.

Despite the excess of $NaBH_4$ in the solution, the reduction of 4-NP over time in the presence of Pt-coated fibrils does not show an entirely linear correlation which can be used to extract a single reaction rate constant sometimes expressed as k_{app} as others have reported [125, 144, 145, 146, 147]. Instead, the amount of 4-NP present as measured by the height of the characteristic peak in the absorption spectra reduces dramatically immediately following the addition of the Pt-coated fibrils. Though this sort of initial decrease in 4-NP absorption peak is often encountered and ignored in the literature, it may also indicate that use of a different kinetic fit may produce better results.

For concentrations of added Pt-coated fibrils over 10 nM, the bulk of the reaction occurs quickly with the rate of 4-NP peak reduction in the first 10 seconds amounting to 10-20 times the reduction rate in the following 10 seconds. This rate of this initial reduction in 4-NP is constant regardless of the fibril morphology. The amount of 4-NP present further reduces following this, but at a much slower rate which varies based on the fibril morphology as caused by induced strain during aggregation. The change in rate may be in part due to lack of convection as consumed reactants are effectively blocking the catalytic surfaces from use by unreacted 4-NP.

Table 3. Comparison of kinetic rate constant to similar studies

Support	**Temperature (°C)**	**Metal concentration (M)**	**k_{app} (s^{-1})**	**k_{norm} (s^{-1} m^{-2} L)**	**Reference**
Insulin fibrils (10% strain)	RT	6.4 E -08	0.01	7.22	This work
Pt – nanoparticles (template-free)	RT	3.3 E -6	0.00087	0.057	Jiang
Pt-coated Fe_3O_4 nanowire	RT	9.2 E -7	0.0354	1.83	Jiang
Pt-nanoparticles (template-free)	RT	0.05	0.0038	7.1 E -6	Chang
Pt- coated DAAQNF	RT	0.05	0.01662	1.58 E -4	Chang
Gold nanoparticle chains	RT	0.0068	0.00473	0.6532	Murugadoss

An efficient catalyst is expected to be present in sufficient quantity such that the reaction is rate-limited only by other reaction components. The apparent kinetic rate constants associated with the second regime of slower 4-NP catalysis are similar to rates reported by others using Pt-coated catalyst surfaces for the conversion even with smaller amounts of platinum added to the 4-NP solution in this study (Table 3). When the kinetic rate constant is normalized to reflect the amount of catalytic surface area available, however, our identified rate is significantly higher than others. While our produced fibril morphologies produce higher kinetic constants, the normalized kinetic constant is comparable to that achieved by Jiang *et al* using Pt-coated Fe_3O_4 nanowires [146]. The large kinetic constants with a smaller added amount of platinum overall indicate greater catalytic

efficiency associated with the morphologies produced of the Pt-coated fibrils as opposed to other structures.

Table 4. Rate constants for 1% strain Pt-coated fibrils in varying temperature.

Temperature	k_{app} (s^{-1})
7°C	0.04 ± 0.02
15°C	0.04 ± 0.02
20°C	0.03 ± 0.01

Interestingly, the influence of temperature on the reaction is difficult to observe from the UV-Vis results. Extraction of k_{app} reaction constants associated with the rate of conversion show that variation is within experimental error (Table 4). Any trends are not statistically significant and the system appears to be very robust in that the conversion occurs rapidly despite lowered temperatures (Figure 18).

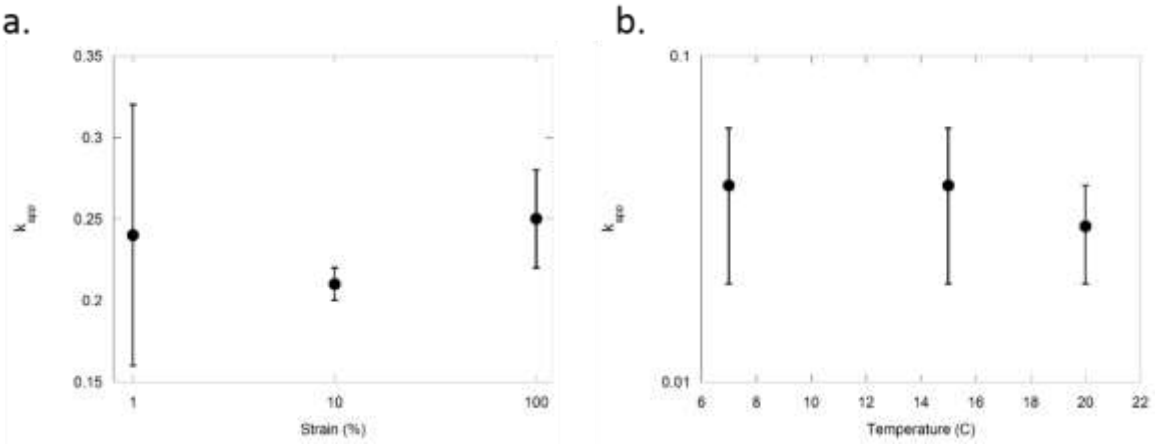

Figure 18. Extracted reaction constant k_{app} variation with a) strain and b) temperature.

The initial reduction of 4-NP which occurs following addition of the metallized-fibrils is dependent on the amount of Pt-coated fibril solution added. Following this initial reaction when the catalyst is added, there is less and less 4-NP to be converted and the surface area available to the 4-NP as a catalytic surface becomes important. Although all solutions of Pt-coated fibrils contain the same amount of insulin protein, the morphological differences result in many short fibrils which were exposed to small amounts of induced strain (1%) or fewer larger fibrils which were exposed to larger strains (100%) during denaturing protocols. The difference in reaction constants for Pt-fibrils of varying morphology is shown to be not statistically significant. This may be due to the addition of an excess of catalyst fibrils such that there is little competition by the 4-NP for access to catalyst surfaces.

The slowest reactions and lowest kinetic rate constants resulted from catalysis carried out with Pt-coated fibrils which were created with heat alone or by seeding insulin solution with fibril nuclei. These nucleation and aggregation protocols result in the longest fibrils, but the fibrils may not be able to easily move through the solution and may be inaccessible to much of the 4-NP for use in

the reduction reaction. It is likely that the length of the fibrils, varied by the impact of strain during early aggregation events, affects the ability of the unreacted 4-NP to access the catalytic surface. Fibrils which are shorter but more numerous may lead to increased ability of unconverted 4-NP to reach the catalytic surface and an increased reaction rate.

3.6 Conclusions

Pt-coated insulin fibrils of various morphologies have been successfully created and used in the converting 4-NP to 4-AP. The amyloid structures produced were observed by TEM and the kinetics of the reaction were tracked using UV-Vis spectrometry. The rate of the reaction depends on the concentration of Pt-coated fibrils added, with a required minimum concentration for reliable completion of the reaction within the experimental time frame. The rate of the reaction was calculated for comparison to other studies and was found to be a pseudo-first order reaction constant rate-limited by the desorption of reacted 4-AP from the catalytic surfaces following filling of the catalytic sites. Fibrils which were created without strain or by seeding with a small amount of strained fibril nuclei showed slower reaction rates. Any effects of temperature or strain-induced morphology on the reaction kinetics were within experimental error.

The use of Pt-coated fibrils to catalyze the nitrophenol reduction is completed within 5 minutes with moderate fibril addition. This is slightly faster than reactions reported by others using protein-based metallic fibrils, but the rate is on the same order. Comparison of kinetic rate constants to other studies shows a higher catalytic activity and faster response associated with the Pt-coated fibril structures. The issues that we experienced related to the local fluctuations in 4-NP content

when small amounts of Pt-coated fibrils were added suggest that some convection during catalysis could aid in creating a more uniform reaction environment.

Conversion of 4-NP to 4-AP by Pt-coated fibril structures in the presence of excess $NaBH_4$ using an amyloid protein precipitation method described here was reliable and robust, as resolved by UV-Vis spectroscopy. Morphological differences in fibrils caused by induced strain was found to impact the catalysis, likely by raising the amount of catalytic surface available and perhaps by increasing convection around the catalyst. More effective control of nanostructured materials and morphologies and their incorporation into devices that can be used for simple catalysis would allow these unique materials to be better utilized.

Chapter 4.

Aggregation kinetics and characterization via sigmoidal equation: Rheology and ThT

Parts of this chapter are from a manuscript published in MSE C as "Agitation of amyloid proteins to speed aggregation measured by ThT fluorescence: A call for standardization."

4.1 Chapter Summary

Rheology can be used not only to trigger denaturing and nucleation events, but also to track the aggregation of proteins in the bulk solution. As proteins unfold and begin to self-assemble during heating and shearing, the bulk solution undergoes a corresponding rise in viscosity which can be measured. By fitting a kinetic equation to the curve associated with the changing bulk complex viscosity over time, kinetic time constants can be extracted and used in comparing aggregation behavior of samples with different compositions or tests with varying parameters. A sigmoidal equation is used here to extract kinetic time constants for comparison between various rheological tests and is also applied to kinetic analysis of a selection of ThT assays from the literature as an example of its usefulness in quantifying other measures of protein aggregation. A short discussion of recommendations for preparing ThT assay experiments to measure protein aggregation is also presented based on these results and observations of the literature.

4.2 Protein kinetics

4.2.1 Introduction

Protein aggregation kinetics are studied for a variety of reasons and by a variety of experimental apparatus. One of the most commonly used tools for analysis of amyloid aggregation kinetics is the Thioflavin-T assay (ThT assay). Other methods for kinetic analysis of the aggregate formation include FTIR, circular dichroism, DSC, various forms of microscopy and rheology. Each of these methods may have specific characteristics that allow the user to better understand some aspect of the kinetics of aggregation, but each also has limitations.

ThT analysis is often used in detecting aggregation of amyloid proteins in studies to determine aggregate inhibition by small molecules [148, 149]. More rarely, ThT is used to track the kinetics associated with failure to inhibit, or purposeful aggregation of the protein [150]. By binding to β-pleated sheets during denaturation and nucleation, ThT assays track the kinetics of the very beginning stages of aggregation [151, 152]. ThT is widely used in the biochemistry field and is the gold standard for determining aggregation or inhibition [153]. Some issues which have been identified with the use of ThT assays include the hydroxylation of the ThT itself at low pH and interference with protein aggregation [154, 155, 156, 157]. Lack of standard protocols and practices, especially with concern to use of stirring, shaking and agitation are also of concern in ThT studies of protein aggregation behavior and kinetics [158].

Use of microscopy allows the user to better resolve the actual aggregate morphologies which are being created. Unfortunately, in order to visualize most proteins AFM or TEM are required. The protein aggregates which are imaged are typically static rather than continuously changing and it is difficult to resolve the aggregation process. Experiments which set out to understand the kinetics

of aggregation using microscopy must be very well planned in order to create a cohesive picture of the aggregation process. An exemplary experiment in this realm is the work by Jansen *et al* [53]. In this study, Jansen *et al* track the size of aggregates created during heating over time and are able to resolve important aspects of the aggregate process including the addition of protein clusters to the end-caps of the fibrils thus elongating the fibril. The work by Podesta *et al* also uses time-lapse AFM to resolve early events in the aggregation of insulin protein into fibrils [159].

There are few studies which make use of rheology to understand the kinetics associated with protein aggregation [72, 104]. Rheology is able to resolve details related to the bulk properties and behavior of the protein solution. Thus, unlike ThT assays, rheology is typically not capable of detecting initial events in the aggregation process. Rheology is useful in the study of aggregation kinetics in that protein aggregation, in solutions of large enough concentration, leads to a kind of gelation and formation of a 'soft gel' [72]. The accompanying changes in viscosity and storage and loss moduli allow the user to better understand the kinetics associated with the protein interactions and development of structure within the solution. Details related to aggregation can be extracted by use of models and by use of rheology in conjunction with another experimental method.

Here we study the aggregation kinetics by rheology in order to better understand the process that we are exploiting and to determine the relationship between the aggregation kinetics and the resulting aggregate morphology. We also compare the results with literature studies of ThT assays and apply a kinetic model to the literature data to draw conclusions about the protein aggregation as well as typical methods used in ThT assay testing.

4.2.2 Kinetics of aggregation with shear

The impact of agitation and shearing on the kinetics associated with protein denaturing and aggregate nucleation is not entirely clear [96]. Many studies have shown the aggregation rate and resulting aggregate structure to be impacted by the presence of shear or agitation. Others have shown that the parameter which drives aggregate formation is not the agitation or shearing but rather the interactions between proteins at the liquid-air or liquid-solid interface which arise with the application of shear or agitation [117, 132, 133, 134, 135]. A review by Thomas and Geer finds that shear forces alone are unlikely to cause sufficient protein deformation and changes to initiate aggregation, but that interfacial interactions, particularly at liquid/air interfaces created in turbulent agitated and sheared conditions lead to protein interactions and aggregation [160]. Studies of amyloid proteins have demonstrated that the presence of turbulent agitation induces aggregate formation in a variety of proteins, including β-lactoglobulin [90, 91], amyloid-β [93, 94], insulin [13, 95, 96, 97] and glucagon protein, also associated with diabetes management [92].

Shear is thought to accelerate aggregate formation, but exposure to large deformations can lead to the breakup of large aggregate clusters into smaller components [98] or to fibril degradation resulting in shorter fibrils and loss of ThT binding sites [90]. Although several groups have shown that shear alone is sufficient to initiate fibril formation without the presence of heat [50, 90, 95, 99, 100], concerns about the mechanisms responsible for protein unfolding remain [96, 133, 134, 160]. Prolonged exposure to shear can impart energy which can influence the conformation of macromolecular backbones and increase the likelihood of protein association [90, 122] and can lead to preferential orientation that is conducive to aggregation [93, 95, 101]. While studies have shown accelerated aggregation and fibril development with exposure to shear [90, 91, 94, 100, 102], reports have also confirmed that exposure to large deformations may serve to inhibit fibril formation or lead to fibril breakup [91, 98, 102].

Shear-response of proteins is of practical interest. For example, insulin is sheared during cardiovascular transport [103] and during pharmaceutical processing and delivery by manual or automated syringe pump. Thus, experiments exploring the effect of shear and other forms of agitation are necessary and justified. Though many amyloid proteins have been documented to undergo increased aggregation in the presence of shear, the mechanisms of inducing shear protein interactions leading to aggregation are often difficult to exactly replicate.

4.3 Development of kinetic model

Kinetic experiments tracking the aggregation of proteins with respect to time often result in a profile which is sigmoidal in shape. This is true for rheological tracking of the complex viscosity of the bulk protein solution during aggregation as well as for ThT assays which track the development of β-pleated sheets as a measure of aggregation. This sigmoidal shape occurs due to the transition from one phase to another; a low-viscosity protein solution to a higher viscosity solution containing larger protein structures in the case of rheology and from proteins in their natural protein conformations to denatured proteins with β-pleated sheets for ThT assays. Though these two methods of tacking protein aggregation make use of different mechanisms to detect changes in the proteins, they share the sigmoid-shaped profile due to the respective change in protein state that they each measure.

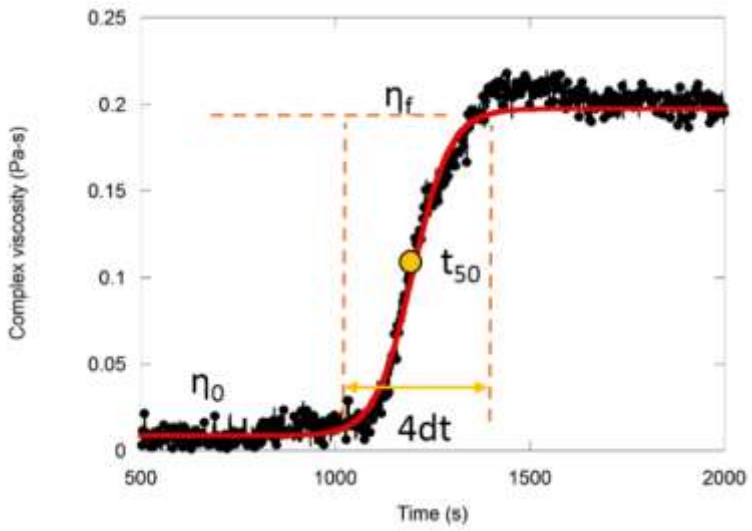

Figure 19. Rheological profile fit with sigmoidal fit to extract kinetic analysis.

The sigmoidal profiles for rheological and ThT assay tests of protein aggregation can be fit with a sigmoidal curve in order to extract kinetic time constants. Such equations have been previously used to quantify kinetics of rapidly polymerizing acrylamide systems [161] and have been employed in protein aggregation studies of insulin under similar fibril-forming conditions by Nielsen *et al* and Sorci *et al* [15, 44]. This technique was especially useful in the analysis of ThT assays in the literature, as methods of quantitatively reporting the kinetics of aggregation extracted from ThT measurements vary greatly across experiments and are sometimes not included at all.

The use of the sigmoidal model to extract time constants associated with aggregation as tracked by increased fluorescence allowed for limited comparison across ThT studies. The range of the kinetic constants extracted from the studies explored in this chapter illustrates the scale of the problem resulting from use of such varied experimental parameters.

The sigmoidal model used to characterize the datasets is described by equation 4.1:

$$P(t) = P_\infty + \frac{P_0 - P_\infty}{(1+e^{k(t-t_{50})})} \quad \text{(eq. 4.1)}$$

Where P_0 and P_∞ represent the baseline fluorescence before aggregate formation and after aggregation, respectively. The two time constants (t_{50} and k) can be used to identify the lag time before the onset of aggregation and the rapidity of the transition from the pre- to post- aggregated states. The time constant, t_{50}, is the time to toggle from the initial to half the fluorescence of the final state of aggregation, and k (units of time^{-1}) is a kinetic time constant related to the inverse of the time to complete the transition beyond the lag time. The pre-aggregation lag time is related to the sigmoidal time constants by equation 4.2:

$$t_{lag} = t_{50} - \frac{2}{k} \quad \text{(eq. 4.2)}$$

Lastly a rate of change can be extracted by using the extracted kinetic constants in order to better compare between the aggregation kinetics of various tests and parametric studies. The rate of change has units which depend on the specific test being conducted (rheological or ThT assay, for example). The rate may be used to compare within one such study to determine the rate at which the change from one protein state to another occurs within the experimental set up. The equation for the calculation of the rate is as follows in equation 4.3:

$$Rate = \frac{k}{4}(P_\infty - P_0) \quad \text{(eq. 4.3)}$$

Here the term aggregation has been used loosely to indicate the change that occurs in the protein solution in response to environmental stimuli, moving the protein from one state to a second state with the exposure of the protein to experimental protocols which cause a measurable change in the protein structure. The experimental protocols in the cases discussed here are intended to cause protein unfolding and the formation of preliminary aggregate structures. In the case of ThT

fluorescence studies, P_0 indicates the baseline of fluorescence detected when the protein is in its native conformation. P_∞ indicates the plateau value of detected fluorescence at which all proteins have been unfolded and formed β-sheet structures. For rheology P_0 indicates the baseline complex viscosity associated with the protein in the bulk solution and the plateau denoted by P_∞ is reached after exposure to denaturing protocols which cause unfolding and aggregation such that an increase in viscosity is detected. In ThT and rheology studies the environmental stimuli designed to cause protein unfolding and self-association are typically heating and agitation, though pH and salt concentrations are also often used.

4.4 Protein kinetics – rheology

4.4.1 Protein rheology

The rheology of proteins in solution is important to understand for applications in pharmaceutical development, tissue engineering, food science, drug delivery and microfluidics [41, 72]. Since proteins undergo shear forces *in vivo* and in pharmaceutical processing and delivery it is equally important to understand the rheological response of protein solutions to shear stresses.

Rheological studies of proteins can be divided into two types of experimental purposes. One focuses on rheological properties of protein solutions for pharmaceutical and biomedical purposes and explore the rheology of a protein solution in its natural or active conformation. Other studies seek to understand the aggregation or gelation of proteins in solution in response to environmental conditions. In these latter tests, the protein behavior varies with pH, temperature, concentration and species. Some proteins form globular aggregates which disperse throughout the solution to

form a gel while others form fibrous aggregates. Some proteins may form both types of aggregates depending on the solution pH in relation to the isoelectric point [72].

Protein rheology allows us to understand the bulk behavior of the protein solution and to draw conclusions about the aggregation of the proteins based on use of models or additional measurements. Pochan *et al* use SANS and cryo-TEM in combination with rheology to better understand the formation of hydrogel networks [70]. In another study, Manno *et al* use rheology and a variety of models to suggest a mechanism for insulin fibrillation in solution [104].

A neat explanation of the molecular mechanism responsible for the increase in viscosity observed with unfolding and aggregation of the protein in solution is developed by Kholodenko *et al* [162] and summarized by Amin *et al* [41]. Briefly, the rise in viscosity can be attributed to the attractive inter-molecular interactions between the proteins during the self-association process. The increased attraction between molecules following unfolding suppresses the mean square displacement of the ensemble average $<r^2(t)>$ that molecules undergo during Brownian diffusion. The reduced value of $<r^2(t)>$ is reflected in the diffusion coefficient:

$$D \approx \frac{\langle r^2(t) \rangle}{\tau} \qquad \text{(eq. 4.4)}$$

Where τ is relaxation time. According to the Stokes-Einstein relationship, $D \times \tau$ must be constant and thus the reduced value of D leads to an increased η of the solution. Though the Stokes-Einstein relationship is intended for use in dilute solutions, the generalized Stokes-Einstein equation has been developed for concentrated systems where the correlation length replaces the hydrodynamic size [162].

The reliance of the viscosity on the size of growing protein clusters in solution has also been developed into a relationship by Lilyestrom *et al* [163]. The relationship between the viscosity of the

solution, η, and the size of clusters, N, is reported to be linear in protein formulations which allow reversible self-assembly of globular protein aggregates. The viscosity is considered to be the ensemble average of the friction coefficient (ζ) experienced by the proteins in the solution during Brownian motion. The force per unit velocity experienced by the soluble protein species scale with the size of the protein clusters N such that a protein of N monomers experiences a frictional force of $N\zeta$ [41, 163]. The understanding of the bulk viscosity of the system as a result of frictional forces between proteins and protein aggregates in solution is instructive. Though the insulin protein aggregates created in this experiment are fibrillar in nature, the clusters of aggregate fragments and the elongating nuclei and fibrils surely contribute to the bulk viscosity. Additionally, there are components of torque and frictional forces which are due to proteins adsorbed to the air/water and solid/water interfaces which add to the bulk viscosity measurement.

One caution regarding the use of rheology to study protein aggregation is that the experiment may impact the outcome due to the inherent requirement of applied shear and existence of an air/water interface in rheological tests. It has been shown that the effects of shear may include increased aggregation rate and interactions at the air/water interface due to agitation, turbidity or changes in pressure may lead to protein aggregation as well. For example, van der Linden *et al* reports on concentration effects and the impact of shear flow on aggregation [98, 164]. In addition contributions to measured torque from the bulk solution and the proteins at the air/water interface may exist, as demonstrated by Sharma *et al* [165].

4.4.2 Materials and methods

Rheometry:

The rheological analysis was conducted using a TA Instruments (New Castle, DE) ARES rheometer in dynamic oscillatory mode outfitted with a 25 mm parallel plate geometry and heated air oven. Before rheological testing, the solution was equilibrated to room temperature, approximately 25°C. The solution was briefly inverted before an aliquot of 0.25 ml of solution was transferred by pipette onto the bottom plate for each test. After the gap dimension between the parallel plates was set to 0.5 ± 0.1 mm, a small amount (<50 μl) of 5cst silicone oil from Dow Corning (Midland, MI) was dispensed circumferentially around the exposed gap dimension in order to limit evaporation. The tests were conducted in the dynamic mode using a programmed heating schedule allowing for the sample to be heated from room temperature at 10°C/min to 65°C. The solution was then maintained at this incubation temperature for ~60 minutes. Figure 20 illustrates the increase in viscosity as a function of time concurrent with the temperature increase for a representative experiment. Dynamic tests of the 5 mg/ml solution were conducted with strains of both 18% and 100% and a strain rate of 10 rad/s was applied.

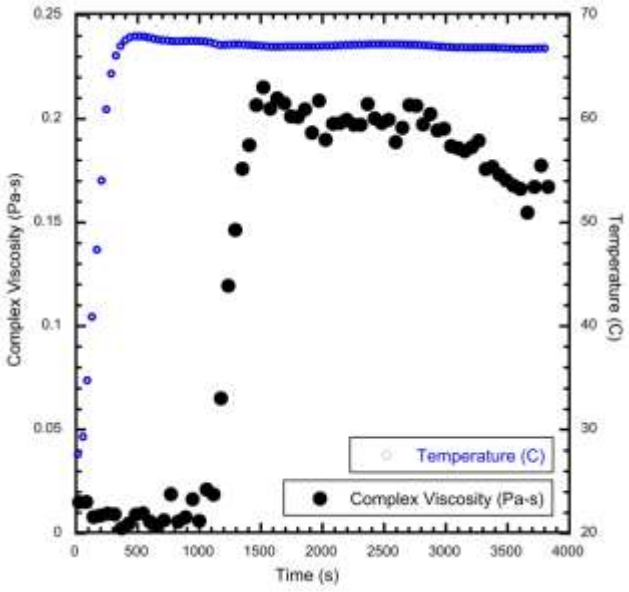

Figure 20. Representative rheological profile with heating to 65C

The low torque on the transducer during the initial heating and incubation phases of each test led to an overly high initial viscosity measurement from the dynamic tests. The initial viscosity was separately determined by conducting dynamic frequency sweeps ranging from a frequency of 0.5 rad/s to 15 rad/s at ambient temperature using a strain of 1% and a step size of 0.05 rad/s.

Data Analysis and Fitting:

The kinetic time constants associated with gelation for experimental results heated at 10°C/min was resolved by use of the logarithmic form of the sigmoidal model (eq 4.1) to fit the complex viscosity using Kaleidagraph software. This, P_∞ is presented as η_∞ for the rheological data.

4.4.3 Kinetics of aggregation

Rheological analysis of the 5 mg/ml insulin solution at various temperatures revealed the formation of weak gels as it was heated. An example rheological advancement experiment is shown in Figure

20. The formation of the gel is seen in the progressive rise in solution viscosity as the time at elevated temperature is extended. The plateau region is taken to be an indication of formation of protein structure which spans the sample volume. In other tests, G' plateaus have been interpreted as the formation of entangled networks [41, 166].

Concentration Dependence:

Rheological tests of insulin in concentrations of 2 mg/ml, 5 mg/ml, and 20 mg/ml showed that there was a drastic difference in aggregation rate as determined by sigmoidal analysis between the low concentrations of 2 and 5 mg/ml and the high concentration of 20 mg/ml. With increasing concentration of insulin in the solution, there is a faster rate of aggregation, meaning that the formation of a network occurs more rapidly at high concentrations than at low ones. Table 5 reports the results of analysis of rheological samples heated to 65°C for the three tested concentrations. Though the final viscosities of each concentration do not vary appreciably between 5 mg/ml and 20 mg/ml, the final viscosity achieved by 2 mg/ml insulin in solution is slightly less. The time constants measured by sigmoidal fitting and the rate calculated from this, however, do vary with concentration. As shown in Table 5, solutions with insulin concentration of 20 mg/ml achieved its final viscosity about three times faster than 5 mg/ml concentration and 15 times faster than 2 mg/ml insulin concentration.

Table 5. Kinetic time constants from sigmoidal fitting of different insulin concentration

Concentration (mg/ml)	**η_∞ (Pa-s)**	**t_{50} (s)**	**k (s)**	**Rate (x10^{-3} Pa-s/s)**
2	0.11	1803.4 ± 7.4	622 ± 18	0.17
5	0.21	1097.9 ± 1.1	177.6 ± 4	1.2
20	0.22	560.3 ± 1.0	63.2 ± 3.2	3.2

Predictably, the rate of viscosity change increases with increased protein concentration while the midpoint in this change (t_{50}) comes earlier (Figure 21). This points to the importance of protein availability and percolation throughout the volume in the development of aggregate structures. When there are more proteins present in the solution, it is easier to form nearly all stages of the protein aggregate. End-growth of fibrils is also hastened due to increased availability of proteins which are denatured once the denaturing temperature has been reached. Insulin is known to denature when exposed to temperatures of 60°C [53]. In the temperature ramp used in our protocol, the final incubation temperature of 65°C is achieved within approximately 240 seconds of the start of the experiment.

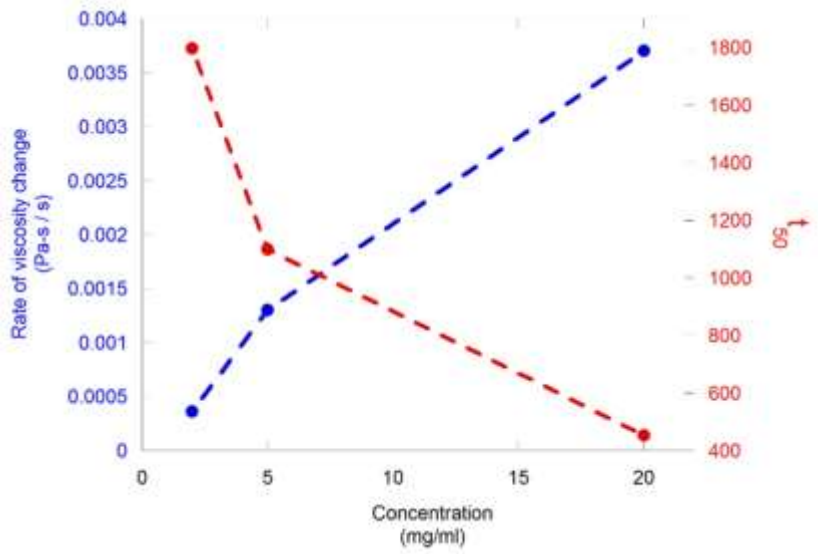

Figure 21. Concentration dependent time constants extracted from rheological data.

Increased protein availability in high-protein concentration solutions leads to faster development of protein structures and subsequent detection of aggregates in the solution by rheology. The process is speeded not only in the amount of time from the beginning of the experiment to when changes in complex viscosity are detected, but also in the rate at which the system toggles between the initial state and the final state with increased protein aggregates.

Species Dependence:

Bovine and porcine-derived insulin vary at only one residue [167], yet the rheology associated with the aggregation behavior of the two insulin species show major differences in the lag-time before aggregation is detected.

The two species of insulin were both obtained in lyophilized states from Sigma Aldrich and suspended into a pH 2 solution according to the same method. Bovine and porcine insulins are less easily aggregated than human insulin, and porcine insulin is generally held to be more stable than

bovine insulin [15, 167]. However, the robust and repeatable rheological profiles associated with 5 mg/ml porcine and bovine insulins show that that porcine insulin undergoes aggregation events resulting in a change in complex viscosity much earlier than bovine insulin does.

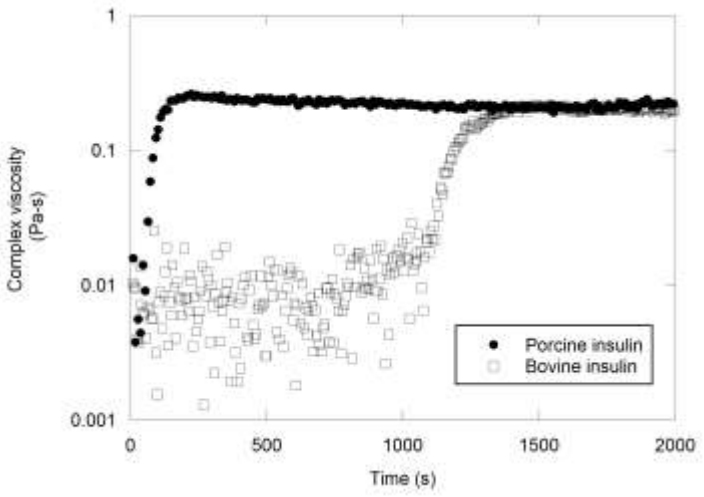

Figure 22. Denaturing and beginning stages of aggregation of porcine and bovine insulin is tracked by rheology. Porcine insulin is shown to aggregate before bovine in this system.

Though the results of these tests appear to go against the commonly held understanding that porcine insulin is more stable than bovine, there are several explanations for this aggregation behavior. Porcine insulin is more stable than bovine insulin in its native conformation. Self-association of proteins in their native state primarily occurs due to weak and transient interactions [41]. It is safe to say, however, that we are pushing the insulin well-outside the native conformation by using low pH, high temperature and shear. After the proteins are denatured, the aggregation behavior is dependent on the amino acid make-up of the protein which are largely the same between the two proteins. They differ at two points, at residue A8 and residue A10. This is a portion of the protein which has many cysteine residues which are important in the folding of the

protein into β-sheet structures after denaturing [168, 169]. At A8 bovine insulin has an alanine residue, while porcine has a threonine, and at A10 bovine insulin has a valine residue while porcine has an isoleucine. It is likely that the bovine insulin residues at A8 and A10 are bulkier and more difficult to fold into the required positions necessary for creation of β-pleated sheets which delays the formation of aggregate structures. Due to these two variations in the amino acid sequence, the bovine and porcine species of insulin have slightly different aggregation behavior kinetics.

4.4.4 Conclusions – rheology

In these experiments, rheology was used to probe the gelation of bovine insulin in denaturing conditions. Experimental parameters of temperature, concentration and shear strain were varied in order to determine the effects of these parameters on the aggregation behavior of the system. The concentration of insulin in solution has an impact on the speed and strength of the network formed and a clear difference was observed between tests conducted on higher concentrations of 20 mg/ml as opposed to concentrations of 2 mg/ml or 5 mg/ml insulin. Differences in aggregation rates of different insulin species were resolved by sigmoidal fitting and may be traced to residue substitutions which inhibit β-sheet formation or interfere with hydrophobic interactions.

4.5 Protein kinetics – ThT assay

4.5.1 ThT assay for measuring amyloid aggregation

Amyloid proteins aggregate into a variety of morphologies, including fibrils with high aspect ratios. Due to the wide clinical relevance of amyloid aggregation in the progression of neurodegenerative and other diseases, their aggregation characteristics have been extensively

studied and prior research has focused on understanding the conditions and pathways leading to protein aggregation, as well as methods to inhibit it after onset [57, 62]. The standard protocol for assessing aggregate formation is a Thioflavin T fluorescence assay (ThT) [15, 170] where increased fluorescence is associated with β-sheet formation in the aggregate [15, 171].

While ThT fluorescence assays are understood to be standard practice in tracking protein aggregation, the technique is not without issues. ThT assays are known to give ambiguous results due to variations in solution composition and sensitivity to pH, preparation of the initial protein solution and interference of added ThT with the protein or other solution additives [155, 172, 173, 174]. ThT assays are also often used as qualitative measures of aggregation without reporting of quantitative kinetic data related to the protein aggregation behavior. Most vexing, perhaps, is the wide range of protocols with which ThT assay aggregation experiments are performed rendering it in many cases impossible to compare between experiments. Temperatures, protein and ThT concentration and the scheme for homogenization (many commercial plate readers are capable only of orbital oscillation at designated time points) all vary widely across experiments.

To summarize, there is consensus that ThT fluorescence is a viable assay confirming β-sheet formation in protein aggregates, that agitation by a variety of techniques facilitates the formation of amyloid structures, and in side by side comparisons, raising protein concentration in solution and temperature both increase the chances for protein-protein interaction leading to faster kinetics of formation. We find it useful to analyze previously published studies retrospectively by comparing different aggregation datasets using similar kinetics determinations. With the time-resolved fluorescence showing a nucleation-based lag response, sigmoidal models that allow comparisons of lag time and aggregation rate are appropriate to consider in making parametric comparisons. Here we have reviewed other published work and extracted time constants to

compare between studies and offer some recommendations for standardized procedures which may yield better comparison and expanded knowledge in this important field.

4.5.2 Materials and Methods

Datasets

Published datasets were used that include temporal ThT fluorescence measurements in either a continuous measurement mode or by measuring aliquots from aggregating solutions at discrete time points. Table 6 includes kinetic constants extracted from a wide range of studies for which the protein, temperature of aggregation, protein concentration and pH of the solutions are given. We omitted datasets that compare the fluorescence at a single time point as might happen with specific inhibition studies. Details regarding the type of agitation are included if provided in the studies. The most common agitation method was stirring at a specific rotational speed.

Aggregation studies using the amyloid proteins amyloid-$\beta_{1\text{-}40}$, amyloid-$\beta_{1\text{-}42}$, β-lactoglobulin, and insulin were selected, though this is not an exhaustive list of proteins for which aggregation can be tracked by ThT fluorescence or of studies using these proteins. The source and species of these proteins was often reported, but not in every case. The initial and final fluorescence values are not significant in this retrospective study since the concentration of ThT and maximum fluorescence varies from study to study.

4.5.3 Observed trends in ThT assay kinetic data

Dynamic ThT fluorescence measurement tracking amyloid aggregation typically shows a sigmoidal curve associated the binding of ThT to nucleating β-sheet structures that form as a result of denaturing. As proteins are initially exposed to denaturing conditions at early time points there

is typically no fluorescence detected. As the incubation time increases and protein denaturing and aggregation progress in response to environmental stimuli, the amount of fluorescence increases until a plateau is reached (Figure 23). This plateau is indicative of three potential scenarios describing the binding. It is possible that protein aggregation has progressed to a point such that all fluorescent molecules are bound, no new β-sheet formation is detected, or the pathway for fluorescent molecules to bind to evolving sheets is blocked. The specific shape of the curve and associated kinetic constants may change depending on the stimulus used to promote protein denaturing and aggregation and the composition of the solution, but in most all cases the sigmoidal shape is conserved.

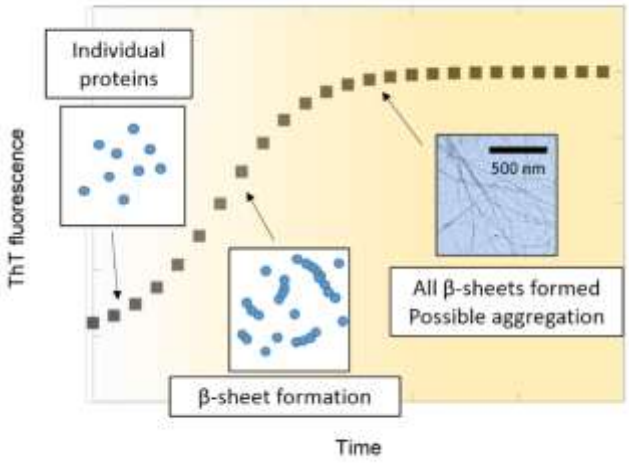

Figure 23. Example of a typical sigmoidal curve common to ThT fluorescence assays.

Presented in Table 6 are the kinetic time constants derived from ThT aggregation datasets fit using a sigmoidal equation. The wide range of experimental conditions used to perform the same general aggregation protocol is striking. Within individual experimental investigations such as the one

executed by Hellstrand *et al*, an amyloid-β aggregation rate is clearly seen to be concentration dependent while fixing other parameters [175]. An even more comprehensive study on insulin was carried out by Nielsen *et al* showing decreasing lag time and increasing aggregation rate with increased protein concentration [13]. It is generally understood that some proteins are inherently more susceptible to aggregation than others, for example the comparison of Aβ 1-40 vs Aβ 1-42 by Tiiman *et al* [176]. The experimental work reported by Dunstan *et al* and Hill *et al* both use the same concentration of β-lactoglobulin which allows for some comparisons between them [90, 91]. However, amongst the studies analyzed here few use the same experimental conditions in the same protein or across different protein species, making direct comparison difficult.

Table 6. Experimental details and kinetic constants derived from sigmoidal fit to ThT fluorescence data in literature

Protein	**Concentration (μM) at T(ºC), salt concentration if noted**	**Agitation mode**	**T_{50} (sigmoid) (hrs)**	**k (hr^{-1})**	**t_{lag} (hrs)**	**Lead Author**
Aβ 1-40	60 @ 37	Periodic vortexing 700 rpm, 1-2 s	4.75	1.14	3	Cook
	10 @ 50 100mM NaCl	Turbulent mixing 250 rpm	0.13	66.7	0.1	Tiiman
	17 @ 20 0.138M NaCl	Couette flow 150 sec^{-1}	46	0.26	38.5	Dunstan
	17 @ 37 0.138M NaCl	None	8.8	0.46	4.45	Dunstan
Aβ 1-42	5 @ 25 100 mM NaCl	Turbulent mixing 250 rpm	0.85	4.8	0.43	Tiiman
	5 @ 25, 100mM NaCl	Turbulent mixing 800 rpm	0.13	24.7	0.05	Tiiman

	1.2 @ 37 20mM Na_2HPO_4	Shaking 100 rpm in plate reader	2.1	4.1	1.6	Hellstrand
	5.8 @ 37 20mM Na_2HPO_4	Shaking 100 rpm in plate reader	0.44	13	0.3	Hellstrand
β-lactoglobulin	360@ 20	Couette flow 50 sec^{-1}	10.1	0.52	6.25	Hill
	360 @ 20	100 sec^{-1}	7.23	0.97	5.2	Hill
	360 @ 20	200 sec^{-1}	4.2	1.3	2.7	Hill
	360@ 80	Couette flow 150 sec^{-1}	1.66	2.03	0.07	Dunstan
Insulin	25 @ 37 in Na_2HPO_4 0.05M	Stirring 300 rpm	1.01	4.9	0.6	Malik
	25 @ 60, no salts indicated	None	14.3	0.3	7.75	Scherzer-Attali
	2.5 @ 50	Magnetic stirrer 250 rpm	0.3	19.2	0.2	Noormägi
	34 @ 60	None	5.3	2.8	4.6	Nielsen
	170 @ 60	None	4.6	1.5	3.3	Nielsen
	340 @ 60 0.05M NaCl	None	3.9	3.5	3.3	Nielsen
	340 @ 37 0.05M NaCl	Stirred 960 rpm	18.2	0.12	1.6	Nielsen
	340 @ 60 0.2M NaCl	None	4.1	1.3	2.6	Nielsen
	340 @ 60 0.2M NaCl	Stirred 960 rpm	19.4	0.11	1.3	Nielsen
	340 @ 60 0.5M NaCl	None	4.6	0.8	2.1	Nielsen
	340 @ 60 0.5M NaCl	Stirred 960 rpm	41.5	0.05	1.5	Nielsen
	1720 @ 60	None	2.0	3.4	1.7	Nielsen
	3440 @ 60	None	1.2	4.9	0.8	Nielsen
	2.5 @ 50 0.1M NaCl 20mM Hepes	Turbulent mixing 250 rpm	0.38	17.8	0.27	Tiiman

Trend 1: Increasing protein collision rate increases the kinetics:

From Table 6 several observations can be made. First, it is expected that Brownian motion of proteins in solution should increase interactions as well as aggregation rate as the protein concentration rises. The Nielsen [13] and Hellstrand [175] datasets show shorter lag times, larger k values and shorter experimental time periods required with increased protein and salt concentration. Increases in mixing or agitation also increase protein interactions. The takeaway is that agitation, greater protein concentration and increased temperature increase protein motion and shorten the kinetics.

The presence of secondary nucleating surfaces in solution may also lead to increased protein aggregation and faster kinetics. The presence of seeds in solution, whether purposeful or accidental, short-circuit nucleation and increase aggregate formation compared to solutions devoid of the seeds [177]. Proteins may also nucleate on surfaces such as vial or well-plate walls and stir bars used in the solution to similar results.

Trend 2: Rising temperature leads to more rapid amyloid formation:

Denaturing should rise with elevated temperature, yielding faster rates of aggregation and a faster increase in fluorescence reading. But what is commonly shown is quiescent data at high temperatures regulated by free convection as opposed to forced convection triggered by various agitation schemes at lower temperature. Nielsen *et al* make individual comparisons from quiescent versus shaken at the same conditions, but both temperature and agitation are manipulated simultaneously so the individual effects of elevated temperature and agitation are not present [13]. The study of denaturing and aggregation in a larger temperature range should be pursued, but

complications could arise due to evaporation at higher temperatures. With so much current research focused on inhibitors and their blocking strategies at body temperatures there is rationale for study of aggregation at 37˚C as well as room temperature. A larger temperature range could lead to a thermodynamic interpretation of the driving force and an Arrhenius-type activation energy assessment.

Trend 3: Agitation also increases the rate of amyloid formation:

Using a variety of agitation methods the papers explored here describe increased aggregation kinetics in protein solutions which are stirred, shaken, or sheared. Researchers use different units to quantify shaking and stirring and obviously the physical differences between mixing apparati would be difficult to replicate exactly. The lag times described for insulin vary between 0.2 hours and 8 hours depending on the method of forced agitation and extent to which the protein is agitated. Scherzer-Attali *et al* report the longest lag time (8 hours) in an experiment performed at 60˚C with moderate insulin concentration in a solution devoid of salts without agitation [178]. The shortest lag times for insulin aggregation are described by experiments by Noormägi *et al* with a 2.5 μM concentration incubated at 50°C with stirring by a magnetic stir bar at 250 rpm. Similar experimental protocols reported by Tiiman *et al* yield a similar lag time in the presence of stirring with salts. Tiiman mentions a difference in mixing efficiency with off-axis stirring [176] that shortens aggregate formation times dramatically. However, studies with increased stirring conducted by Nielsen *et al* in the presence of varying salts show longer associated lag times [13].

The study by Hill *et al* which documents the aggregation of β-lactoglobulin with increasing applied shear between 50 and 200^{-s} shows a decrease in associated lag time to observe aggregation [90]. The

Dunstan [91] and Nielsen [13] efforts show the effect of agitation on the aggregation of stirred and non-stirred mixtures of amyloid–β and insulin at two different temperatures. Overall, mixing leads to faster kinetics over quiescent aggregation, though a controlled study of temperature response would allow for activation energy determination.

Trend 4: Shaken vs. Stirred—Not all forms of mixing yield the same aggregation response:

Here the data is more variable and trends are less clear due to a variety of agitation mechanisms used in the selected studies. Both Hill and Dunstan have considered the variability associated with turbulence using stirring bars as agitators [90] [91]. Though the rotational speed of a stir bar as an agitation mechanism is often reported, the geometries of the setup can lead to experimental unknowns in the mixing protocols and increased turbulence. Using a Couette controlled-shear system both groups tracked aggregation resulting from a strain rate as high as 200 sec^{-1}. Both studies note that higher shear rates are tied to a faster and more pronounced fluorescence response, as denoted by the effect on aggregation rate (k) and lag time for both insulin and amyloid-β. It also suggests that shear rate could be a more accurately controlled and replicated parameter as opposed to rotational speed in mixing apparatus. Uncontrolled mixing with stir bars results in a less homogeneous shear profile and turbulence which may be key to aggregate formation, but leads to a much less controlled induction scheme.

Both increased turbulence and protein fibril strain likely lead to an increased driving force for aggregation. Above a certain threshold of extensional strain, aggregate formation could be reduced if chain fracture results from the shear strain, changing both protein chain length and making the fibril mixture in solution more heterogeneous [122].

While ThT fluorescence is a validated assay to probe aggregate formation in denatured proteins, the added complexity of agitation during aggregation is confounding. Mixing by stirring bar or shaker table does not take into account the key variables associated with effects of exposing the proteins to turbulent flow and exposure to the liquid/air or liquid/solid interfaces. The Couette flow apparatus adapted for an in situ fluorescence assay is a step forward in more independently controlling shear than the rotational speed of a stirring bar apparatus.

4.5.4 Recommendations for standardization

The studies which we have selected for this study are excellent examples of well-crafted explorations of protein aggregation in a variety of conditions. The variety of denaturing conditions explored and the means by which they are created, particularly agitation and shearing, do not allow for easy recreation of experimental protocols or for comparisons between them. The variances in protein response in individual experiments are likely due to subtleties in detailed experimental methodology including the reporting of protein selection, the species from which proteins were purified from, details of solution preparation and initial peptide state, temperature and agitation control, size and shape of stirring bars and size of vessel, and the presence of stabilizers. Some of these, such as the initial peptide state, may not even be possible to report in all cases. This suggests that more details of how the experiments are executed, with particular focus on the use and means of agitation, are important to include, even if relegated to supplemental information.

The experimental phase space of protein aggregation is vast and further exploration is required. However, a standardized approach to aggregation experiments or a combinatorial scheme for analysis would lead to greater scientific gain by allowing more direct comparisons. Attributes of a refined protocol would include a specified ThT concentration and use of controlled agitation

methods which control for or at least document the geometric parameters which control agitation. Extended analysis time frames may be able to capture more effectively the subtleties of protein aggregation. Thermal effects may still be studied by varying temperature protocols for comparison of critical aggregation temperatures and the aggregation potential of proteins. The effect of shear and agitation on amyloid aggregation is of particular interest to the scientific and medical communities. Greater understanding of the flow characteristics and use of controlled shear protocols may lead to better understanding of the driving force for aggregation.

It is worth considering whether other biophysical assays such as rheometry [104] or birefringence [100] have additional potential to yield kinetic parameters that can be linked to the experimental conditions under which aggregates form. If the rheometer is a more controlled shear apparatus, perhaps it is a more standardized gauge to observe a shear induced response as well. The caveat is the threshold for sensing aggregation is higher for rheological studies which will likely detect bulk properties and fibrillar interactions affecting the fluid viscosity rather than interactions of individual proteins as in ThT assays. Thus, the lag times which are observed by rheometry or by birefringence are likely longer than those observed by the ThT fluorescence assay. Though use of rheology may allow for greater control of added shear, issues related to protein aggregation at air/liquid and liquid/solid interfaces are not mitigated by its use. Experiments by Biddlecombe *et al* and others have shown that films of protein aggregates may occur at interfaces in shear cells [117].

Due to the use of differing agitation protocols depending on the fluorescence assay plate reader used and experimental set up, direct comparison between experiments is difficult. The effects of agitation resulting from the different mixing protocols can be quantified and reported by use of a dissolved oxygen probe which would measure the oxygen incorporated into the solution during mixing as an indication of the amount of mixing occurring. Reporting the amount of oxygen

content in the solution may help to explain differences between experimental set-ups and allow replication of experimental conditions by others. Alternatively, an additional standard experiment, such as lysosome could be used as a machine-to-machine cross reference to help to understand and control for experimental differences across studies. Results from the standard could be included with details of experimental set-up to aid in calibration between experiments.

4.5.5 Conclusions regarding ThT assay kinetics

This retrospective study of protein aggregation measured by ThT fluorescence assay in published literature has assessed protein sensitivity to denaturing conditions that include elevated temperatures, fluctuations in pH, concentration and, in particular, agitation to induce amyloid structure formation. The dynamic tracking of fluorescence shows a sigmoidal evolution as aggregates form; the resulting kinetics of association have been analyzed to explore the range of aggregation behavior which occurs based on environmental parameters. Comparisons between the experimental results of different groups have been historically difficult due to subtleties of experimental procedures including denaturing temperature, protein type and concentration, formulation differences, and how agitation is achieved. While it is clear that agitation has a strong influence on the driving force for aggregation, the use of magnetic stirring bar or shaker table rotational speed is insufficient to characterize the degree of turbulence produced during shear. The pathway forward in resolving dependence of aggregate formation on shear may require alternative methodologies or better standardization of the experimental protocols.

4.6 Chapter conclusions

Measurements of amyloid aggregation typically exhibit a sigmoid-shaped curve associated with the progression of protein denaturing and aggregation. Although the specific events which are measured by the testing mechanisms are different, use of an equation to extract constants associated with the aggregation process is beneficial as it leads to better understanding of the aggregation process and allows for comparison between tests and samples. Application of a sigmoidal equation to aggregation data acquired by rheology and ThT allow for comparison between tests and better understanding of trends.

Chapter 5.

Textile-immobilized insulin-based platinum catalysts

5.1 Chapter Summary

Immobilization of catalytic surfaces onto a textile substrate allows for simple insertion and removal from a reaction vessel. Such immobilization of protein-templated metallic catalytic surfaces has not been documented in the literature. Here, we document our initial work showing successful association of the protein-templated Pt-nanowires with nylon fabric and testing of catalytic ability in reducing 4-nitrophenol to 4-aminophenol. Results show that the nanowires adsorbed on the fabric substrate are able to catalyze the initial reduction and show some continued catalytic performance in subsequent reductions following retrieval and installation. Though the continued catalytic performance in additional reductions of 4-nitrophenol is promising, the rate of reduction and associated reaction constant indicate that the second reduction takes place at a slower rate, suggesting loss or poisoning of the catalyst. Additionally, there is some cause for concern that the reduction of the second vessel of 4-nitrophenol may actually be due to adsorption of 4-nitrophenol to the nylon catalyst and removal from the vessel with the catalyst, rather than complete conversion. In either case, optimization of the immobilization protocol is required. The protocols, methods and results of our work to immobilize platinum-coated protein fibrils onto textiles for use in reduction of 4-nitrophenol to 4-aminophenol is reported.

5.2 Catalyst textiles

Use of nanoparticle catalysts to facilitate specific types of chemical reactions in promising. The ability to purify the reaction products and to maintain the catalyst for continued use are compounded by their small sizes. Metal nanoparticles or nanoclusters exhibit interesting characteristics but are also likely to form aggregates or larger clusters. The stabilization of nanoparticles against aggregation is required in order to fully utilize catalytic efficiency of the nanoparticles. While electrostatic and steric methods are typically employed to stabilize the nanoparticles, we have effectively stabilized them by attaching them to insulin-based fibril structures. Association of the metal nanoparticles onto the insulin fibrils influences the shape and size of the catalyst surface available for reaction. The further aggregation of the platinum-coated insulin nanowires can be accomplished by immobilization of the nanowires onto a textile substrate which further serves the purpose of allowing facile introduction and removal of the catalyst to the reaction vessel. The immobilization of catalyst surfaces onto a retrievable textile fabric or other substrate is a plausible way in which catalyst surfaces might be isolated from a reaction vessel and potentially redeployed.

The creation and use of textile catalysts is of interest as the fabric provides a substrate for the catalysts which allows for the retrieval and potential reuse of the catalyst as well as perhaps providing a larger surface on which the reaction can occur. Additionally, fabric supports are inexpensive and can be easily transported when dry. Polymeric materials that can be used as supports for catalysts are highly flexible, durable, versatile and accessible. Textile catalysis may be of use in treatment of water supplies in remote locations where it would be difficult to set up sophisticated chemical processes.

The association of platinum nanoparticles with nylon textile has been documented in the literature with critical studies dating back to the 1970s. Platinum and nylon-based catalysts were of initial interest for use in the selective hydrogenation of benzene for conversion to cyclohexane for industrial applications [179, 180, 181]. In studies by Harrison and Rase on the selectivity of platinum catalysts supported on nylon, microscope images indicated that platinum nanoparticles associate with nylon in a geometric pattern coinciding with amide groups. Furthermore, they found that the arrangement of platinum at amide linkages exist on all types of nylon used [179, 182], though the geometric effect was contested by Dini *et al* [181]. Work by Sermon *et al* using Pt-nylon catalysts in the selective hydrogenation of benzene highlighted the importance of reactant product diffusion into the nylon substrate in order to fully utilize the platinum catalyst surfaces available throughout the substrate [183].

More recent studies have been published which examine the use of platinum on organic polymer substrates and their subsequent use in catalysis [184]. The most commonly used functional polymer supports for metal catalyst particles are resins, but use of other polymers including polyacrylates, and polyimides are growing. Of particular research interest are the use of polymer supports which are involved in the specific catalyst activity. For example, metal catalyst supports which have acidic functionalities are useful for use with multifunctional catalysts which have acid catalysis as a reaction step, while polymers with nitrogen moieties are useful in redox catalysis as they interact with groups on the surface of metal nanoclusters [184]. A study by Dimeska *et al* illustrates the natural tendency of uncoated nylon fabric to adsorb platinum in a series of experiments testing its use in the recovery of platinum from solution [185]. The recovery of platinum from solution by nylon fabric was attributed here to the reactions between the platinum complex and functional groups on the textile surface in addition to the coordination of platinum to the amide groups in the nylon.

The association of protein with various nonpolar surfaces are well documented, and of little use here if we assume that the majority of the protein nanowire is coated with platinum nanoparticles via the metallization process. The metallization process allows us to image the fibrils via TEM without negative stain, and the fibrils are fully visible without breaks or patches, suggesting a full coverage. Though we assume that interactions between the metal coating and the nylon substrate are the most important interactions in the adsorption of the catalysts to the nylon substrate, there may be small interactions between the protein and the polymer textile that contribute. Typically the association of proteins like insulin with a polymer substrate are due to charges at the interface and the interaction between positively charged portions of the protein and negatively charged interfaces [186].

A variety of textiles are used in the literature as fabric supports for nano-molecules and other nanoscale components including graphene and carbon nanotubes which are immobilized onto the fabrics by adsorption or adhesion [187, 188, 189]. The effects of irradiation on certain textiles provides an alternative means for immobilization of molecules and components onto the fabric substrate. Irradiation of textiles can cause photochemical production of surface radicals which can be used to functionalize or graft the textile with organic molecules, biocatalysts, or other components [190, 191, 192]. Studies by Gao *et al* and Opwis *et al* suggest that grafted functional groups and molecules engage in covalent bonding with the polymer surface following the UV irradiation and production of free radicals [191, 192]. In addition, the capillary action which textiles display allows for uniform wetting of the material with the catalyst before photo-induced immobilization resulting in 3-dimensional coating. Active surface area can be adjusted by varying of the diameter of textile fibers and the fabric weave density [193].

Recent work by Lu *et al* successfully attached a variety of organic catalysts to nylon polyamide textiles using UV-irradiation to immobilize the organometallic catalysts onto the fabric by covalent bonding. The immobilized catalysts facilitated the desired reaction and lost little functionality over time [193]. The irradiation time of the textile proved to regulate the successful immobilization of the catalysts, as degradation of the textile and catalysts occurred with overexposure.

Although the work by Lu *et al* involves the immobilization of organometallic catalysts which would normally be in the same phase as the reactants in the catalysis, a similar methodology can be used to facilitate the immobilization of Pt-templated nanowires which we have used in the heterogeneous catalysis of 4-nitrophenol (4-NP) as described in Chapter 3. In Chapter 3 the Pt-nanowires are dispersed in solution and used to catalyze the reduction of 4-NP to 4-AP. Here, we explore the immobilization of these nanowires onto textile fabrics for simplified retrieval of the catalysts from the reaction vessel and their potential reuse in subsequent reactions.

We have been interested in 4-NP as a rather ubiquitous contaminant in a range of fresh water and other aqueous reservoirs. 4-NP has a significant toxicity to bacterial species and as a result, it persists in a range of groundwaters [136]. Its reduction to 4-aminophenol is thought to enhance its ability to be more effectively degraded through bacterial digestion pathways. We selected 4-NP as a model marker of the protein-templated Pt-catalyst conversion given that its conversion is easy to identify by absorption spectroscopy and dynamic measurements of conversion could be taken to identify reaction kinetics.

Here we describe the initial attempts to produce a templated and metallized cotton fabric to characterize the rate of 4-NP conversion with the constraint that the catalyst is removed and

reinstalled in a fresh solution of 4-NP. We include our protocols for fabric synthesis, sequential 4-NP exposure, and our analysis of 4-NP conversion by UV-Visible spectroscopy.

5.3 Materials and Methods

5.3.1 Platinum-coated insulin fibrils

Platinum-coated fibrils were created from insulin protein as described in previous chapters using a method partially adapted from the metallizing of insulin fibers by Zhang *et al* [77]. The protein fibrils were produced using the combined heating and deformation protocol. For simplicity, the fibrils were produced with 10% applied strain, as this created a reliably large number of fibrils. The fibrils were left to aggregate overnight in quiescent conditions before coating with an electrolessly deposited platinum as described previously in Chapter 3. Following platinum metallization, the coated fibrils are subsequently distributed onto the fabric. For simplicity, the Pt-coated insulin fibrils are referred to as Pt-nanowires in this chapter.

5.3.2 Preparation of fabric

A 100% nylon mesh with a fabric density of $2x10^{-6}$ g/cm^2 was selected as a substrate for the catalyst Pt-nanowires. The nylon fabric has a medium weave, easily absorbs aqueous solution and is highly flexible allowing simple insertion and removal from the reaction vessels. Strips of the nylon fabric were prepared which were approximately 1.5 by 8 cm to allow their insertion into UV-Visible spectroscopy cuvettes.

Textile-immobilized catalysts were prepared by immersion of the nylon fabric in the catalyst dispersion to allow for absorption of the solution into the textile weave. The textile was immersed

for 60 seconds before extraction and UV-irradiation. During UV-irradiation, textiles were placed under direct UV-light with an intensity of 100 mW/cm^2 for 5 minutes before flipping the fabric to irradiate the other side for an additional 5 minutes. Following UV-irradiation the fabric strips were allowed to air dry. Additional tests were conducted using small weave nylon fabric which was immersed in the Pt-nanowire dispersion for 24 hours rather than the typical 60 seconds prior to removal, irradiation and drying.

The fabric strips were weighed before and after coating to determine the amount of catalyst absorbed. The strips were allowed to dry overnight and were again weighed in order to determine the water content lost to evaporation and drying and the amount of catalyst available on the textile.

5.3.3 Testing protocols

The catalytic efficiency of the textile-bound catalysts was tested in the reduction of 4-NP to 4-AP. The 4-NP solution was prepared as described in chapter 3, including 4-NP and an excess of $NaBH_4$ for the reaction. The progress of the reaction was tracked by UV-Visible spectroscopy.

Efficiency in subsequent reactions was tested by introducing the catalyst textile to additional reaction cuvettes to catalyze subsequent reductions of 4-NP. After an initial spectrum was taken, the catalytic fabric swatch was introduced into the cuvette. The complete conversion of 4-NP to 4-AP results in a color change from yellow to clear, so the reaction is easily monitored for completion. If the reaction completed within the first 5 minutes, the catalyst textile was removed from the reaction vessel and introduced into a new vessel with fresh 4-NP solution to test the continued catalysis. If the reduction was not completed within 5 minutes, the fabric was removed from the cuvette and another spectrum was captured in order to determine the progression of the reaction. If the reaction was not complete (i.e. all 4-nitrophenol had not been converted to 4-

aminophenol as judged by the lack of 4-NP peak and presence of 4-AP peak), the fabric was re-introduced into the cuvette for another 5 minute period, after which the fabric was again removed and the spectra taken by UV-Vis. UV-Vis spectra were taken at several time point during the reaction so that the conversion of 4-NP could be tracked and reaction rate constants extracted.

5.3.4 Control experiments

Additional testing was conducted to determine that there would be no leaching of the fabric itself into the 4-nitrophenol/ $NaBH_4$ solution which might interfere with results and that the nylon fabric does not catalyze the reaction on its own. A swatch of the nylon fabric was introduced to a vial of 4-NP solution after weighing and measuring. The fabric was weighed again in the wet state after 15 minutes of immersion and also after 24 hours of immersion. The fabric was then dried and weighed. Lastly the fabric was washed in distilled water and weighed in wet and dry states. The 4-NP/$NaBH_4$ solution was also tested by UV-Vis before and after the introduction of the nylon fabric to determine if there was any change in the solution spectra. The results of these tests indicate that there is no loss of nylon material into the solution.

In order to test the efficiency of the Pt-nanowire associated fabric compared to catalysis with Pt-nanoparticles, nylon fabric samples were metallized with Pt-nanoparticles. These swatches were prepared using the same 60 second immersion in platinum solution followed by UV-irradiation and air drying method.

5.4 Results

5.4.1 Incorporation of platinum-fibrils into fabric

One important factor for the catalysis of 4-NP into 4-AP is the amount of Pt-coated fibrils introduced into the reaction and thus the available catalytic surface area. It was previously found that adding too few Pt-fibrils to the reaction vessel resulted in an incomplete or immeasurable reaction. The minimum amount of added Pt-fibril surface area required for a successful reduction of 4-NP to 4-AP within the experimental timeframe was found to be 200 µl of Pt-coated protein solution such that the final concentration of protein in the reaction vessel was approximately 12 nM as described in Chapter 3.

The swatches of nylon absorbed approximately 250 µl of catalyst solution after 60 seconds of immersion. The liquid solution absorbed by the nylon and the amount of solids remaining after drying are recorded in Table 7 where the amount of Pt-nanowire or Pt-nanoparticle catalyst solution initially absorbed by the textile as well as the remaining catalyst after drying are reported as percentages of the textile weight and are averaged over 3 trials.

Table 7. Catalyst adsorption

Catalyst	**Catalyst solution absorbed as a percentage of textile weight**	**Dried catalyst as a percentage of textile weight**
Pt-nanowire	495%	2.5%
Pt-nanoparticle	840%	6%

5.4.3 Catalytic performance

The immobilization of Pt-nanowires on nylon resulted in a catalyst textile which was able to completely reduce 4-NP to 4-AP in a first reaction and continue to reduce 4-NP when introduced to a second reaction vessel, albeit at a slower conversion rate. The immobilization of Pt-nanoparticles on the nylon fabric created a textile which was able to catalyze the reduction of 4-NP to 4-AP in an initial reaction, but was unable to complete the first reaction within a 120 minute experimental period. Thus, the Pt-nanoparticle coated textile was not tested in subsequent reactions as it was unable to fully catalyze the first.

The Pt-nanowire coated nylon successfully and rapidly reduced 4-nitrophenol in preliminary reactions and displayed continued catalytic activity based on the reduction of 4-NP absorption peak in subsequent reactions, though at a reduced reaction rate. This reduced rate of reaction may be due to loss of catalyst in the first reaction vessel or poisoning of the catalysts.

Figure 24 shows the successful reduction of an initial test of 4-NP to 4-AP by nylon-bound Pt-nanowires as well as catalysis in a second reaction vessel after removal of the textile from the first and immersion in the second vessel. The initial reduction occurs within 15 seconds of insertion of the catalyst textile into the vessel, yielding a Pt-surface area normalized reaction constant (k_{norm}) of 1303 s^{-1} m^{-2} L. Retrieval of the textile and insertion into another reaction vessel results in catalysis at a slower rate with an average normalized reaction constant of 14 s^{-1} m^{-2} L. The reduction of the second 4-NP solution is nearing completion at 120 minutes and the normalized reaction constant is reduced to 1% of that of the first reaction. Despite this, the continued catalytic activity is promising as it indicates that at least some of the catalyst has been successfully bound

to the textile, retained its ability to participate in catalysis of the reaction during drying, and is capable of being removed from an initial reaction to go on to catalyze another.

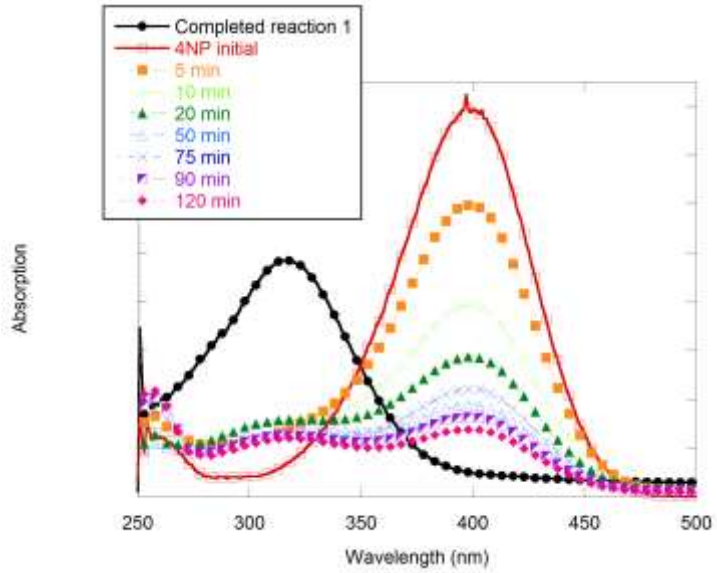

Figure 24. UV-Vis spectra tracking successful reduction of 4-NP and continued catalytic activity in 2nd reaction vessel.

Of interest in figure 24 is the fact that the peak associated with 4-aminophenol which is achieved during the second reaction is less than 25% as high as the 4-aminophenol peak achieved in the initial reduction. Furthermore, though the 4-aminophenol peak does increase during the initial timepoints of the second reaction experiment, the 4-aminophenol peak *decreases* as time increases from 20 minutes. This suggests that 4-aminophenol is being removed from the reaction vessel, which could be due to two different mechanisms. The removal of 4-aminophenol from the reaction may be due to re-adsorption to the Pt-nylon catalyst along with a failure to successfully desorb after reacting on the catalyst surface. Alternatively, the 4-aminophenol may be removed by simple absorption of the solution into the nylon which is removed from the vessel during the UV-Vis test

at each timepoint. The loss of the 4-aminophenol from the reaction solution is concerning, and causes pause in the assertion of continued catalytic efficiency of the Pt-nylon catalyst. However, the point still remains that the first reaction is indeed catalyzed, and some catalytic efficiency is shown in the initial rise in 4-aminophenol in the solution before the peak begins to decrease.

The lack of an appropriately sized increase in the 4-aminophenol peak to correspond to the decrease in the 4-nitrophenol peak is troubling. The potential loss of catalytic efficiency due to chemical poisoning of the 4-nitrophenol through oxidation is expected to result in no reduction of the 4-nitrophenol peak. The fact that we observe the unusual response of a decrease in 4-nitrophenol peak without an accompanying increase in the 4-aminophenol peak is indicative that there may be another unexpected reaction occurring. Analysis of the components which remain in the reaction vessel may lead to a better understanding of the process by which the catalytic efficiency is lost, as discussed in chapter 6.

Despite the inability of the Pt-nanoparticle based textiles to completely convert the 4-NP to 4-AP within the 120 minute timeframe, they did catalyze the initial reaction over the time period. For the first reaction using the Pt-nanoparticle coated nylon and for the second 4-NP reaction employing the Pt-nanowire coated textile, the UV-Vis spectra taken at time points within the 120 minutes time period are used to determine the surface area normalized reaction constant.

Table 8 lists the normalized reaction constants from the UV-Vis spectra collected during the reactions and calculated according to the method in Chapter 3. Note that the nylon textile coated with Pt-nanowires has higher catalytic performance than nylon coated only with Pt-nanoparticles in the first reaction, but after removal and reinsertion into fresh 4-NP solution the Pt-nanowire

coated textile has a lower reaction constant. Recall that Pt-nanoparticle coated nylon does not fully reduce the 4-NP within the experimental timeframe and so there is only data for the first reaction.

The catalytic performance of the Pt-nanowire nylon sample in the second reaction vessel is approximately one quarter of the reaction constant for the Pt-nanoparticle-coated nylon. The performance of the Pt-nanowire based sample in the first reaction is nearly 10x more than the Pt-nanoparticle rate constant. The reaction constants calculated here reflect the 4-nitrophenol peak in the UV-Vis data and thus the reaction constant reported for the second reaction catalyzed by the platinum nanowire and nylon catalyst is likely over-estimated due to loss of 4-nitrophenol from the reaction via absorption by the nylon and loss outside the vessel during testing.

Table 8. Normalized reaction constants for 4-NP reduction by textile-bound catalysts

Sample preparation	k_{norm} (s^{-1} m^{-2} L) Reaction 1	k_{norm} (s^{-1} m^{-2} L) Reaction 2
Pt-nanowire	1303	15
Pt-nanoparticle only	117	N/A

Examples of the UV-Vis spectra associated with reduction of 4-NP by nylon-bound nanowire and nanoparticle catalysts are shown in Figure 25. Nylon coated with the fibril-based nanowires was able to completely catalyze the reaction in the first reaction vessel and continue to catalyze the reaction at a slower rate in a subsequent reaction vessel. Nylon coated with only platinum nanoparticles was able to catalyze the initial reaction but did not complete the reaction. The spectra in 25a shows catalysis by Pt-nanowires bound to nylon with the initial complete reaction shown in

black along with the 4-NP peaks associated with the reduction of a second 4-NP solution after retrieval of the fabric substrate and introduction into the second vessel. Figure 25b shows a similar spectra associated with a nylon sample prepared by immersing the nylon swatch in the nanowire catalyst solution for 24 hours rather than the 60 seconds used in other preparations. The similar spectra indicate that the longer immersion time in catalyst does not significantly impact the association of the catalyst with the fabric. Figure 25c demonstrates the catalytic activity of nylon fabric coated with platinum nanoparticles on an initial reaction. The Pt-nanoparticle coated nylon does not completely reduce the 4-NP.

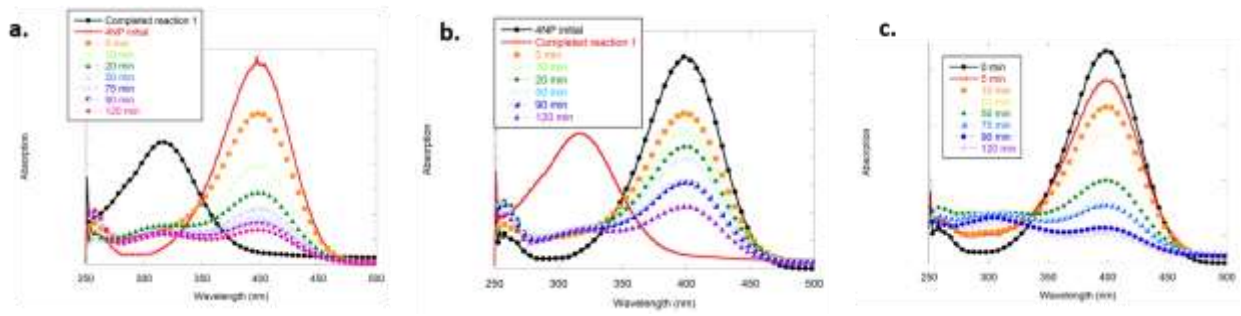

Figure 25. UV-Vis spectra from a.) Pt-nanowire coated nylon, b) Pt-nanowire coated nylon immersed in catalyst solution for 24 hours and c) nylon coated only with Pt-nanoparticles.

UV-Vis spectra can also be used to determine the amount of 4-NP reacted at a given time point using a 4-NP concentration curve. The amount of 4-NP left in the reaction vessel at the time points of 30 and 120 minutes are given in table 9. Both the nylon catalysts that were immersed in Pt-nanowire solution for 60 seconds and 24 hours were able to fully catalyze the initial reaction. The complete reduction of 4- NP in the first reaction vessel occurs rapidly, and so the reported amounts of 4-NP left in the reaction recorded in table 9 are from reaction of the second vessel for these

tests. The Pt-nanoparticle based nylon catalyst does not fully catalyze the initial reaction and so the associated amount of remaining 4-NP recorded in table 9 is from the first reaction only.

Table 9. Concentration of 4-NP at key time points for reduction with a variety of nylon-bound catalysts

Sample preparation	Completed reaction 1?	[4-NP] after 30 minutes (μM)	[4-NP] after 120 minutes (μM)
Pt-nanowire, 60 seconds	X	18.6	15.5
Pt-nanowires, 24 hours	X	12	7
Pt-nanoparticle only		13	9.5

5.5 Chapter conclusions

We have shown that it is possible to create protein-based metallic nanowires which can be adsorbed onto polymeric mesh networks. Based on sequential catalyst studies we have shown in a limited way that there is residual catalyst function in subsequent reaction vessels in the reduction of 4-NP. Nylon-bound catalysts can be formed based on optimization of a catalyst association and UV-irradiation method which are capable of fully catalyzing the initial 4-NP reduction and are functional in subsequent reactions, albeit at a slower reaction rate.

The continued catalytic activity and efficiency of the platinum-nylon catalysts should be qualified with the statement that the catalytic efficiency of the catalyst in the second reaction vessel is likely over-exaggerated by the UV-Vis results, as it is clear that 4-aminophenol is not being produced at a rate that matches the reduction of 4-nitrophenol. This suggests that either 4-aminophenol is being lost, either by removal from the reaction through absorption or by failure to desorb from the

substrate. Alternatively, the 4-nitrophenol may be disappearing from the reaction vessel through similar means which would also explain the lack of increase in the 4-aminophenol peak measured by UV-Vis spectroscopy. Although the second reaction does not take place at the rate suggested by the UV-Vis results, there is some continued efficiency observed in the initial reduction of 4-nitrophenol to 4-aminophenol which should be further investigated and optimized.

A more complete mass balance is required to resolve the amount of catalyst remaining in the reaction vessel and to determine the cause of the reduced reaction rate in sequential reactions. The reduced reaction rate despite continued catalyst function after retrieval and reinstallation of the catalyst-coated fabric indicates that there may be loss of catalyst into the initial reaction vessel or poisoning of the catalyst. Additionally, better methods of adsorbing or covalently bonding the protein-based Pt-nanowires to the fabric substrate are crucial for the development of a more robust textile-based catalyst system.

Chapter 6.

Development and use of insulin-based platinum nanowires: Conclusions & future work

6.1 Chapter Summary

A protocol has been developed for the reliable production of insulin fibril structures for which the morphology of fibers is influenced by applying varying amounts of deformation during a brief denaturing period. Large deformation during denaturing results in shorter fibrils on average compared with small deformations, 1350 nm compared to 1750 nm for small deformation preparations. The produced insulin fibrils have been metallized with platinum (Pt) for use as catalyst surfaces in reducing 4-nitrophenol to 4-aminophenol. The metallized fibrils have been shown to be robust and efficient catalysts with a normalized reaction rate of 7.22 $s^{-1}m^{-1}L$. The kinetics related to the aggregation of insulin are discussed and a means for comparison of aggregation kinetics by use of sigmoidal fitting is discussed and extended to ThT studies in the literature. Finally, initial studies investigating the immobilization of the protein-templated Pt-catalysts into textile substrates have been conducted showing potential for use of fabric-based catalysts for efficient catalysis of 4-nitrophenol reduction as well as retrieval and reuse in subsequent reactions. Future directions for subsequent work are also suggested here.

6.2 Conclusions

6.2.1 Development of protocol for creation of insulin fibrils

In this work a heat and deformation-based protocol is proposed for robust creation of fibrillar structures from moderate concentrations of porcine and bovine insulin suspended in solution of pH 2. By employing both heat above the denaturing temperature and controlled displacement of the proteins, fibrils are reliably formed following a 15 minute protocol and 24 hours of incubation at room temperature.

Fibrils which are formed using this protocol are more numerous than fibrils nucleated in non-agitated conditions and are also morphologically different. Fibrils which undergo the heat and deformation protocol are typically shorter than fibrils which are not deformed. A likely cause of this difference is the increased nucleation at the air/water interface in the deformed samples that undergo deformation by rheometer-induced displacement and due to increased motion of proteins in the solution during this protocol. The formation of many nuclei during the denaturing protocol leads to more fibrils in the following incubation period.

The formation of short fibrils and fibrils fragments during the deforming and heating protocol has been confirmed via TEM. Following the incubation period, TEM images of the fibrils show that the fibers are much longer, moving from 300 ± 150 nm to 2000 ± 1000 nm with overnight incubation. Though nucleation and denaturing occurs during the initial deforming and heating, the aggregation of the amyloid fibrils continues at room temperature via chain elongation, as well as fibrillar network formation. Furthermore, the fibrils form nanostructured networks which may have wider interest as fibrillar nanowires.

6.2.2 Effect of deformation on fibril morphologies

The effects of deformation of varying magnitudes was determined via rheology and TEM imaging of resulting fibrils. Morphological differences in the fibrils and networks produced were observed between large and small deformations. It was found that small oscillatory deformations resulted in the creation of numerous nuclei and the eventual growth of relatively long fibers (when compared with fibrils nucleated in large deformation conditions) which made up dense fibril networks with small average pore sizes. These fibrils have an average length of 1750 nm, though fibrils which are much shorter and much longer are also observed. In comparison, larger oscillatory deformations during denaturing resulted in stunted fibrils which were shorter, straight and angular rather than long and more curled. These fibrils were observed to have an average length of 1350 nm. The networks produced by these fibers had lower fibril density than networks created with fibrils nucleated in small deformation conditions.

The use of applied oscillatory strain on a parallel plate rheometer to control deformation resulted in a varying amount of applied deformation depending on the location of a protein on the plate. TEM images of proteins which were retrieved from the edges of the plate versus the center of the plate illustrate the differences in the amount of sensed displacement, as protein aggregates near the edges were straighter, more numerous and more fragmented. Protein fibrils which were located in the center of the plate where less deformation was sensed were more curved, longer and less numerous. Important follow on studies would expose protein solutions to controlled strain using a cone and plate rheometer, but these are beyond the scope of this dissertation. The distinction between sampling in the middle vs the edge yields differences in structure, likely due to both increased nucleation at the edges and issues related to protein fragmentation and breakup closer to the moving air/water interface.

6.2.3 Metallization of fibrils to create catalytic surfaces

Protein-templated nanowires and nanostructures are of potential use in a variety of nanoscaled devices such as biosensors, solar cells and electrodes. Additionally, protein-templated nanowires can provide high surface area catalytic surfaces for use in catalyzing reactions. A protocol for metallizing the pre-formed fibrils is detailed in this work which uses electroless chemistry to coat the fibrils in platinum (Pt). The fibril morphologies are preserved following Pt-coating and the coating is well-adhered to the fibril surfaces.

6.2.4 Efficiency of protein-templated nanowires as catalysts

The produced Pt-coated insulin nanowires are efficient catalysts in reducing 4-nitrophenol to 4-aminophenol in the presence of $NaBH_4$. The efficiency of the protein-templated catalysts was higher than the use of an equivalent amount of platinum nanoparticles alone in our tests and compared favorably to reported efficiencies of other nanowire-like catalysts in the literature.

The catalytic efficiency of the protein-based nanowires in the reaction was tracked by UV-Visible absorption spectroscopy and reaction constants were extracted from the resulting data to compare with literature values. The normalized reaction constant for the Pt-coated fibril catalysts was found to be 7.22 $s^{-1}m^{-1}L$, which was on the order of reaction constants for similar nanowire-like catalyst surfaces reported in the literature. The reduction of 4-nitrophenol using the amyloid Pt-catalysts followed pseudo-first order kinetics which was expected for Pt-based catalysts in this reaction.

6.2.5 Characterization of aggregation kinetics

Aggregation kinetics associated with the denaturing protocol making use of heat and deformation were resolved by the application of a sigmoidal model fit to rheological data. The sigmoidal model

was fit to the complex viscosity which undergoes an increase during denaturing, thought to be due to forming larger protein structures throughout the bulk of the solution and the decreased mean square value and increased friction and resulting torque detected by the rheometer with the increasing size of the protein aggregates.

There is likely some contribution to the viscosity increase due to proteins adsorbed at the air/water and water/solid interfaces. These interfaces serve as locations for increased association of proteins and the formation of nuclei and larger aggregate structures which may also desorb from interface to recombine with the bulk of the solution.

The use of the sigmoidal model allows the extraction of kinetic time constants that allowed comparisons between experimental results to better understand the effects of environmental and other extensive parameters on protein aggregation. Concentration effects were resolved using these kinetic constants which show that aggregation begins earlier and occurs at an increased rate for higher protein concentrations. The effects of amino acid residue substitutions in bovine and porcine insulin species are also detected by fitting with the sigmoidal model showing porcine insulin to more quickly denature and aggregate in the conditions of our heat and deformation experiment.

Additionally, the sigmoidal model was applied to ThT fluorescence assay data from the literature in order to extend its application to quantify aggregation data obtained by other methods and allow for comparison between studies and extraction of common trends. The sigmoidal model was successfully applied to the literature data, but the variety of experimental parameters employed throughout the studied literature made comparison difficult. Trends in the data indicated expected results related to increased rate of aggregation with increasing concentration and temperature as

well as the increased aggregation rate when solutions were continuously stirred, mixed or otherwise agitated. This exercise also lead to suggested methods for standardization of ThT assay experimental procedures.

6.2.6 Immobilization of protein-templated catalysts into textiles

The efficiency of the produced protein-based catalysts can be increased by immobilizing the catalysts onto textile substrates providing a means for simple use and easy retraction and reuse. Although the creation of such catalyst fabrics with organic and non-metallic molecules is currently a topic of much research, the creation of catalyst textiles incorporating protein-based metallic nanowires has not yet been reported in the literature.

Protein-templated catalysts were immobilized onto nylon using UV irradiation. Protein-based nanowires adsorbed to the fabric and were immobilized there by UV irradiation of the textile and subsequent drying. The catalyst textiles were efficient at catalyzing initial reductions of 4-nitrophenol to 4-aminophenol and showed some continued catalytic activity when retrieved from the initial reaction vessel and introduced into a fresh 4-nitrophenol solution. A reduced reaction rate in the second reaction vessel indicates that there may be loss of the catalyst or poisoning of the catalyst. Additionally, there is evidence that suggests loss of 4-aminophenol and/or nitrophenol from the reaction system in the second reaction vessel which results in an over-estimation of catalytic activity based on the reduction of the 4-nitrophenol peak measured by UV-Vis. Nylon textiles prepared with Pt-coated insulin nanowires showed higher catalytic efficiency than nylon textiles prepared with only Pt-nanoparticles, as fabrics coated in platinum only were unable to fully catalyze the initial 4-nitrophenol reaction within the experimental timeframe of 2 hours in which

the fabric prepared with the insulin nanowires was able to fully reduce one solution of 4-nitrophenol and nearly complete the reduction of the second reaction.

6.3 Future directions

6.3.1 Protein-based nanowire applications

The protocol presented here repeatable and reliably produces large amounts of robust insulin fibrils which can be coated in metal to produce protein-templated nanowires. Their use as catalytic surface is presented in this work, but alternative applications of these nanowires have been suggested in the literature but not yet adequately explored. The high efficiency of these nanowires as catalysts suggests that they may successfully be implemented and incorporated into other applications and devices. The development of devices making use of the interesting materials properties of these nanowires is a worthy direction of research.

6.3.2 Catalyst textiles

One application of the produced catalytic protein-based nanowires which began here was their incorporation into textiles for creation of catalyst fabrics which would allow simple use of the catalysts and removal for reuse. A series of tests were presented which point to a potentially successful method for production of nylon fabric with incorporated catalyst nanowires via use of UV irradiation. The production of such catalyst fabric and confirmation of its robustness in a retrieve and reuse scenario with continued efficiency is important in using the catalytic properties of protein-based nanowires.

A better understanding of the events which lead to the loss of catalytic efficiency of the textile catalyst after the initial catalytic reduction may be achieved through analysis of the components of the solution in the second reaction vessel. A variety of chemistry tools could be employed to better understand what is being produced and what reaction is or is not taking place, including gas chromatography or high performance liquid chromatography (HPLC).

6.3.3 Network properties

The formation and characterization of 2-dimensional networks of insulin fibrils is potentially useful in incorporation of fibril-based nanowires into devices like electrodes. In such a device, the connectivity of the fibers and the density of the wires may be of importance to the conductivity of the network mesh. Other applications where an understanding of the network properties may be of use can also be imagined such a use in solar cells or fibril-based filters.

Methods to influence the morphology of the produced networks may also be of interest if the network structure is an important component of the desired device. Along with the influence of deformation explored here, concentration effects, seeding or peptide engineering might also be considered as parameters which may be tuned in order to influence network structure.

Though the 2-dimensional structure can be visualized using TEM and other forms of microscopy, the extrapolation to 3-dimensional network structure is not so easily understood. Use of methods such as SAXS or SANS could potentially help in the understanding of these structures that exist within the protein solution and within the soft gels which are formed during denaturing and aggregation.

The formation of fibrils could be tracked using NMR which would show the depletion of monomers and would give an understanding of the percentage of available protein which is used

in the formation of the fibrils and how much is left in the solution following the incubation period. This may be useful in determining whether the 24 hour incubation period is sufficient and analyzing the loss of protein which is not incorporated into the fibrils. Additionally, monomer and solubilized oligomers and protofibrils which remain in the solution following the metallization process may interact with the protein sidechains and serve to block the nanowire surface, reducing the catalytic efficiency of the nanowires. Knowing how much monomer remains in the solution would be useful in determining if this these interactions may be causing loss of catalytic efficiency and could determine whether additional steps should be added to isolate the fibrils before metallizing and use as catalysts.

6.3.4 Deformation and interfacial effects

The current discourse regarding the effects of applied strain on denaturing and aggregation of proteins is fragmented. While one group claims that shear forces can provide the impetus for protein unfolding and aggregation, the other maintains that it is not the shear forces, but rather effects of the shear forces on the creation of air/water interfaces which lead to protein unfolding.

While it was not the intent of this work, we have found ourselves drawn into the debate due to the mechanism which we have chosen to speed fibril nucleation for the creation of protein aggregates. The true nature of strain and shear effects are difficult to parse as the creation of shear and creation of interfaces are connected in most studies. Some elegant studies which point to the impacts of the shear itself or the interfacial effects have been conducted, but these remain colored by the author's allegiance to their position in the debate [46, 118, 133].

The results of interfacial effects on the morphologies and characteristics of fibrils which are grown from nuclei formed in the heating and deforming protocol could be better understood using a

variety of analyses. The elimination of an air/water interface, if possible, could definitively answer the question of what role the movement at the interface produces. Since this would be very difficult to achieve, alternative tests may be employed to increase understanding, such as the use of continuous shear rather than oscillatory straining and comparison of the fibrils created via this method which lacks the compression/dilation that oscillation produces. Changing the size of the available interface while holding the concentration of protein constant by simply altering the size of the parallel plate used or changing the gap size might also lead to better understanding of how much the nucleation of proteins depends on the interface and how available surface area for protein adsorption and turnover affects the number of resulting nuclei produced.

Shear forces, agitation, and strain all exist *in vivo* and *in vitro* in pharmaceutical, manufacturing and processing of proteins [194]. We understand that concentration and temperature stability also are important regulatory parameters on protein structure. Understanding the effects of both the fluid forces and the interactions which occur at created and bulk interfaces are important to elucidate. My dissertation has probed several facets of this interdisciplinary area and the field of templated nanostructures and these topics remain of current interest both amongst scientists interested in structure and engineers interested in performance characteristics and attributes.

Bibliography

(1) Gazit, E. Self-assembled peptide nanostructures: the design of molecular building blocks and their technological utilization. *Chemical Society Reviews* **2007**, *36*, 1263-1269.

(2) Cherny, I.; Gazit, E. Amyloids: Not only pathological agents but also ordered nanomaterials. *Angewandte Chemie-International Edition* **2008**, *47*, 4062-4069.

(3) Dobson, C. M. Experimental investigation of protein folding and misfolding. *Methods* **2004**, *34*, 4-14.

(4) Dobson, C. M. Protein aggregation and its consequences for human disease. *Protein and Peptide Letters* **2006**, *13*, 219-227.

(5) Krebs, M. R. H.; Domike, K. R.; Donald, A. M. Protein aggregation: more than just fibrils. *Biochemical Society Transactions* **2009**, *37*, 682-686.

(6) Rochet, J. C.; Lansbury, P. T. Amyloid fibrillogenesis: themes and variations. *Current Opinion in Structural Biology* **2000**, *10*, 60-68.

(7) Hill, R. T.; Lyon, J. L.; Allen, R.; Stevenson, K. J.; Shear, J. B. Microfabrication of three-dimensional bioelectronic architectures. *Journal of the American Chemical Society* **2005**, *127*, 10707-10711.

(8) Haas, J.; Vohringer-Martinez, E.; Bogehold, A.; Matthes, D.; Hensen, U.; Pelah, A.; Abel, B.; Grubmuller, H. Primary Steps of pH-Dependent Insulin Aggregation Kinetics are Governed by Conformational Flexibility. *Chembiochem* **2009**, *10*, 1816-1822.

(9) Hua, Q. X.; Liu, M.; Hu, S. Q.; Jia, W. H.; Arvan, P.; Weiss, M. A. A conserved histidine in insulin is required for the foldability of human proinsulin - Structure and function of an Ala(B5) analog. *Journal of Biological Chemistry* **2006**, *281*, 24889-24899.

(10) Dodson, G.; Steiner, D. The role of assembly in insulin's biosynthesis. *Current Opinion in Structural Biology* **1998**, *8*, 189-194.

(11) Rhodes, E.; Gafni, A. Micelle Formation by a Fragment of Human Islet Amyloid Polypeptide. *Biophysical Journal* **2003**, *84*, 3480-3487.

(12) Brange, J.; Andersen, L.; Laursen, E. D.; Meyn, G.; Rasmussen, E. Toward understanding insulin fibrillation. *Journal of Pharmaceutical Sciences* **1997**, *86*, 517-525.

(13) Nielsen, L.; Khurana, R.; Coats, A.; Frokjaer, S.; Brange, J.; Vyas, S.; Uversky, V. N.; Fink, A. L. Effect of environmental factors on the kinetics of insulin fibril formation: Elucidation of the molecular mechanism. *Biochemistry* **2001**, *40*, 6036-6046.

(14) Brange, J.; Dodson, G. G.; Edwards, D. J.; Holden, P. H.; Whittingham, J. L. A model of insulin fibrils derived from the x-ray crystal structure of a monomeric insulin (despentapeptide insulin). *Proteins-Structure Function and Genetics* **1997**, *27*, 507-516.

(15) Nielsen, L.; Frokjaer, S.; Brange, J.; Uversky, V. N.; Fink, A. L. Probing the mechanism of insulin fibril formation with insulin mutants. *Biochemistry* **2001**, *40*, 8397-8409.

(16) Attri, A. K.; Fernandez, C.; Minton, A. P. pH-dependent Self-association of Zinc-free Insulin Characterized by Concentration-gradient Static Light Scattering. *Biophysical Chemistry* **2010**, *148*, 28-33.

(17) Dzwolak, W.; Ravindra, R.; Lendermann, J.; Winter, R. Aggregation of bovine insulin probed by DSC/PPC calorimetry and FTIR spectroscopy. *Biochemistry* **2003**, *42*, 11347-11355.

(18) Uversky, V. N. Intrinsically Disordered Proteins and Their Environment: Effects of Strong Denaturants, Temperature, pH, Counter Ions, Membranes, Binding Partners, Osmolytes, and Macromolecular Crowding. *Protein Journal* **2009**, *28*, 305-325.

(19) Whittingham, J. L.; Scott, D. J.; Chance, K.; Wilson, A.; Finch, J.; Brange, J.; Dodson, G. G. Insulin at pH 2: Structural analysis of the conditions promoting insulin fibre formation. *Journal of Molecular Biology* **2002**, *318*, 479-490.

(20) Krebs, M. R. H.; Bromley, E. H. C.; Rogers, S. S.; Donald, A. M. The mechanism of amyloid spherulite formation by bovine insulin. *Biophysical Journal* **2005**, *88*, 2013-2021.

(21) Langton, M.; Hermansson, A. M. Fine-stranded and particulate gels of Beta-lactoglobulin and whey-protein at varying pH. *Food Hydrocolloids* **1992**, *5*, 523-539.

(22) Clark, A. H.; Saunderson, D. H. P.; Suggett, A. Infrared and laser-Raman spectroscopy studies of thermally-induced globular protein gels. *International Journal of Peptide and Protein Research* **1981**, *17*, 353-364.

(23) Clark, A. H.; Judge, F. J.; Richards, J. B.; Stubbs, J. M.; Suggett, A. Electron-microscopy of network structures in thermally-induced globular protein gels. *International Journal of Peptide and Protein Research* **1981**, *17*, 380-392.

(24) Fandrich, M.; Dobson, C. M. The behaviour of polyamino acids reveals an inverse side chain effect in amyloid structure formation. *Embo Journal* **2002**, *21*, 5682-5690.

(25) Ivanova, M. I.; Sievers, S. A.; Sawaya, M. R.; Wall, J. S.; Eisenberg, D. Molecular basis for insulin fibril assembly. *Proceedings of the National Academy of Sciences of the United States of America* **2009**, *106*, 18990-18995.

(26) Jimenez, J. L.; Nettleton, E. J.; Bouchard, M.; Robinson, C. V.; Dobson, C. M.; Saibil, H. R. The protofilament structure of insulin amyloid fibrils. *Proceedings of the National Academy of Sciences of the United States of America* **2002**, *99*, 9196-9201.

(27) Vestergaard, B.; Groenning, M.; Roessle, M.; Kastrup, J. S.; van de Weert, M.; Flink, J. M.; Frokjaer, S.; Gajhede, M.; Svergun, D. I. A helical structural nucleus is the primary elongating unit of insulin amyloid fibrils. *Plos Biology* **2007**, *5*, 1089-1097.

(28) Beychok, S. Side-chain optical activity in cystine-containing proteins - Circular dichroism studies. *Proceedings of the National Academy of Sciences of the United States of America* **1965**, *53*, 999-&.

(29) Mercola, D. A.; Morris, J. W. S.; Arquilla, E. R.; Bromer, W. W. Ultraviolet circular dichroism of bovine insulin and desoctapeptide insulin. *Biochimica Et Biophysica Acta* **1967**, *133*, 224-+.

(30) Ettinger, M. J.; Timashef.Sn. Optical activity of insulin .1. Nature of circular dichrosim bands. *Biochemistry* **1971**, *10*, 824-&.

(31) Uversky, V. N.; Garriques, L. N.; Millett, I. S.; Frokjaer, S.; Brange, J.; Doniach, S.; Fink, A. L. Prediction of the association state of insulin using spectral parameters. *Journal of Pharmaceutical Sciences* **2003**, *92*, 847-858.

(32) Ahmad, A.; Millett, I. S.; Doniach, S.; Uversky, V. N.; Fink, A. L. Partially Folded Intermediates in Insulin Fibrillation. *Biochemistry* **2003**, *42*, 11404-11416.

(33) Bouchard, M.; Zurdo, J.; Nettleton, E. J.; Dobson, C. M.; Robinson, C. V. Formation of insulin amyloid fibrils followed by FTIR simultaneously with CD and electron microscopy. *Protein Science* **2000**, *9*, 1960-1967.

(34) Hua, Q. X.; Weiss, M. A. Mechanism of insulin fibrillation - The structure of insulin under amyloidogenic conditions resembles a protein-folding intermediate. *Journal of Biological Chemistry* **2004**, *279*, 21449-21460.

(35) Huus, K.; Havelund, S.; Olsen, H. B.; van de Weert, M.; Frokjaer, S. Thermal dissociation and unfolding of insulin. *Biochemistry* **2005**, *44*, 11171-11177.

(36) Loksztejn, A.; Dzwolak, W. Chiral bifurcation in aggregating insulin: An induced circular dichroism study. *Journal of Molecular Biology* **2008**, *379*, 9-16.

(37) Ji, X.; Ma, X.; Bian, L. Spectral Studies on the Conformational Transitions of Bovine Insulin During Denaturant-induced Unfolding. *Chemical Research in Chinese Universities* **2014**, *30*, 222-227.

(38) Krebs, M. R. H.; Domike, K. R.; Cannon, D.; Donald, A. M. Common motifs in protein self-assembly. *Faraday Discussions* **2008**, *139*, 265-274.

(39) Krebs, M. R. H.; MacPhee, C. E.; Miller, A. F.; Dunlop, L. E.; Dobson, C. M.; Donald, A. M. The formation of spherulites by amyloid fibrils of bovine insulin. *Proceedings of the National Academy of Sciences of the United States of America* **2004**, *101*, 14420-14424.

(40) Babenko, V.; Dzwolak, W. Amino acid sequence determinants in self-assembly of insulin chiral amyloid superstructures: Role of C-terminus of B-chain in association of fibrils. *Febs Letters* **2013**, *587*, 625-630.

(41) Amin, S.; Barnett, G. V.; Pathak, J. A.; Roberts, C. J.; Sarangapani, P. S. Protein aggregation, particle formation, characterization & rheology. *Current Opinion in Colloid & Interface Science* **2014**, *19*, 438-449.

(42) Groenning, M.; Frokjaer, S.; Vestergaard, B. Formation Mechanism of Insulin Fibrils and Structural Aspects of the Insulin Fibrillation Process. *Current Protein & Peptide Science* **2009**, *10*, 509-528.

(43) Kelly, J. W. The alternative conformations of amyloidogenic proteins and their multi-step assembly pathways. *Current Opinion in Structural Biology* **1998**, *8*, 101-106.

(44) Sorci, M.; Grassucci, R. A.; Hahn, I.; Frank, J.; Belfort, G. Time-dependent insulin oligomer reaction pathway prior to fibril formation: Cooling and seeding. *Proteins-Structure Function and Bioinformatics* **2009**, *77*, 62-73.

(45) Li, Y.; Roberts, C. J. Lumry-Eyring Nucleated-Polymerization Model of Protein Aggregation Kinetics. 2. Competing Growth via Condensation and Chain Polymerization. *Journal of Physical Chemistry B* **2009**, *113*, 7020-7032.

(46) Campioni, S.; Carret, G.; Jordens, S.; Nicoud, L.; Mezzenga, R.; Riek, R. The Presence of an Air-Water Interface Affects Formation and Elongation of alpha-Synuclein Fibrils. *Journal of the American Chemical Society* **2014**, *136*, 2866-2875.

(47) Castellanos, M. M.; Pathak, J. A.; Colby, R. H. Both protein adsorption and aggregation contribute to shear yielding and viscosity increase in protein solutions. *Soft Matter* **2014**, *10*, 122-131.

(48) Trigg, B. J.; Lee, C. F.; Vaux, D. J.; Jean, L. The air-water interface determines the outcome of seeding during amyloidogenesis. *Biochemical Journal* **2013**, *456*, 67-80.

(49) Gosal, W. S.; Clark, A. H.; Pudney, P. D. A.; Ross-Murphy, S. B. Novel amyloid fibrillar networks derived from a globular protein: beta-lactoglobulin. *Langmuir* **2002**, *18*, 7174-7181.

(50) Loveday, S. M.; Wang, X. L.; Rao, M. A.; Anema, S. G.; Singh, H. beta-Lactoglobulin nanofibrils: Effect of temperature on fibril formation kinetics, fibril morphology and the rheological properties of fibril dispersions. *Food Hydrocolloids* **2012**, *27*, 242-249.

(51) Waugh, D. F.; Wilhelmson, D. F.; Commerford, S. L.; Sackler, M. L. Studies of the Nucleation and Growth Reactions of Selected Types of Insulin Fibrils. *Journal of the American Chemical Society* **1953**, *75*, 2592-2600.

(52) Waugh, D. F. A Fibrous Modification of Insulin .1. The Heat Precipitate of Insulin. *Journal of the American Chemical Society* **1946**, *68*, 247-250.

(53) Jansen, R.; Dzwolak, W.; Winter, R. Amyloidogenic self-assembly of insulin aggregates probed by high resolution atomic force microscopy. *Biophysical Journal* **2005**, *88*, 1344-1353.

(54) Corrigan, A. M.; Donald, A. M. Particle tracking microrheology of gel-forming amyloid fibril networks. *European Physical Journal E* **2009**, *28*, 457-462.

(55) Blundell, T. L.; Cutfield, J. F.; Dodson, G. G.; Dodson, E.; Hodgkin, D. C.; Mercola, D. Structure and Biology of Insulin. *Biochemical Journal* **1971**, *125*, P50-&.

(56) Jahn, T. R.; Makin, O. S.; Morris, K. L.; Marshall, K. E.; Tian, P.; Sikorski, P.; Serpell, L. C. The Common Architecture of Cross-beta Amyloid. *Journal of Molecular Biology* **2010**, *395*, 717-727.

(57) Wang, W. Protein aggregation and its inhibition in biopharmaceutics. *International Journal of Pharmaceutics* **2005**, *289*, 1-30.

(58) Findeis, M. A. Approaches to discovery and characterization of inhibitors of amyloid beta-peptide polymerization. *Biochimica Et Biophysica Acta-Molecular Basis of Disease* **2000**, *1502*, 76-84.

(59) Kim, Y. S.; Randolph, T. W.; Stevens, F. J.; Carpenter, J. F. Kinetics and energetics of assembly, nucleation, and growth of aggregates and fibrils for an amyloidogenic protein - Insights into transition states from pressure, temperature, and co-solute studies. *Journal of Biological Chemistry* **2002**, *277*, 27240-27246.

(60) Mauro, M.; Craparo, E. F.; Podesta, A.; Bulone, D.; Carrotta, R.; Martorana, V.; Tiana, G.; San Biagio, P. L. Kinetics of different processes in human insulin amyloid formation. *Journal of Molecular Biology* **2007**, *366*, 258-274.

(61) Murphy, R. M. Kinetics of amyloid formation and membrane interaction with amyloidogenic proteins. *Biochimica Et Biophysica Acta-Biomembranes* **2007**, *1768*, 1923-1934.

(62) Bartolini, M.; Andrisano, V. Strategies for the Inhibition of Protein Aggregation in Human Diseases. *Chembiochem* **2010**, *11*, 1018-1035.

(63) MacPhee, C. E.; Woolfson, D. N. Engineered and designed peptide-based fibrous biomaterials. *Current Opinion in Solid State & Materials Science* **2004**, *8*, 141-149.

(64) Gazit, E. Use of biomolecular templates for the fabrication of metal nanowires. *Febs Journal* **2007**, *274*, 317-322.

(65) Wang, W.; Nema, S.; Teagarden, D. Protein aggregation-Pathways and influencing factors. *International Journal of Pharmaceutics* **2010**, *390*, 89-99.

(66) Brunsteiner, M.; Flock, M.; Nidetzky, B. Structure Based Descriptors for the Estimation of Colloidal Interactions and Protein Aggregation Propensities. *Plos One* **2013**, *8*.

(67) Dinca, V.; Kasotakis, E.; Catherine, J.; Mourka, A.; Ranella, A.; Ovsianikov, A.; Chichkov, B. N.; Farsari, M.; Mitraki, A.; Fotakis, C. Directed three-dimensional patterning of self-assembled peptide fibrils. *Nano Letters* **2008**, *8*, 538-543.

(68) Sarkar, S.; Guibal, E.; Quignard, F.; SenGupta, A. K. Polymer-supported metals and metal oxide nanoparticles: synthesis, characterization, and applications. *Journal of Nanoparticle Research* **2012**, *14*.

(69) Villegas, V.; Zurdo, J.; Filimonov, V. V.; Aviles, F. X.; Dobson, C. M.; Serrano, L. Protein engineering as a strategy to avoid formation of amyloid fibrils. *Protein Science* **2000**, *9*, 1700-1708.

(70) Hule, R. A.; Nagarkar, R. P.; Hammouda, B.; Schneider, J. P.; Pochan, D. J. Dependence of Self-Assembled Peptide Hydrogel Network Structure on Local Fibril Nanostructure. *Macromolecules* **2009**, *42*, 7137-7145.

(71) Kasotakis, E.; Mossou, E.; Adler-Abramovich, L.; Mitchell, E. P.; Forsyth, V. T.; Gazit, E.; Mitraki, A. Design of Metal-Binding Sites Onto Self-Assembled Peptide Fibrils. *Biopolymers* **2009**, *92*, 164-172.

(72) Yan, C. Q.; Pochan, D. J. Rheological properties of peptide-based hydrogels for biomedical and other applications. *Chemical Society Reviews* **2010**, *39*, 3528-3540.

(73) Acar, H.; Garifullin, R.; Aygun, L. E.; Okyay, A. K.; Guler, M. O. Amyloid-like peptide nanofiber templated titania nanostructures as dye sensitized solar cell anodic materials. *Journal of Materials Chemistry A* **2013**, *1*, 10979-10984.

(74) Ottova, A.; Tvarozek, V.; Racek, J.; Sabo, J.; Ziegler, W.; Hianik, T.; Tien, H. T. Self-assembled BLMs: biomembrane models and biosensor applications. *Supramolecular Science* **1997**, *4*, 101-112.

(75) Viguier, B.; Zor, K.; Kasotakis, E.; Mitraki, A.; Clausen, C. H.; Svendsen, W. E.; Castillo-Leon, J. Development of an Electrochemical Meta-Ion Biosensor Using Self-Assembled Peptide Nanofibrils. *Acs Applied Materials & Interfaces* **2011**, *3*, 1594-1600.

(76) Colby, R.; Hulleman, J.; Padalkar, S.; Rochet, J. C.; Stanciu, L. A. Biotemplated synthesis of metallic nanoparticle chains on an alpha-synuclein fiber scaffold. *Journal of Nanoscience and Nanotechnology* **2008**, *8*, 973-978.

(77) Zhang, L. G.; Li, N.; Gao, F. M.; Hou, L.; Xu, Z. M. Insulin Amyloid Fibrils: An Excellent Platform for Controlled Synthesis of Ultrathin Superlong Platinum Nanowires with High Electrocatalytic Activity. *Journal of the American Chemical Society* **2012**, *134*, 11326-11329.

(78) Tang, Q.; Solin, N.; Lu, J.; Inganas, O. Hybrid bioinorganic insulin amyloid fibrils. *Chemical Communications* **2010**, *46*, 4157-4159.

(79) Gysemans, M.; Snauwaert, J.; Van Haesendonck, C.; Leroux, F.; Goris, B.; Bals, S.; Van Tendeloo, G. AFM and TEM study of Ag coated insulin-derived amyloid fibrils. In *European Microscopy Congress*, S. Richter, A. S., Ed., 2008; Vol. Volume 2: Materials Science, pp 739-740.

(80) Leroux, F.; Gysemans, M.; Bals, S.; Batenburg, K. J.; Snauwaert, J.; Verbiest, T.; Van Haesendonck, C.; Van Tendeloo, G. Three-Dimensional Characterization of Helical Silver Nanochains Mediated by Protein Assemblies. *Advanced Materials* **2010**, *22*, 2193-+.

(81) Hsieh, S.; Hsieh, C. W. Nanoparticle alignment on various surfaces using insulin fibrils as a biotemplate. *Abstracts of Papers of the American Chemical Society* **2011**, *242*.

(82) Padalkar, S.; Hulleman, J. D.; Kim, S. M.; Rochet, J. C.; Stach, E. A.; Stanciu, L. A. Protein-templated semiconductor nanoparticle chains. *Nanotechnology* **2008**, *19*.

(83) Miller, A. F. Gelation of misfolded proteins. In *Polymer-Solvent Complexes and Intercalates V*, Grohens, Y., Ed., 2005; Vol. 222, pp 109-114.

(84) Bohidar, H. B. Light scattering and viscosity study of heat aggregation of insulin. *Biopolymers* **1998**, *45*, 1-8.

(85) Domike, K. R.; Donald, A. M. Thermal dependence of thermally induced protein spherulite formation and growth: Kinetics of beta-lactoglobulin and insulin. *Biomacromolecules* **2007**, *8*, 3930-3937.

(86) Dirix, C.; Meersman, F.; Smeller, L.; Heremans, K. Unfolding and fibrillogenesis of insulin: Temperature, pressure and chemistry. *High Pressure Research* **2002**, *22*, 733-736.

(87) Donald, A. M. Why should polymer physicists study biopolymers? *Journal of Polymer Science Part B-Polymer Physics* **2007**, *45*, 3257-3262.

(88) Domike, K. R.; Donald, A. M. Kinetics of spherulite formation and growth: Salt and protein concentration dependence on proteins beta-lactoglobulin and insulin. *International Journal of Biological Macromolecules* **2009**, *44*, 301-310.

(89) Kjoniksen, A. L.; Zhu, K. Z.; Behrens, M. A.; Pedersen, J. S.; Nystrom, B. Effects of Temperature and Salt Concentration on the Structural and Dynamical Features in Aqueous Solutions of Charged Triblock Copolymers. *Journal of Physical Chemistry B* **2011**, *115*, 2125-2139.

(90) Hill, E. K.; Krebs, B.; Goodall, D. G.; Howlett, G. J.; Dunstan, D. E. Shear flow induces amyloid fibril formation. *Biomacromolecules* **2006**, *7*, 10-13.

(91) Dunstan, D. E.; Hamilton-Brown, P.; Asimakis, P.; Ducker, W.; Bertolini, J. Shear-induced structure and mechanics of beta-lactoglobulin amyloid fibrils. *Soft Matter* **2009**, *5*, 5020-5028.

(92) De Jong, K. L.; Incledon, B.; Yip, C. M.; DeFelippis, M. R. Amyloid fibrils of glucagon characterized by high-resolution atomic force microscopy. *Biophysical Journal* **2006**, *91*, 1905-1914.

(93) Hamilton-Brown, P.; Bekard, I.; Ducker, W. A.; Dunstan, D. E. How Does Shear Affect A beta Fibrillogenesis? *Journal of Physical Chemistry B* **2008**, *112*, 16249-16252.

(94) Dunstan, D. E.; Hamilton-Brown, P.; Asimakis, P.; Ducker, W.; Bertolini, J. Shear flow promotes amyloid-beta fibrilization. *Protein Engineering Design & Selection* **2009**, *22*, 741-746.

(95) Bekard, I. B.; Dunstan, D. E. Shear-Induced Deformation of Bovine Insulin in Couette Flow. *Journal of Physical Chemistry B* **2009**, *113*, 8453-8457.

(96) Bekard, I. B.; Asimakis, P.; Bertolini, J.; Dunstan, D. E. The Effects of Shear Flow on Protein Structure and Function. *Biopolymers* **2011**, *95*, 733-745.

(97) Sluzky, V.; Tamada, J. A.; Klibanov, A. M.; Langer, R. Kinetics of insulin aggregation in aqueous-solutions upon agitation in the presence of hydrophobic surfaces. *Proceedings of the National Academy of Sciences of the United States of America* **1991**, *88*, 9377-9381.

(98) Veerman, C.; Sagis, L. M. C.; Venema, P.; van der Linden, E. Shear-induced aggregation and break up of fibril clusters close to the percolation concentration. *Rheologica Acta* **2005**, *44*, 244-249.

(99) Webster, G. T.; Dusting, J.; Balabani, S.; Blanch, E. W. Detecting the Early Onset of Shear-Induced Fibril Formation of Insulin in situ. *Journal of Physical Chemistry B* **2011**, *115*, 2617-2626.

(100) Akkermans, C.; Venema, P.; Rogers, S. S.; van der Goot, A. J.; Boom, R. M.; van der Linden, E. Shear Pulses Nucleate Fibril Aggregation. *Food Biophysics* **2006**, *1*, 144-150.

(101) Ashton, L.; Dusting, J.; Imomoh, E.; Balabani, S.; Blanch, E. W. Shear-Induced Unfolding of Lysozyme Monitored In Situ. *Biophysical Journal* **2009**, *96*, 4231-4236.

(102) Humblet-Hua, N. P.; Sagis, L. M. C.; van der Linden, E. Effects of Flow on Hen Egg White Lysozyme (HEWL) Fibril Formation: Length Distribution, Flexibility, and Kinetics. *Journal of Agricultural and Food Chemistry* **2008**, *56*, 11875-11882.

(103) Stroev, P. V.; Hoskins, P. R.; Easson, W. J. Distribution of wall shear rate throughout the arterial tree: A case study. *Atherosclerosis* **2007**, *191*, 276-280.

(104) Manno, M.; Giacomazza, D.; Newman, J.; Martorana, V.; San Biagio, P. L. Amyloid Gels: Precocious Appearance of Elastic Properties during the Formation of an Insulin Fibrillar Network. *Langmuir* **2010**, *26*, 1424-1426.

(105) Zhang, L. G.; Gao, F. M. Self-assembled gold nanochains hybrid based on insulin fibrils. *Journal of Nanoparticle Research* **2012**, *14*.

(106) Barrau, S.; Zhang, F.; Herland, A.; Mammo, W.; Andersson, M. R.; Inganas, O. Integration of Amyloid Nanowires in Organic Solar Cells. *Applied Physics Letters* **2008**, *93*.

(107) Estrada, D.; Pop, E. Imaging dissipation and hot spots in carbon nanotube network transistors. *Applied Physics Letters* **2011**, *98*.

(108) Williams, L. N.; Elder, S. H.; Horstemeyer, M. F.; Harbarger, D. Variation of diameter distribution, number density, and area fraction of fibrils within five areas of the rabbit patellar tendon. *Annals of Anatomy-Anatomischer Anzeiger* **2008**, *190*, 442-451.

(109) Underwood, E. E. Stereology, or the quantitative evaluation of microstructures. *Journal of Microscopy* **1969**, *89*, 161-180.

(110) Rothenberg, G. Data mining in catalysis: Separating knowledge from garbage. *Catalysis Today* **2008**, *137*, 2-10.

(111) Bee, J. S.; Chiu, D.; Sawicki, S.; Stevenson, J. L.; Chatterjee, K.; Freund, E.; Carpenter, J. F.; Randolph, T. W. Monoclonal Antibody Interactions With Micro- and Nanoparticles: Adsorption, Aggregation, and Accelerated Stress Studies. *Journal of Pharmaceutical Sciences* **2009**, *98*, 3218-3238.

(112) Bee, J. S.; Davis, M.; Freund, E.; Carpenter, J. F.; Randolph, T. W. Aggregation of a Monoclonal Antibody Induced by Adsorption to Stainless Steel. *Biotechnology and Bioengineering* **2010**, *105*, 121-129.

(113) Bee, J. S.; Randolph, T. W.; Carpenter, J. F.; Bishop, S. M.; Dimitrova, M. N. Effects of Surfaces and Leachables on the Stability of Biopharmaceuticals. *Journal of Pharmaceutical Sciences* **2011**, *100*, 4158-4170.

(114) Hoehne, M.; Samuel, F.; Dong, A.; Wurth, C.; Mahler, H.-C.; Carpenter, J. F.; Randolph, T. W. Adsorption of Monoclonal Antibodies to Glass Microparticles. *Journal of Pharmaceutical Sciences* **2011**, *100*, 123-132.

(115) Kreilgaard, L.; Jones, L. S.; Randolph, T. W.; Frokjaer, S.; Flink, J. M.; Manning, M. C.; Carpenter, J. F. Effect of Tween 20 on freeze-thawing- and agitation-induced aggregation of recombinant, human factor XIII. *Journal of Pharmaceutical Sciences* **1998**, *87*, 1597-1603.

(116) Webb, S. D.; Golledge, S. L.; Cleland, J. L.; Carpenter, J. F.; Randolph, T. W. Surface adsorption of recombinant human interferon-gamma in lyophilized and spray-lyophilized formulations. *Journal of Pharmaceutical Sciences* **2002**, *91*, 1474-1487.

(117) Biddlecombe, J. G.; Smith, G.; Uddin, S.; Mulot, S.; Spencer, D.; Gee, C.; Fish, B. C.; Bracewell, D. G. Factors Influencing Antibody Stability at Solid-Liquid Interfaces in a High Shear Environment. *Biotechnology Progress* **2009**, *25*, 1499-1507.

(118) Bee, J. S.; Schwartz, D. K.; Trabelsi, S.; Freund, E.; Stevenson, J. L.; Carpenter, J. F.; Randolph, T. W. Production of particles of therapeutic proteins at the air-water interface during compression/dilation cycles. *Soft Matter* **2012**, *8*, 10329-10335.

(119) Wiesbauer, J.; Prassl, R.; Nidetzky, B. Renewal of the Air-Water Interface as a Critical System Parameter of Protein Stability: Aggregation of the Human Growth Hormone and Its Prevention by Surface-Active Compounds. *Langmuir* **2013**, *29*, 15240-15250.

(120) Li, J. L.; Liu, X. Y. *Soft fibrillar materials: Fabrication and applications*; Wiley Science Publishing2013.

(121) Underwood, E. E. Stereology of projected images. *Journal of Microscopy-Oxford* **1972**, *95*, 25-&.

(122) Fandrich, M.; Dobson, C. M. Protein folding aspects of amyloid fibril formation. *Amyloid-Journal of Protein Folding Disorders* **2001**, *8*, 26-26.

(123) Loveday, S. M.; Rao, M. A.; Creamer, L. K.; Singh, H. Factors Affecting Rheological Characteristics of Fibril Gels: The Case of beta-Lactoglobulin and alpha-Lactalbumin. *Journal of Food Science* **2009**, *74*, R47-R55.

(124) Hamada, D.; Yanagihara, I.; Tsumoto, K. Engineering amyloidogenicity towards the development of nanofibrillar materials. *Trends in Biotechnology* **2004**, *22*, 93-97.

(125) Chang, G. H.; Luo, Y. L.; Qin, X. Y.; Lu, W. B.; Asiri, A. M.; Al-Youbi, A. O.; Sun, X. P. Synthesis of Pt Nanoparticles Decorated 1,5-Diaminoanthraquinone Nanofibers and Their Application Toward Catalytic Reduction of 4-Nitrophenol. *Journal of Nanoscience and Nanotechnology* **2012**, *12*, 7075-7080.

(126) Zhang, Y.; Franklin, N. W.; Chen, R. J.; Dai, H. J. Metal coating on suspended carbon nanotubes and its implication to metal-tube interaction. *Chemical Physics Letters* **2000**, *331*, 35-41.

(127) Scheibel, T.; Parthasarathy, R.; Sawicki, G.; Lin, X. M.; Jaeger, H.; Lindquist, S. L. Conducting nanowires built by controlled self-assembly of amyloid fibers and selective metal deposition. *Proceedings of the National Academy of Sciences of the United States of America* **2003**, *100*, 4527-4532.

(128) Chi, E. Y.; Krishnan, S.; Randolph, T. W.; Carpenter, J. F. Physical stability of proteins in aqueous solution: Mechanism and driving forces in nonnative protein aggregation. *Pharmaceutical Research* **2003**, *20*, 1325-1336.

(129) Morris, A. M.; Finke, R. G. alpha-Synuclein aggregation variable temperature and variable pH kinetic data: A re-analysis using the Finke-Watzky 2-step model of nucleation and autocatalytic growth. *Biophysical Chemistry* **2009**, *140*, 9-15.

(130) Hamada, D.; Dobson, C. M. A kinetic study of beta-lactoglobulin amyloid fibril formation promoted by urea. *Protein Science* **2002**, *11*, 2417-2426.

(131) Malik, R.; Roy, I. Probing the mechanism of insulin aggregation during agitation. *International Journal of Pharmaceutics* **2011**, *413*, 73-80.

(132) Wiesbauer, J.; Cardinale, M.; Nidetzky, B. Shaking and stirring: Comparison of controlled laboratory stress conditions applied to the human growth hormone. *Process Biochemistry* **2013**, *48*, 33-40.

(133) Bee, J. S.; Stevenson, J. L.; Mehta, B.; Svitel, J.; Pollastrini, J.; Platz, R.; Freund, E.; Carpenter, J. F.; Randolph, T. W. Response of a Concentrated Monoclonal Antibody Formulation to High Shear. *Biotechnology and Bioengineering* **2009**, *103*, 936-943.

(134) Jaspe, J.; Hagen, S. J. Do protein molecules unfold in a simple shear flow? *Biophysical Journal* **2006**, *91*, 3415-3424.

(135) Kiese, S.; Papppenberger, A.; Friess, W.; Mahler, H. C. Shaken, not stirred: Mechanical stress testing of an IgG1 antibody. *Journal of Pharmaceutical Sciences* **2008**, *97*, 4347-4366.

(136) Uberoi, V.; Bhattacharya, S. K. Toxicity and degradability of nitrophenols in anaerobic systems. *Water Environment Research* **1997**, *69*, 146-156.

(137) Pradhan, N.; Pal, A.; Pal, T. Catalytic reduction of aromatic nitro compounds by coinage metal nanoparticles. *Langmuir* **2001**, *17*, 1800-1802.

(138) Pradhan, N.; Pal, A.; Pal, T. Silver nanoparticle catalyzed reduction of aromatic nitro compounds. *Colloids and Surfaces a-Physicochemical and Engineering Aspects* **2002**, *196*, 247-257.

(139) Schweitzer, P. A. *Corrosion Engineering Handbook*; 2 ed.; CRC Press2006.

(140) Wu, Y. P.; Zhang, T.; Zheng, Z. H.; Ding, X. B.; Peng, Y. X. A facile approach to Fe3O4@Au nanoparticles with magnetic recyclable catalytic properties. *Materials Research Bulletin* **2010**, *45*, 513-517.

(141) Dotzauer, D. M.; Dai, J. H.; Sun, L.; Bruening, M. L. Catalytic membranes prepared using layer-by-layer adsorption of polyelectrolyte/metal nanoparticle films in porous supports. *Nano Letters* **2006**, *6*, 2268-2272.

(142) Huang, J. F.; Vongehr, S.; Tang, S. C.; Lu, H. M.; Shen, J. C.; Meng, X. K. Ag Dendrite-Based Au/Ag Bimetallic Nanostructures with Strongly Enhanced Catalytic Activity. *Langmuir* **2009**, *25*, 11890-11896.

(143) Lin, F. H.; Doong, R. A. Bifunctional Au-Fe3O4 Heterostructures for Magnetically Recyclable Catalysis of Nitrophenol Reduction. *Journal of Physical Chemistry C* **2011**, *115*, 6591-6598.

(144) Lin, F. H.; Doong, R. A. Magnetically Recyclable Gold-Magnetite Nanocatalysts for Reduction of Nitrophenols. *Sustainable Nanotechnology and the Environment: Advances and Achievements* **2013**, *1124*, 291-305.

(145) Chang, G. H.; Luo, Y. L.; Lu, W. B.; Qin, X. Y.; Asiri, A. M.; Al-Youbi, A. O.; Sun, X. P. Ag nanoparticles decorated polyaniline nanofibers: synthesis, characterization, and applications toward catalytic reduction of 4-nitrophenol and electrochemical detection of H2O2 and glucose. *Catalysis Science & Technology* **2012**, *2*, 800-806.

(146) Jiang, Y. J.; Li, G. Z.; Li, X. D.; Lu, S. X.; Wang, L.; Zhang, X. W. Water-dispersible Fe3O4 nanowires as efficient supports for noble-metal catalysed aqueous reactions. *Journal of Materials Chemistry A* **2014**, *2*, 4779-4787.

(147) Zhang, Y. W.; Liu, S.; Lu, W. B.; Wang, L.; Tian, J. Q.; Sun, X. P. In situ green synthesis of Au nanostructures on graphene oxide and their application for catalytic reduction of 4-nitrophenol. *Catalysis Science & Technology* **2011**, *1*, 1142-1144.

(148) Quinn, S. D.; Dalgarno, P. A.; Cameron, R. T.; Hedley, G. J.; Hacker, C.; Lucocq, J. M.; Baillie, G. S.; Samuel, I. D. W.; Penedo, J. C. Real-time probing of beta-amyloid self-assembly and inhibition using fluorescence self-quenching between neighbouring dyes. *Molecular Biosystems* **2014**, *10*, 34-44.

(149) Brandenburg; Berlepsch, H.; Koksch, B. Inhibition of amyloid formation in model peptides. *Journal of Peptide Science* **2010**, *16*, 117-118.

(150) Bartolini, M.; Naldi, M.; Fiori, J.; Valle, F.; Biscarini, F.; Nicolau, D. V.; Andrisano, V. Kinetic characterization of amyloid-beta 1-42 aggregation with a multimethodological approach. *Analytical Biochemistry* **2011**, *414*, 215-225.

(151) Biancalana, M.; Makabe, K.; Koide, A.; Koide, S. Molecular Mechanism of Thioflavin-T Binding to the Surface of beta-Rich Peptide Self-Assemblies. *Journal of Molecular Biology* **2009**, *385*, 1052-1063.

(152) Bolder, S. G.; Sagis, L. M. C.; Venema, P.; van der Linden, E. Thioflavin T and birefringence assays to determine the conversion of proteins into fibrils. *Langmuir* **2007**, *23*, 4144-4147.

(153) Robbins, K. J.; Liu, G.; Selmani, V.; Lazo, N. D. Conformational Analysis of Thioflavin T Bound to the Surface of Amyloid Fibrils. *Langmuir* **2012**, *28*, 16490-16495.

(154) Fodera, V.; Groenning, M.; Vetri, V.; Librizzi, F.; Spagnolo, S.; Cornett, C.; Olsen, L.; van de Weert, M.; Leone, M. Thioflavin T Hydroxylation at Basic pH and Its Effect on Amyloid Fibril Detection. *Journal of Physical Chemistry B* **2008**, *112*, 15174-15181.

(155) Hudson, S. A.; Ecroyd, H.; Kee, T. W.; Carver, J. A. The thioflavin T fluorescence assay for amyloid fibril detection can be biased by the presence of exogenous compounds. *Febs Journal* **2009**, *276*, 5960-5972.

(156) Noormai, A.; Primar, K.; Tougu, V.; Palumaa, P. Interference of low-molecular substances with the thioflavin-T fluorescence assay of amyloid fibrils. *Journal of Peptide Science* **2012**, *18*, 59-64.

(157) Buell, A. K.; Dobson, C. M.; Knowles, T. P. J.; Welland, M. E. Interactions between Amyloidophilic Dyes and Their Relevance to Studies of Amyloid Inhibitors. *Biophysical Journal* **2010**, *99*, 3492-3497.

(158) Batzli, K. M.; Love, B. J. Agitation of amyloid proteins to speed aggregation measured by ThT fluorescence: A call for standardization. *MSE C* **2014**.

(159) Podesta, A.; Tiana, G.; Milani, P.; Manno, M. Early events in insulin fibrillization studied by time-lapse atomic force microscopy. *Biophysical Journal* **2006**, *90*, 589-597.

(160) Thomas, C. R.; Geer, D. Effects of shear on proteins in solution. *Biotechnology Letters* **2011**, *33*, 443-456.

(161) Savart, T.; Dove, C.; Love, B. J. In situ Dynamic Rheological Study of Polyacrylamide during Gelation Coupled with Mathematical Models of Viscosity Advancement. *Macromolecular Materials and Engineering* **2010**, *295*, 146-152.

(162) Kholodenko, A. L.; Douglas, J. F. Generalized stokes-Einstein equation for spherical-particle suspensions. *Physical Review E* **1995**, *51*, 1081-1090.

(163) Lilyestrom, W. G.; Yadav, S.; Shire, S. J.; Scherer, T. M. Monoclonal Antibody Self-Association, Cluster Formation, and Rheology at High Concentrations. *Journal of Physical Chemistry B* **2013**, *117*, 6373-6384.

(164) Veerman, C.; Sagis, L. M. C.; Venema, P.; van der Linden, E. The effect of shear flow on the percolation concentration of fibrillar protein assemblies. *Journal of Rheology* **2005**, *49*, 355-368.

(165) Sharma, V.; Jaishankar, A.; Wang, Y.-C.; McKinley, G. H. Rheology of globular proteins: apparent yield stress, high shear rate viscosity and interfacial viscoelasticity of bovine serum albumin solutions. *Soft Matter* **2011**, *7*, 5150-5160.

(166) Chambon, F.; Winter, H. H. Stopping of crosslinking reaction in a PDMS polymer at the gel point. *Polymer Bulletin* **1985**, *13*, 499-503.

(167) Brange, J. *Stability of Insulin*; 1 ed.; Springer-Verlag: New York, 1940.

(168) Sarkar, N.; Kumar, M.; Dubey, V. K. Effect of sodium tetrathionate on amyloid fibril: Insight into the role of disulfide bond in amyloid progression. *Biochimie* **2011**, *93*, 962-968.

(169) Johansson, J.; Nerelius, C.; Willander, H.; Presto, J. Conformational preferences of non-polar amino acid residues: An additional factor in amyloid formation. *Biochemical and Biophysical Research Communications* **2010**, *402*, 515-518.

(170) Ahmad, A.; Uversky, V. N.; Hong, D.; Fink, A. L. Early Events in the Fibrillation of Monomeric Iinsulin. *Journal of Biological Chemistry* **2005**, *280*, 42669-42675.

(171) Levine, H. Thioflavin-T interaction with synthetic Alzheimer's-disease beta-amyloid peptides - Detection of amyloid aggregation in solution. *Protein Science* **1993**, *2*, 404-410.

(172) Jha, S.; Snell, J. M.; Sheftic, S. R.; Patil, S. M.; Daniels, S. B.; Kolling, F. W.; Alexandrescu, A. T. pH Dependence of Amylin Fibrillization. *Biochemistry* **2014**, *53*, 300-310.

(173) Suzuki, Y.; Brender, J. R.; Hartman, K.; Ramamoorthy, A.; Marsh, E. N. G. Alternative Pathways of Human Islet Amyloid Polypeptide Aggregation Distinguished by F-19 Nuclear Magnetic Resonance-Detected Kinetics of Monomer Consumption. *Biochemistry* **2012**, *51*, 8154-8162.

(174) Khurana, R.; Coleman, C.; Ionescu-Zanetti, C.; Carter, S. A.; Krishna, V.; Grover, R. K.; Roy, R.; Singh, S. Mechanism of thioflavin T binding to amyloid fibrils. *Journal of Structural Biology* **2005**, *151*, 229-238.

(175) Hellstrand, E.; Boland, B.; Walsh, D. M.; Linse, S. Amyloid beta-Protein Aggregation Produces Highly Reproducible Kinetic Data and Occurs by a Two-Phase Process. *Acs Chemical Neuroscience* **2010**, *1*, 13-18.

(176) Tiiman, A.; Noormagi, A.; Friedemann, M.; Krishtal, J.; Palumaa, P.; Tougu, V. Effect of agitation on the peptide fibrillization: Alzheimer's amyloid-beta peptide 1-42 but not amylin and insulin fibrils can grow under quiescent conditions. *Journal of Peptide Science* **2013**, *19*, 386-391.

(177) Bernhardt, N. A.; Berhanu, W. M.; Hansmann, U. H. E. Mutations and Seeding of Amylin Fibril-Like Oligomers. *Journal of Physical Chemistry B* **2013**, *117*, 16076-16085.

(178) Scherzer-Attali, R.; Shaltiel-Karyo, R.; Adalist, Y. H.; Segal, D.; Gazit, E. Generic inhibition of amyloidogenic proteins by two naphthoquinone-tryptophan hybrid molecules. *Proteins-Structure Function and Bioinformatics* **2012**, *80*, 1962-1973.

(179) McDuffie, N. G. Selectivity of platinum and platinum-nylon catalysts. *Journal of Catalysis* **1979**, *57*, 193-194.

(180) Galvagno, S.; Staiti, P.; Antonucci, P.; Giannetto, A.; Giordano, N. Effect of pretreatment in benzene hydrogenation on Pt/Nylon catalyst. *Reaction Kinetics and Catalysis Letters* **1982**, *21*, 157-162.

(181) Dini, P.; Dones, D.; Montelat.S; Giordano, N. Study of platinum-polyamide catalysts - Catalytic behavior in benzene hydrogenation reaction. *Journal of Catalysis* **1973**, *30*, 1-12.

(182) Harrison, D. P.; Rase, H. F. Nylon-platinum catalysts with unusual geometric and selective characteristics. *Industrial & Engineering Chemistry Fundamentals* **1967**, *6*, 161-&.

(183) Sermon, P. A.; Azhari, C. H. Formation, reactivity and catalytic selectivity of Pt(ClX)(CONH)Y species prepared by interaction of H2PtCl6 with Nylon supports. *Journal of Molecular Catalysis* **1990**, *59*, 267-277.

(184) Kralik, M.; Biffis, A. Catalysis by metal nanoparticles supported on functional organic polymers. *Journal of Molecular Catalysis a-Chemical* **2001**, *177*, 113-138.

(185) Dimeska, R.; Little, S.; Ralph, S. R.; Wallace, G. G. Platinum recovery using inherently conducting polymers and common fabrics. *Fibers and Polymers* **2007**, *8*, 463-469.

(186) Browne, M.; Cecil, R.; Miller, J. C. Some reactions of insulin at nonpolar surfaces. *European Journal of Biochemistry* **1973**, *33*, 233-240.

(187) Hu, L.; Pasta, M.; La Mantia, F.; Cui, L.; Jeong, S.; Deshazer, H. D.; Choi, J. W.; Han, S. M.; Cui, Y. Stretchable, Porous, and Conductive Energy Textiles. *Nano Letters* **2010**, *10*, 708-714.

(188) Pasta, M.; La Mantia, F.; Hu, L.; Deshazer, H. D.; Cui, Y. Aqueous supercapacitors on conductive cotton. *Nano Research* **2010**, *3*, 452-458.

(189) Yu, G.; Hu, L.; Vosgueritchian, M.; Wang, H.; Xie, X.; McDonough, J. R.; Cui, X.; Cui, Y.; Bao, Z. Solution-Processed Graphene/MnO2 Nanostructured Textiles for High-Performance Electrochemical Capacitors. *Nano Letters* **2011**, *11*, 2905-2911.

(190) Praschak, D.; Bahners, T.; Schollmeyer, E. PET surface modifications by treatment with monochromatic excimer UV lamps. *Applied Physics a-Materials Science & Processing* **1998**, *66*, 69-75.

(191) Gao, S. L.; Hassler, R.; Mader, E.; Bahners, T.; Opwis, K.; Schollmeyer, E. Photochemical surface modification of PET by excimer UV lamp irradiation. *Applied Physics B-Lasers and Optics* **2005**, *81*, 681-690.

(192) Opwis, K.; Knittel, D.; Schollmeyer, E. Functionalization of catalase for a photochemical immobilization on poly(ethylene terephthalate). *Biotechnology Journal* **2007**, *2*, 347-352.

(193) Lee, J.-W.; Mayer-Gall, T.; Opwis, K.; Song, C. E.; Gutmann, J. S.; List, B. Organotextile Catalysis. *Science* **2013**, *341*, 1225-1229.

(194) Randolph, T. W.; Carpenter, J. F. Engineering challenges of protein formulations. *Aiche Journal* **2007**, *53*, 1902-1907.